AD NUMBER
AD334868
CLASSIFICATION CHANGES
TO: **UNCLASSIFIED**
FROM: **CONFIDENTIAL**
LIMITATION CHANGES
TO: **Approved for public release; distribution is unlimited. Document partially illegible.**
FROM: **Distribution authorized to U.S. Gov't. agencies and their contractors; Administrative/Operational Use; FEB 1963. Other requests shall be referred to Aeronautical Systems Division, Wright-Patterson AFB, OH 45433. Document partially illegible.**
AUTHORITY
1 Jul 1965, per document markings; AFFDL ltr, 21 Oct 1974

AD 334868

DISCLAIMER NOTICE

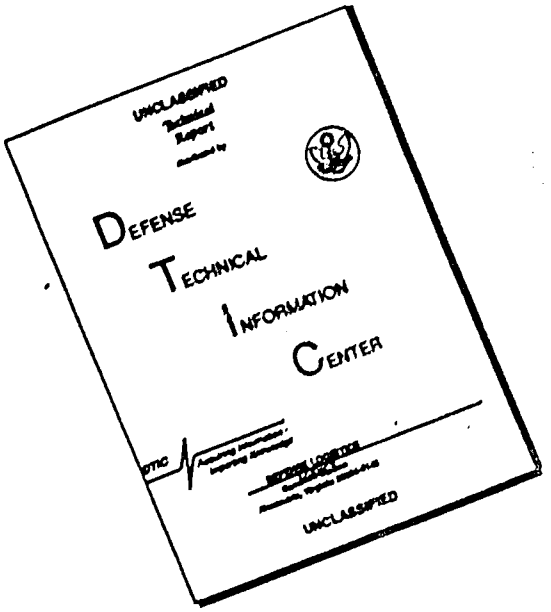

THIS DOCUMENT IS BEST QUALITY AVAILABLE. THE COPY FURNISHED TO DTIC CONTAINED A SIGNIFICANT NUMBER OF PAGES WHICH DO NOT REPRODUCE LEGIBLY.

ASD-TDR-62-844

CONFIDENTIAL

30

(Unclassified Title)

Analytical And Experimental Investigation Of Supersonic Parachute Phenomena

TECHNICAL DOCUMENTARY REPORT ASD-TDR-62-844
February 1963

Flight Accessories Laboratory
Aeronautical Systems Division
Air Force Systems Command
Wright-Patterson Air Force Base, Ohio

Project No. 6065, Task No. 606505

(Prepared under Contract No. AF 33(616)-8459, Item No. II
By Cook Technological Center, A Division of Cook Electric Company
Chicago, Illinois, Author: L. W. Sims)

CONFIDENTIAL

NOTICES

When Government drawings, specifications, or other data are used for any purpose other than in connection with a definitely related Government procurement operation, the United States Government thereby incurs no responsibility nor any obligation whatsoever, and the fact that the Government may have formulated, furnished, or in any way supplied the said drawings, specifications, or other data, is not to be regarded by implication or otherwise as in any manner licensing the holder or any other person or corporation, or conveying any rights or permission to manufacture, use, or sell any patented invention that may in any way be related thereto.

This document contains information affecting the National defense of the United States within the meaning of the Espionage Laws, Title 18, U.S.C., Sections 793 and 794. Its transmission or the revelation of its contents in any manner to an unauthorized person is prohibited by law.

Qualified requesters may obtain copies of this report from the Armed Services Technical Information Agency, (ASTIA), Arlington Hall Station, Arlington 12, Virginia.

Copies of this report should not be returned to the Aeronautical Systems Division unless return is required by security considerations, contractual obligations, or notice on a specific document.

FOREWORD

This report was prepared by the Cook Research Laboratories, Cook Technological Center, a Division of the Cook Electric Company, Chicago, Illinois, in compliance with Contract No. AF33(616)-8459, Project No. 6065 and Task No. 606505. The Retardation and Recovery Branch, Flight Accessories Laboratory, Aeronautical Systems Division, was the initiating agency with Mr. Reinhold Gross, and subsequently Mr. Charles A. Babish, III, serving as project officers. The work at the Cook Technological Center was under the supervision of Mr. Alton D. Anderson, Director; Mr. L. J. Lorenz, Manager of the Aerospace Technology Section; and Mr. Leland W. Sims, Project Engineer. The work was initiated on 30 June 1961 and completed on 10 August 1962.

Acknowledgements are extended to the following staff members who contributed to the project: Mr. R. C. Fredette, formerly Associate Director, Cook Technological Center, for his guidance in the early phases of the program; Messrs. A. Solarski, P. Minerva and P. Reel for their contribution to the analytical study; Messrs. H. Loellbach and F. Ruprecht for parachute model design and fabrication; Messrs. R. Meyer and R. Brent for their contribution to the CTC Wind Tunnel Program; R. Wolter and P. Hoffman for mechanical design, and DR. J. S. Thele for his willing assistance throughout the program.

The generous assistance and cooperation of personnel at the Government test facilities - AEDC, VKF, and NASA Langley, L.S.T. are also highly appreciated.

This report is classified CONFIDENTIAL because data generated during the program constituted a breakthrough in the supersonic parachute area, indicating that the dissemination of configuration and design characteristics should be limited. Pages 39, 46, 48, 50, 64, 66 and 67 of this report are classified CONFIDENTIAL because they contain such information.

(This Abstract is Unclassified)

ABSTRACT

Analytical studies to determine the characteristics of textile parachute canopies in supersonic flow and associated airflow phenomena are described to the point of completion in this program.

Data derived from the wind tunnel test programs which were conducted using six inch and eight inch parachute models, are discussed. Test Mach numbers covered the range from M = 1.5 to M = 4.65, with approximately 200 test conditions tabulated. The over-all test program discussion describes investigations leading to the evolution of canopy shapes which performed satisfactorily through Mach 4.65.

Force data and high speed Schlieren photographs of numerous test conditions are included to illustrate canopy performance characteristics.

Total canopy porosities of 8 to 18 percent with high roof porosities and low inlet region porosity distributions were studied most intensively.

Canopy shapes consisting of bi-conic, conic, modified guide surface, and conventional ribbon types were investigated.

PUBLICATION REVIEW

Publication of this Technical Documentary Report does not constitute Air Force approval of the report's findings or conclusions. It is published only for the exchange and stimulation of ideas.

FOR THE COMMANDER:

George A. Solt, Jr.
Chief, Retardation and Recovery Branch
Flight Accessories Laboratory

TABLE OF CONTENTS

TABLE OF CONTENTS (cont'd)

TABLE OF CONTENTS (cont'd.)

LIST OF ILLUSTRATIONS

LIST OF ILLUSTRATIONS (Cont'd.)

LIST OF ILLUSTRATIONS (Cont'd.)

LIST OF ILLUSTRATIONS (Cont'd.)

LIST OF TABLES

SECTIONS I AND II

SYMBOLS AND NOMENCLATURE

A_E	Exit or open area ($\lambda_T S_o$)
A_i	Inlet Area
a	Guide surface gore dimension
ϵ	Wake parameter
C_{D_c}	Drag coefficient based on maximum constructed frontal area
C_{D_o}	Drag coefficient based on total cloth area
C_{D_p}	Drag coefficient based on design frontal area
D_e	Outer vent diameter
D'_e	Inner vent diameter
d	Forebody base diameter
d_c	Maximum constructed diameter
d_i	Inlet diameter
d_m	Inflated diameter
d_o	Diameter of flat canopy
d_p	Maximum design diameter
L	Guide surface gore dimension
ℓ	Suspension line length
q	Dynamic pressure
S_i	Inlet cone surface area

SYMBOLS AND NOMENCLATURE
(cont'd.)

S_m	Inflated frontal area
S_o	Total Cloth area
S_p	Maximum design frontal area
S_R	Roof area
x	Centerline distance aft of forebody base
x_t	Distance of wake throat aft of forebody base
$\Delta\alpha$	Angular canopy displacement about point of suspension
λ_i	Inlet cone porosity (percent)
λ_R	Roof porosity (percent)
λ_T	Total canopy porosity (percent) $(\lambda_i S_i + \lambda_R S_R)/S_o$
θ_i	Canopy inlet cone half angle
θ_R	Canopy roof half angle
θ_S	Cone half angle
θ_w	Shock wave angle

Canopy inlet cone - Portion of canopy upstream of maximum diameter

Canopy roof - Portion of canopy downstream of maximum diameter

Canopy Inlet - Most upstream cross-section of canopy (skirt)

SECTION I

STATUS OF PARACHUTE DEVELOPMENT AT SUPERSONIC SPEEDS

A. Introduction

At the time of the initiation of this program, June 30, 1961, a considerable amount of parachute testing had been performed at transonic and supersonic speeds. These test programs were conducted using high speed sleds, wind tunnels, and free flight vehicles. A large amount of data was generated as a result of these programs - such as force measurements, high speed photographs, and Schlieren films. Numerous conventional canopy configurations were employed in these tests with ribbon-type constructions predominating. In this part of the report, a brief background of parachute testing and development will be presented. As a result of analysis of the data derived from the early tests, the basic problems associated with the application of conventional parachute configurations at supersonic speeds were determined and will be discussed. Section I will be devoted to this. Subsequent sections of this report will describe the objectives, procedures and results of this program.

This program was initiated in order to explore the applicability of flexible, self-inflating parachute-like configurations in the Mach number range from M = 1.5 to M = 4.0. The program was basically divided into two separate, concurrent, yet interdependent efforts. These consisted of: (1) a theoretical study, and (2) a wind tunnel test program. The theoretical study had as its objective, the development of a mechanized rigorous theoretical method of prediction of the flow field about a trailing decelerator leading to the determination of the surface properties of the decelerator. The development of such a computer program serves to define the environment surrounding a parachute-like configuration so that a shape which will perform satisfactorily in stability and inflation characteristics at supersonic speeds may be predicted. The effects of a non-uniform forebody wake was also considered in the formulation. The wind tunnel program was initially conceived to be a testing program which verified the results of the theoretical prediction. Due, however, to formulation and computer programming difficulties encountered in the analytical study, this program was unable to provide such predictions consistent with available Government facility wind tunnel testing dates. The prediction of feasible canopy configurations was performed by non-rigorous procedures. These involved the study of Schlieren photographs of early tests, coupled with the application of shocktables and employing an empirical formulation of wake flow properties. This procedure led to the prediction of initial modifications to conventional parachute configurations which were indicated to be required to improve their performance characteristics. Successive testing programs, in conjunction with this procedure, resulted

---

Manuscript released by the author, November 29, 1962, for publication as an ASD Technical Documentary Report.

in the gradual improvement of canopy performance and led to the establishment of the apparently significant phenomena which defines the criteria for the determination of satisfactory parachute performance. Unconventional parachute canopy designs which successfully endured tests at Mach numbers through M = 4.65 were developed in this program. The success of these canopies in the final (Phase II) testing program resulted in security classification of the designs of these configurations.

B. Basic Problems Associated with Supersonic Operation of Conventional Parachute Configurations

As discussed in Subsection A above, numerous test programs have been accomplished during the investigation of the performance of conventional parachutes at supersonic speeds. However, such configurations have been found to perform poorly in the supersonic speed range, particularly for Mach numbers above 1.8 to 2.0. Specifications for a particular decelerator configuration require, in general, that the ratio of drag effectiveness to system weight be a maximum, and further that the volumetric requirements of the system be minimized. When self-inflating parachute configurations properly operate, the system drag to weight ratio is lower than other decelerator types such as inflatable devices. For example, an inflatable drag device, whether spherical or conical in shape represents a significantly greater total material surface area (hence weight) for a given drag area. A drag coefficient of approximately 0.2 based upon total cloth area is typical for an inflatable device (not including inflation aids, etc.,) whereas parachute configurations have achieved drag coefficients approaching 1.0 based upon cloth area in the Mach number range for which efficient operation of the conventional parachute is realized. However, for Mach numbers above 1.8 to 2.0, the conventional parachute drag efficiency has been found generally to decrease rapidly with increasing Mach number. In fact, the drag effectiveness of conventional parachutes has been found to be in the order of 1/6 of the expected value at a Mach number of 3.5. This would infer a cross-over in drag efficiency of an inflatable device, for illustration, as compared to a conventional parachute (i.e., previously employed configurations) for Mach numbers in excess of this value.

The following paragraphs of this section will describe the characteristics of conventional parachute configurations when operating in the supersonic range and contribute to their reducing efficiency in an increasing Mach number environment.

1. Inflation Characteristics

Analysis of schlieren movies of conventional parachute configurations has revealed a typical behavior in the supersonic range above

Mach 1.8 - 2.0. This behavior is characterized by a rather violent breathing tendency, or alternate inflation and deflation cycle, which occurs at very high frequencies (the order of 50 to 100 cycles per second). This phenomena is illustrated in Figure I-1 for a 4.0 foot diameter flat circular ribbon parachute with a 19 percent porosity. This film sequence was taken during a wind tunnel test of this configuration at a Mach number of 3.5, during the conduct of a series of tests in the NASA, Cleveland, Ohio, 10 feet by 10 feet section by these Laboratories under Contract AF 33(616)-3346. During this program, both ribbon and guide surface type parachutes were tested in the Mach number range from M = 2.0 to 3.5. A wide number of variations of both types of parachutes was employed. For example, the porosity of the ribbon-type parachutes was varied from 5 to 30 percent. Porosity distributions were also considered in that low skirt porosity with large vent porosity as well as low vent porosity and high skirt porosities were employed in the various configurations. In addition, the tests were conducted both with and without a forebody. In all instances, parachute performances from the standpoint of inflation stability were as mentioned above with high frequency breathing evident.

In addition to the ribbon parachutes, various types of Guide Surface Ribless canopies were also tested. The extremes in breathing are not as pronounced as for the ribbon; however, overinflation of the roof and indentation of the guide surfaces resulted in nearly immediate failure of the canopy at the intersection of the roof and guide surface panels.

In order to evaluate whether this phenomena was associated with the flexible materials of which these configurations are constructed or to an unstable flow field ahead of the canopy, a further test program was conducted employing rigid canopies constructed of steel and simulating the inflated shape of a typical ribbon canopy. These tests were conducted with and without simulated lines, various numbers of lines, and lengths of lines. Based upon the results of these tests, the existence of unsteady flow conditions, and Mach number effects was confirmed. A discussion of these tests, and the preceding fabric model tests along with an analysis of the various associated flow regimes is given in Reference 1. As a result of this analysis it appeared that the nature of the flow regime and shock wave structure ahead of the canopy is significantly dependent upon the forebody wake characteristics, and that parachute configurations are greatly affected by the interaction of the canopy shock wave with velocity gradients existing in the wake of a forebody. Several typical flow types, which are associated with this interaction, are discussed in Reference 1.

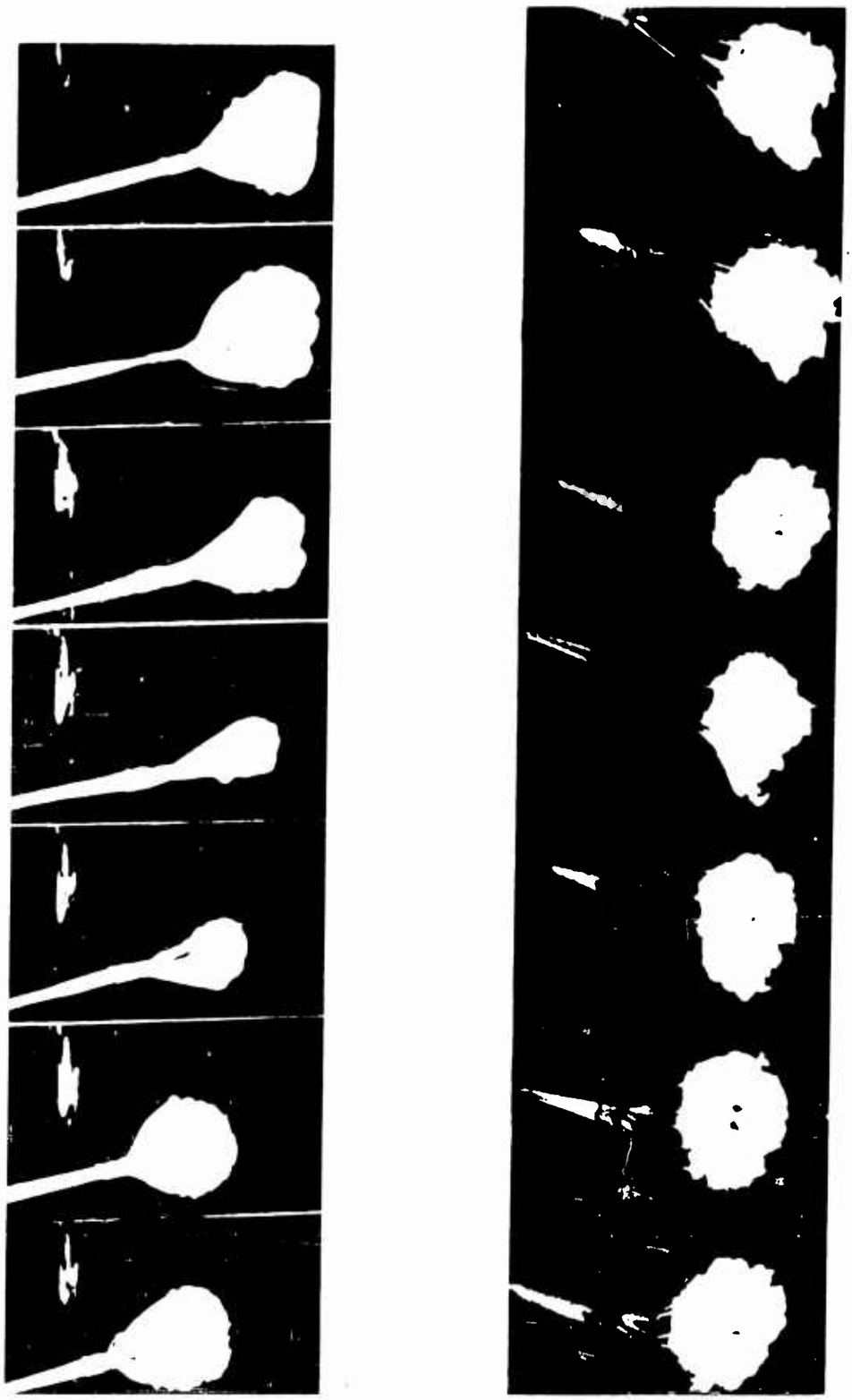

FLAT CIRCULAR RIBBON GUIDE SURFACE RIBLESS

Figure I-1. Characteristics of Two Parachutes at M = 3.5

In later tests, a canopy configuration which was tested in the Cook Technological Center wind tunnel facility (under Contract AF 33(616)-5507), demonstrated that certain configurational characteristics may have a strong effect in suppressing the unfavorable interaction effects which appear to be associated with a parachute configuration immersed in a non-uniform flow field provided by an upstream forebody. The canopy of this configuration consisted of a 15^{o} (half angle) conical frustrum fabricated of a non-porous material with a vent which provided an exit to inlet area ratio of 0.29. A variation of this configuration employing a 45^{o} conical frustrum was also tested. Very high drag coefficients (0.45 and 0.96, respectively) based upon cloth area, were realized with these models at M = 2. Extremely high inflation characteristics were also evident from the schlieren films (Figure 1-2) and very little canopy breathing was evident. However, these canopies exhibited an instability about the point of suspension by oscillation angles up to nearly 20^{o}. In spite of the high oscillation angles, the canopies remained well inflated although subjected to severe disturbances which were associated with the high angular excursions. The instability of these configurations was attributed to the ring airfoil-type lift inherent in this canopy shape. A stabilizing surface extending forward of the maximum diameter had been added to the 45^{o} conical canopy. However, the high inflation tendencies of this canopy resulted in material stretch of this surface to such an extent that it was ineffective in contributing stabilization. It was this basic configuration, along with the indicated necessary modifications which served to establish some of the configurational details of the shapes which were selected for the first testing series in this program.

2. Stability Characteristics

Analysis of the data from early tests indicate that the stability of a parachute canopy about the point of suspension varies directly with porosity. Tests in the present program indicate this trend also. However, it is apparent that the configurational details of the canopy have a significant effect also. An illustration of this, of course, is the guide surface type canopy which is constructed generally with a low porosity material yet, in the subsonic and transonic ranges of Mach numbers, exhibits extreme stability. The contribution of the forward guide surface is considered significant in the attainment of this stability. The flat roof of this configuration contributes negative lift when sufficient porosity allows flow through the canopy. The forward guide surfaces, which are inflated internally with near-stagnation pressures, serve as a stabilizing cone-frustrum and contribute the necessary compensating positive lift for stability. The basic guide surface configuration, along with modifications, served also to provide some of the

Figure I-2 Characteristics of a 15° Conical Parachute, AE/Ai = 0.29, M = 2.0

shapes investigated in the first testing series of this program. These configurations will be discussed in Section II.

3. Shock Wave-Boundary Layer Interaction

Analysis of Schlieren photographs of conventional parachute configurations at supersonic speeds has indicated significant shock wave-suspension line boundary layer interactions. It has appeared from observation of parachute test data, that for those configurations which exhibited low or marginal inflation characteristics that the effect of the shock wave-boundary layer interaction has a significant effect on the inflation stability of the canopy, and has appeared to be somewhat associated with cyclic canopy collapse. In other instances (Figure I-2) it has appeared that this phenomenon does not have a significant effect on the parachute performance. This latter example, of course, applied to a canopy with strong inflation properties as previously described.

This phenomenon has been most evident in those instances where the suspension lines become normal, or near normal to the canopy shock wave. This condition is readily attained in the case of a canopy which is unstable about the point of suspension, allowing excursion angles of the canopy such that the lines approach normalcy to the shock wave, such as illustrated in Figure I-2. This is possible, since examination of Schlieren films appears to indicate that the canopy shock wave translates normal to the wake axis, an amount approximately equal to the width of the forebody wake. Very small rotation of the shock pattern about its vertex was evident. For those canopy types which sustain a strong shock, very small oscillation angles are needed to attain a near normal angle between the suspension lines and the shock wave.

Since separation of a boundary layer by shock wave interaction is associated with a critical pressure ratio (as a function of Mach number) across the shock in the case of a shock wave incident to a flat plate (Reference 2), it is expected that this will be true also for a shock wave intersection with a three dimensional body. The Basic Test program was organized to establish the effects of shock wave interaction with a boundary layer on a cylinder as a function of shock wave angle, shock wave-cylinder intersection angle, Reynolds number and Mach number. The Basic Test program will be discussed in Section II.

C. Indications of Desirable Canopy Geometry Based Upon Early Tests

Reference was made in Subsection B of Section I to a conical canopy

configuration, illustrated in Figure I-2 which had exhibited strong inflation tendencies as well as inflation stability at Mach 2. In the design of this canopy, three features differed extremely from conventional configurations previously applied in the supersonic speed range. These are (1) a much lower exit to inlet area ratio had been employed, (2) a non-porous material was used in the vicinity of the inlet, or skirt region of the canopy, and (3) a much lower total porosity was employed.

The total porosity of a parachute is defined as the open area divided by the total cloth area. Thus, the open area consists of the space between ribbons, as in a ribbon canopy construction and open spaces in a woven fabric which allow the passage of air. In the case of a canopy such as described above which, except for the open vent, is constructed of non-porous material, the over-all porosity was considered as the area of the vent divided by the total area (which includes the vent). This definition will be at variance to some degree with porosity which is expressed as a function of permeability. The latter property of cloth is determined by measuring the rate of flow of air under specified conditions through a fabric. The normally small spaces between fibers will prescribe somewhat different flow conditions than flow through a large vent. However, in all calculations performed in this program to determine the open area, a strictly geometric interpretation has been made. This "open" area is used to determine both total porosity and "exit" area.

Accordingly, the exit to inlet area ratio of the conical canopy discussed above is 0.29, and the total geometric porosity is 9.5 percent. In contrast to this, a conventional ribbon parachute is constructed using a geometric porosity of 15 to 28 percent. If the canopy were constructed in a hemispherical shape, the exit to inlet area ratio would be 0.30 to 0.56, assuming full inflation. In such configurations, the porosity at the skirt is normally greater than that near the vent, making this area less able to sustain the near-stagnation pressures expected in the canopy inlet region. Strong inflation characteristics in the skirt, or inlet regions appear to be essential to provide an outward force at least equal to the inward components of the suspension line loads.

As discussed previously, the stability of a given parachute configuration about the point of suspension appears to vary inversely with porosity. In the case of the Guide Surface configuration, however, the total porosity is low and the stability is good, although structural damage resulted in tests of this configuration at supersonic speeds. The stabilizing effect of the forward guide surface is apparent, although the (conventionally employed) angle of this surface appeared to be too great.

The apparent requirements for low over-all porosity, coupled with the use of stabilizing surfaces appeared essential. A study of the effects of (1) porosity distributions in producing good inflation, (2) stabilizing surface angles and lengths for proper inflation and stability, and (3) the over-all geometric shape of the canopy for optimum drag to weight ratio appeared to prescribe the direction of effort in the Phase I parachute test program.

D. Effects of Forebody Wake on Supersonic Parachute Operation

The importance of the effects of the wake of a forebody on a trailing parachute configuration have been recognized. In Reference 1, calculations were performed to determine the effects of the non-uniform flow field produced by the wake on a shock wave ahead of a blunt trailing decelerator. Significant shock diffraction was verified by employing empirical wake theory for the determination of the wake flow ahead of the canopy and shock wave. Diffraction of the typical near-normal shock wave, which would exist under free stream conditions ahead of a blunt body such as an inflated parachute, into a conical type shock was indicated by these calculations. This has been confirmed by numerous Schlieren photographs of parachutes operating supersonically in a forebody wake. Furthermore, the dependence upon the wake of a forebody for satisfactory parachute operation at supersonic speeds has also been indicated by past tests and applications.

Examination of a Phase Ia model configuration under test will be used as an illustration to establish the flow field ahead of a canopy and associated shock wave. To predict the flow field in the wake, an empirical wake theory will be employed. Drag predictions provided by this procedure on trailing decelerators have been in good agreement with test data.

The velocity, V_w, across the wake as given in Reference 1:

$$V_w = V_\infty \left\{ 1 - \left[1 - \frac{V_{w_1}}{V_\infty} \right] \left[1 - \frac{y}{b} \right]^{3/2} \right\}^2$$

where:

y = the distance from the wake centerline

b = the wake half width

V_∞ = the free stream velocity

$\frac{V_{w_1}}{V_\infty}$ = the wake centerline velocity decrement ratio which is

determined by the expression

$$V_{w_1}/V_\infty = \frac{C}{(x/d - x_t/d)^{2/3} + C}$$

where the constant C is based upon test data. (0.7 used in this report)

Figure I-3 is a trace from a Schlieren photograph of a Phase Ia configuration(discussed in Section II), which was located at an x/d = 10, at a test Mach number of 2.13. Various wake Mach numbers are indicated in the wake ahead of the shock wave and flow deviations through the shock for these Mach numbers and local shock wave angles are also shown. A wake width equal to tne forebody diameter is assumed. It may be seen from Figure I-3 that a subsonic outflow, resulting from the deflection through the shock has a very favorable effect in maintaining the canopy fully inflated. Canopy inlet angles, below the horizontal, approaching 25 degrees will provide a positive "angle of attack" of the canopy inlet to the local flow direction. It is apparent from Figure I-3 that the flow deviation angle based upon the free stream Mach number is sufficient to spread the wake to near the skirt of the canopy. This is further indicated to be required, since the pressure ratio across the normal portion of the shock on the centerline is greater (for the wake centerline Mach number) than the pressure ratio across the oblique shock at the free stream Mach number. Divergence of the wake flow is further encouraged by the high (near stagnation) pressures existing in the canopy. Since wake effects of the parachute confluence point are not considered, it is expected that the wake Mach numbers near the centerline are lower than predicted giving a lower than predicted pressure ratio across the shock at the centerline such that a near constant pressure distribution is realized throughout the diverged wake ahead of the canopy, satisfying pressure boundary requirements.

In the event that the parachute diameter ratio to the wake width were significantly greater, and assuming a similar shock geometry, the flow deviation through the shock wave would not be adequate to spread the wake (if the shock standoff distance remained the same) to the skirt of the canopy, and the flow aft of the shock at greater distances from the wake centerline would be supersonic. A lip shock would then be produced which may, as past tests indicate, further spread the wake upon intersecting the boundary layer until the entire canopy is in subsonic flow. This would possibly lead to a fluctuating flow condition, and reduction in parachute performance. In consideration of this, and other associated phenomena, it is expected that a practical parachute to forebody diameter ratio limit may possibly exist

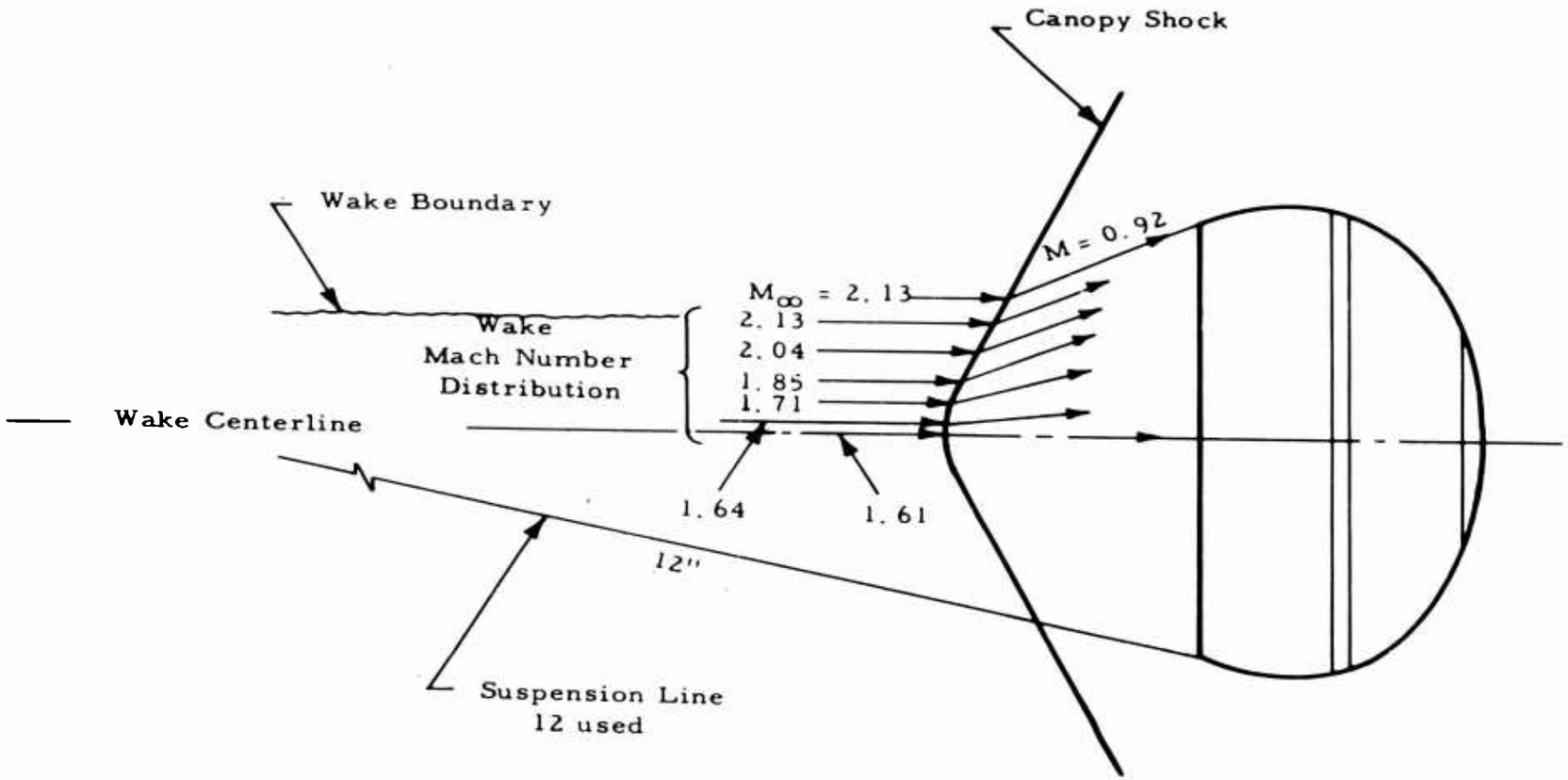

Figure I-3. Flow Field and Shock Configuration Phase Ia Test Model C-6a, $M_\infty = 2.13$

for efficient supersonic parachute operation at a prescribed supersonic Mach number.

E. Purpose and Scope of This Program

As pointed out previously, a number of applied research programs have been conducted to study and to extend the operational capabilities of textile parachute canopies into the supersonic speed regime. Results of these programs revealed problem areas which required further study in order to evolve satisfactory concepts of self-inflating aerodynamic decelerators for supersonic speed applications.

This program was planned to consist of an exclusive analysis, wind tunnel testing, data documentation, and reporting of phenomena associated with the operation of flexible type self-inflating aerodynamic decelerators operating within a Mach number of range of 1.5 to 4.0.

The analytical study was to consist of an application of fluid flow equations to configurations consisting of parachute-like shapes with flow properties surrounding these configurations described by means of the integration of established fluid flow equations. Mechanization of all computations was to be maximized, and correlation of derived fluid flow properties with wind tunnel observations was to serve (1) to establish the adequecy of developed techniques, or (2) to serve as a basis for modification of techniques, so as to produce the required degree of agreement.

The ultimate goal of the analytical approach was to evolve an aerodynamic theory which would serve to both predict and explain the test results, and lead to a means of prediction of parachute canopy geometry for satisfactory performance at supersonic speeds.

An exploratory wind tunnel program was designed to be conducted in order to supplement and verify the analytical study.

In subsequent sections of this report, the analytical procedures and exploratory test programs will be described.

SECTION II

EXPERIMENTAL PROGRAM

Three test phases were completed in this program. The Phase I test program was conducted in the Cook Technological Center wind tunnel and the AEDC-VKF, Tunnel A, Tullahoma, Tennessee. The interim test program (Phase Ia) was conducted in the Cook Technological Center wind tunnel facility, and the third program (Phase II) was conducted in the Langley Research Center Large Supersonic Tunnel, Langley Field, Virginia. In the three phase test program, tests were conducted over a Mach number range of from 1.5 to 4.65.

In order to make maximum use of available testing time in Government wind tunnel facilities, the first testing program was required to be conducted earlier in the over-all program than initially planned. As a result, this program was required to be of a development nature, and model designs were accordingly required to be determined by general trends in geometric shapes which were indicated to be favorable in earlier testing programs, as discussed in Section I, Parts C and D.

A. Phase I Test Program

1. Phase I Test Facilities

The first test phase of this program was conducted at the Cook Technological wind tunnel facility and the Arnold Engineering Development Center, Tullahoma, Tennessee. The AEDC tests were conducted in the 40 inch x 40 inch tunnel A test section which is capable of a Mach number range of 1.5 to 5. A description of these test facilities is given in Appendices I and II.

2. Basic Test Program

a. General

As a result of the study of various Schlieren photographs of past tests, shock wave-suspension line boundary layer interaction appeared to be evident as discussed in Section I. A considerable amount of data appears to be available in the literature on two-dimensional shock wave-boundary layer interaction. Pressure ratios associated with separation of the boundary layer on a flat plate are fairly well established (Ref. 2), and a certain degree of correlation of this data is associated with parachute

data (Ref. 1).

In order to establish correlation of published two-dimensional data with three-dimensional characteristics, the basic test program of this contract was conceived; it was decided to employ rigid models. Since, as discussed above, critical interaction conditions appear to exist when the shock wave and suspension line are approximately normal to each other, appropriate test items appeared to consist of a shock generator to provide a nearly normal shock, and a rod to simulate a line. An adjustment mechanism would provide for a variation of angle between the shock wave and the rod, by variation of the rod angle of attack. The effect of Reynolds number would be determined by an axial position adjustment of the length of the rod ahead of the shock wave or by variation of tunnel total pressure. An apparently appropriate configurational design was conceived for preliminary tests in the CTC wind tunnel facility. This is shown in Figure II-1. The shock generator employed in this test configuration consisted of a solid choked annular ring allowing flow through the center of the ring, and also allowing freedom of motion of the rod inserted through it and penetrating the shock generated by the choked annulus.

b. Cook Technological Center Basic Test Program

These tests were conducted by varying the rod angle every 2 degrees from 0° to 22°, and at each angular position a Schlieren photograph was taken. Table II-1 describes the test schedule. This procedure was repeated providing three different rod lengths ahead of the shock wave. Analysis of the Schlieren photographs indicated that precise measurements, the nature of which were desired in these tests, could not be performed with the test configuration employed. An inherently unstable flow condition had been encountered since upon establishment of a normal shock in front of the annulus, and resultant separation of the boundary layer (Figure II-2) the separated flow is not stagnated on the blunt nose (unlike separation ahead of a blunt body by means of a protruding spike). Once separation is induced, the separated flow must feed through the annulus, thereby establishing the need for a new normal shock on the axis to be established to maintain mass flow requirements through the annulus. This apparently occurs at a high frequency, and the camera speeds employed were not adequate to stop this high frequency phenomenon. The tests indicated that in order to isolate the phenomena of interest, the rod-shock wave intersection must be outside of

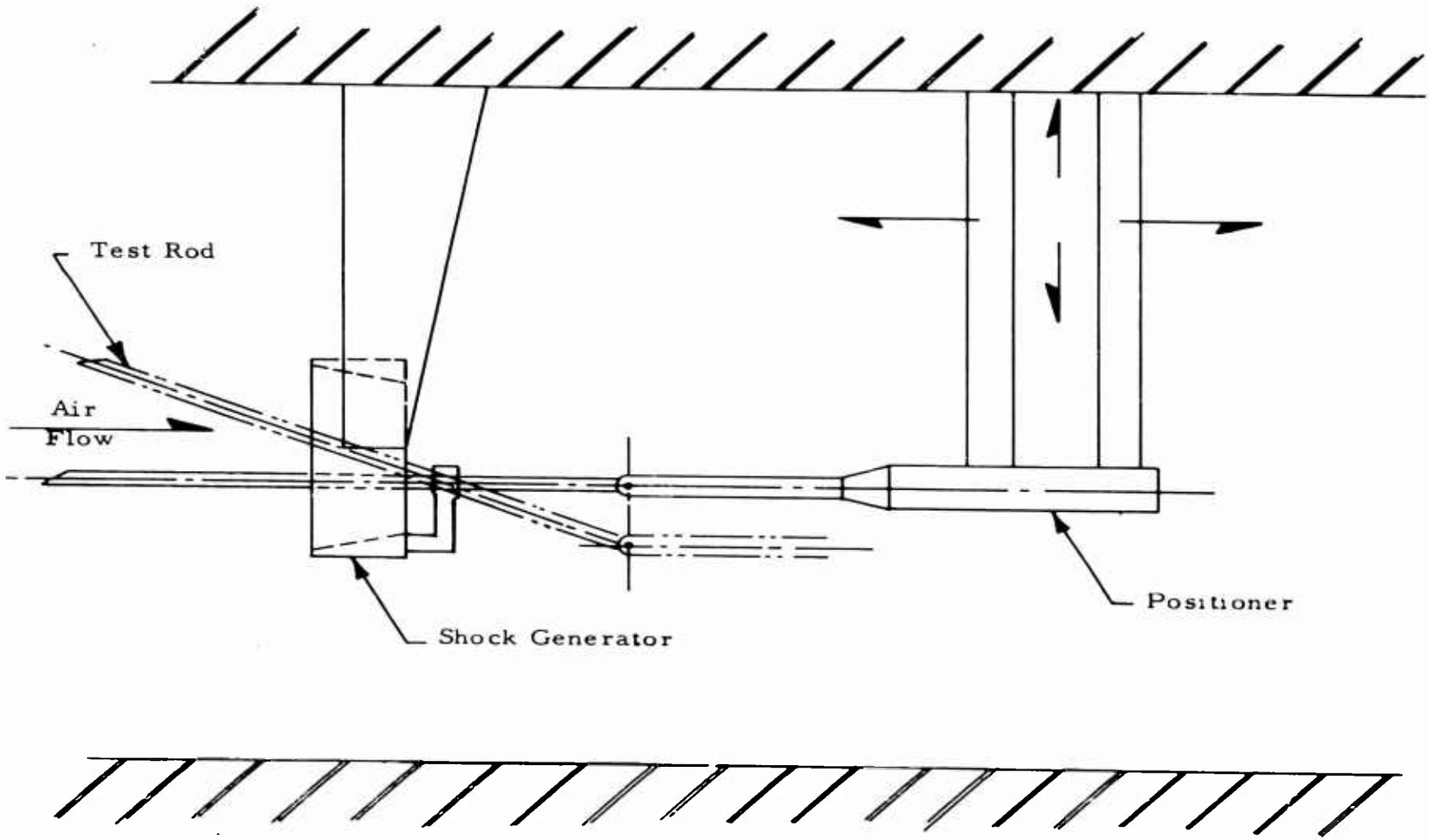

Figure II-1. Phase I Basic Test Installation - CTC Facility

TABLE II-1

PHASE I BASIC TEST PROGRAM

COOK TECHNOLOGICAL CENTER WIND TUNNEL

Run	Mach No.	α_p	θ_w	l_p/d_i
1	2.0	0-22°	90°	1
		$\alpha_{p_{cr}}$ (1)		
	2.0	0-22°	90°	1/2
		$\alpha_{p_{cr}}$ (1)		
	2.0	0-22°	90°	2
		(1)		
2	2.0	$\alpha_{p_{cr}}$	90°	1
		(1)		
3	2.0	$\alpha_{p_{cr}}$	90°	1
		(1)		
4	2.0	$\alpha_{p_{cr}}$	50°	1
		(1)		
5	2.0	$\alpha_{p_{cr}}$	$\theta_{w_{cr}}$ (1) ±5°	1
	2.0	$\alpha_{p_{cr}}$ (1)	$\theta_{w_{cr}}$ (1) ±5°	1/2
	2.0	$\alpha_{p_{cr}}$ (1)	$\theta_{w_{cr}}$ (1) ±5°	2

(1) Inception of boundary layer separation

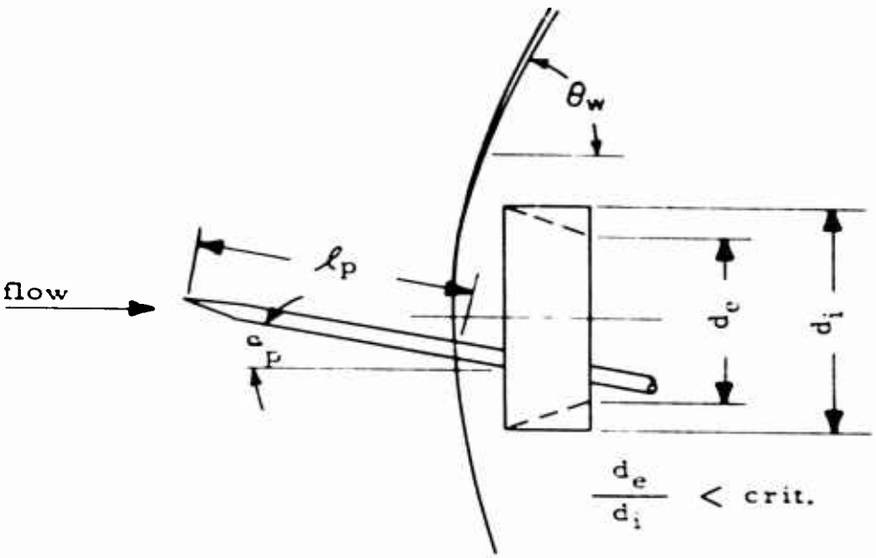

Illustration of Symbols

Figure II-2 Typical Schlieren Photograph, Phase I Basic Test, CTC Wind Tunnel. Film Speed: 24 fps, M = 2.1, $\alpha = 8^{\circ}$

the ring, so as to be unaffected by the downstream flow through the annulus. In anticipation of a more thorough and detailed study, the test method was modified for the basic test phase in the AEDC Tunnel A. This test program and associated equipment are discussed below.

c. AEDC Basic Test Program

In Figure II-3 is shown the test installation in the AEDC Tunnel A, where the investigation of shock wave-boundary layer interaction studies were performed as part of the Phase I test program.

A remotely controlled actuator which is capable of limited transverse and angular movement, to which the rod is attached, coupled with the AEDC Tunnel A positioner to which the shock generator is attached, provides a system which is capable of producing relative variation in two linear dimensions and one angular (pitch) movement for the rod mounted to the actuator, and the shock generator which is mounted to the axial positioner.

This investigation was conducted over a Mach number range of from M = 1.5 to M = 3, with variation of Reynolds number in some cases. The test program is described in Table II-2. In Figure II-4 is shown the shadowgraph pictures of the shock wave produced by the shock generator. These photographs were made by focusing the Schlieren system on the rear wind tunnel window. Traces of these shock wave configurations were made during wind tunnel test runs which were performed during Schlieren system checkout. Some considerable degree of difficulty with the Tunnel A Schlieren system was encountered and the shock wave sketches above were made in order to save tunnel running time in accomplishing basic tests. The test rod (Figure II-3) is equippped with two sets of four holes each. The sets are located an inch apart, with holes in each set located at 90^{o} intervals around the rod and in a plane perpendicular to the rod axis. From these holes, pressure lines were run through the rod and axial positioner hub to the outside of the tunnel. Static pressure measurements were thereby made possible at desired rod positions. The rod was positioned such that the shock wave location would be intermediate to the two sets of static orifices. Since the shock wave position could not be adequately determined theoretically, the shadowgraphs described above were used. Accordingly, the coordinates of three points on the shock wave

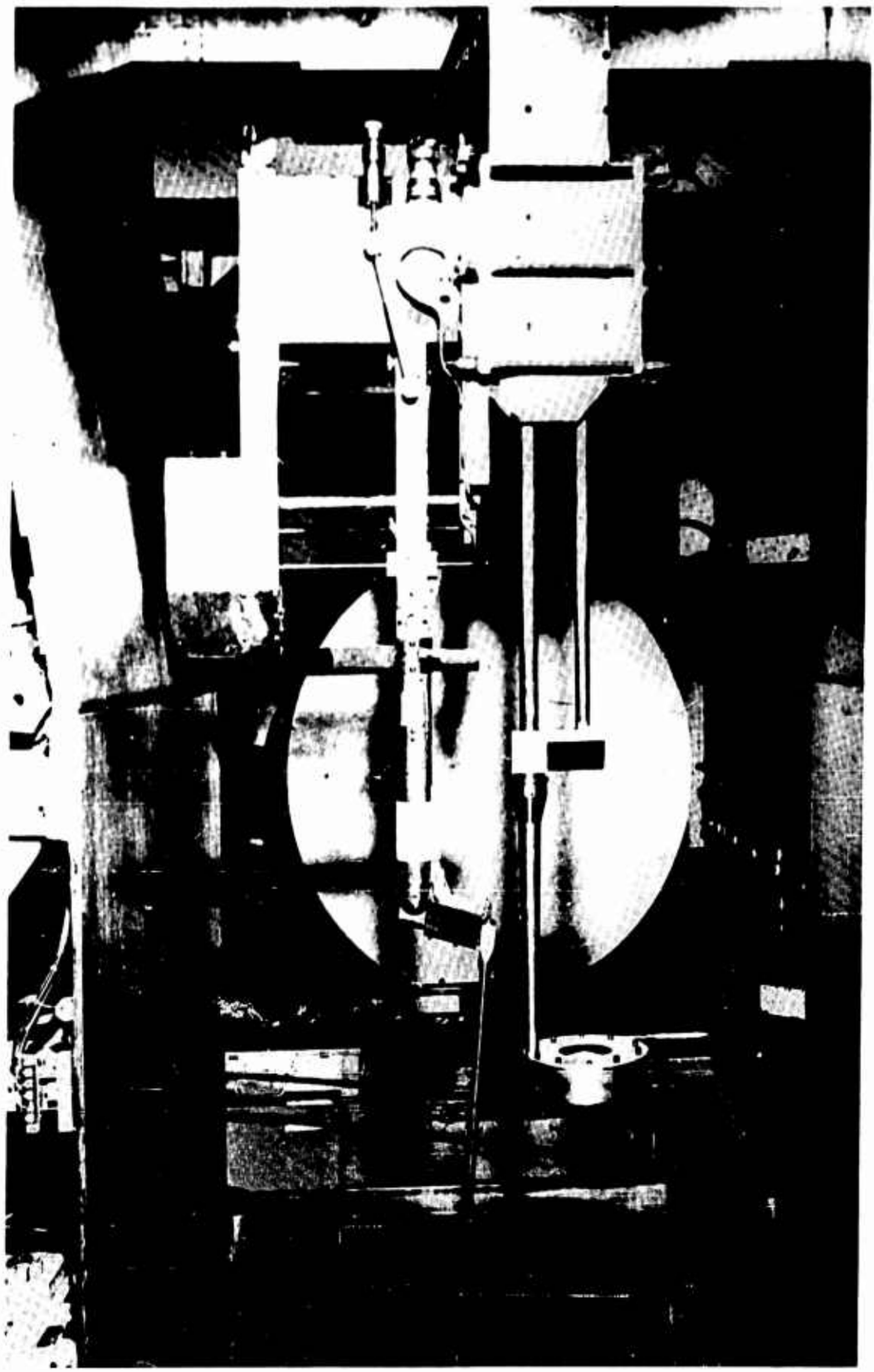

Figure II-3. Phase I Basic Test Installation

TABLE II-2

PHASE I BASIC TEST PROGRAM

TUNNEL A, VKF, AEDC

MACH NO.	REYNOLDS NO.	ROD POSITION	REMARKS
2.0	Mean Value	P_1 (1)	Rod angle of attack sweep. Observation of flow and Schlieren photo coverage. Determination of rod critical angle and limits due to hysteresis effects. Record all pressures at angles of ±2°, 0°, 8°, and 16°.
		P_1	Pressure distribution and Schlieren photo coverage with rod angle setting equivalent to lower critical value.
		P_2 (2)	Same as above.
		P_3 (2)	Same as above.
		P_1	Pressure distribution and Schlieren photo coverage with rod angle setting equivalent to lower critical value plus 1/2 incremental critical range.
		P_2	Same as above.
		P_3	Same as above.
		P_1	Pressure distribution and Schlieren photo coverage with rod angle setting equivalent to lower critical value plus the whole incremental critical range.
		P_2	Same as above.
		P_3	Same as above.
		P_1	Pressure distribution and Schlieren photo coverage with rod angle setting equivalent to upper critical value plus 1/2 incremental critical range.
		P_2	Same as above.
		P_3	Same as above.
	Maximum Value	P_1	Initial rod angle setting at critical value determined for mean Reynolds No. case. Angle sweep within critical angle limits established previously at mean Reynolds No. case. Observation of flow and Schlieren photo coverage to determine absolute critical angle at this maximum Reynolds No. condition.
		P_1	Pressure distribution and Schlieren photo coverage with rod angle setting equivalent to critical value established from the immediately preceding case.
		P_2	Same as above.
		P_3	Same as above.
	Minimum Value	P_1	Initial rod angle setting at critical value determined for mean Reynolds No. case. Angle sweep within critical angle limits established previously at mean Reynolds No. Observation of flow and Schlieren photo coverage to determine absolute critical angle at this minimum Reynolds No. condition.
		P_1	Pressure distribution and Schlieren photo coverage with rod angle setting equivalent to critical value established from the immediately preceding case.
		P_2	Same as above.
		P_3	Same as above.
1.5	Mean Value	P_1	Rod angle of attack sweep. Observation of flow and Schlieren photo coverage. Determination of rod critical angle and limits due to hysteresis effects. Record all pressures at angles of ±2°, 0°, 8°, and 16°.
		P_1	Pressure distribution and Schlieren photo coverage with rod angle setting equivalent to lower critical value.
		P_2	Same as above.
		P_3	Same as above.
		P_1	Pressure distribution and Schlieren photo coverage with rod angle setting equivalent to lower critical value plus 1/2 incremental critical range.
		P_2	Same as above.
		P_3	Same as above.
		P_1	Pressure distribution and Schlieren photo coverage with rod angle setting equivalent to lower critical value plus the whole incremental critical range.
		P_2	Same as above.
		P_3	Same as above.
3.0	Mean Value	P_1	Rod angle of attack sweep. Observation of flow and Schlieren photo coverage. Determination of rod critical angle and limits due to hysteresis effects. Record all pressures at angles of ±2°, 0°, 8°, and 16°.
		P_1	Pressure distribution and Schlieren photo coverage with rod angle setting equivalent to lower critical value.
		P_2	Same as above.
		P_3	Same as above.
		P_1	Pressure distribution and Schlieren photo coverage with rod angle setting equivalent to lower critical value plus 1/2 incremental critical range.
		P_2	Same as above.
		P_3	Same as above.
		P_1	Pressure distribution and Schlieren photo coverage with rod angle setting equivalent to lower critical value plus the whole incremental critical range.
		P_2	Same as above.
		P_3	Same as above.

(1) Rod positioned so that shock wave is at midpoint of space between rows of pressure taps.

(2) Alternate rod positions for pressure surveys.

M = 1.5 M = 2 M - 3

Figure II-4. Typical Shock Configurations Phase I Basic Tests

(at which three local shock wave angles were measured) were determined relative to the control counts on the actuator and on the tunnel axial positioner. On the basis of these initial positions, actuation mechanism positions were then determined so as to provide angular variation of the rod relative to the shock wave, while maintaining the shock wave intermediate to the two sets of static pressure taps (providing a constant rod length ahead of the shock wave). It may be added here that since the rod actuation mechanism was not capable of axial movement, movement of the rod in an axial direction relative to the shock wave was accomplished by axial movement of the shock generator (provided by the tunnel axial positioner on which it was mounted), resulting in axial translation of the shock wave.

The tests as outlined in Table II-2 were conducted in subsequent tunnel A runs. The correlation of rod angle, inception of boundary layer separation on the rod and associated pressure measurements before and after separation were dependent upon the inspection of the corresponding still Schlieren films and Schlieren movies. Due to the difficulty with the tunnel Schlieren system, a negligible number of Schlieren pictures were provided. Consequently the tests contributed little to the over-all program. Associated with the conduct of the tests described above, another phenomenon was made apparent. At some points on the shock wave where tests were being conducted through large ranges of rod angular variation, it was noted that for large negative angles of attack and after boundary layer separation on the rod had been initiated, the entire shock wave separated to the forward end of the rod. An explanation of this phenomenon is not possible at this time since it does not appear to be associated with a centerline disturbance ahead of the shock generator, since it occurred at various rod end locations relative to the centerline of the shock generator.

These tests were immediately followed by the first parachute test program.

3. Parachute Test Program

a. Wind Tunnel Test Installation and Deployment Method

All test models in the Phase I program were tested behind a bi-conic forebody (Figure II-5) which was strut mounted to the tunnel side wall. A spring actuated deployment mechanism was

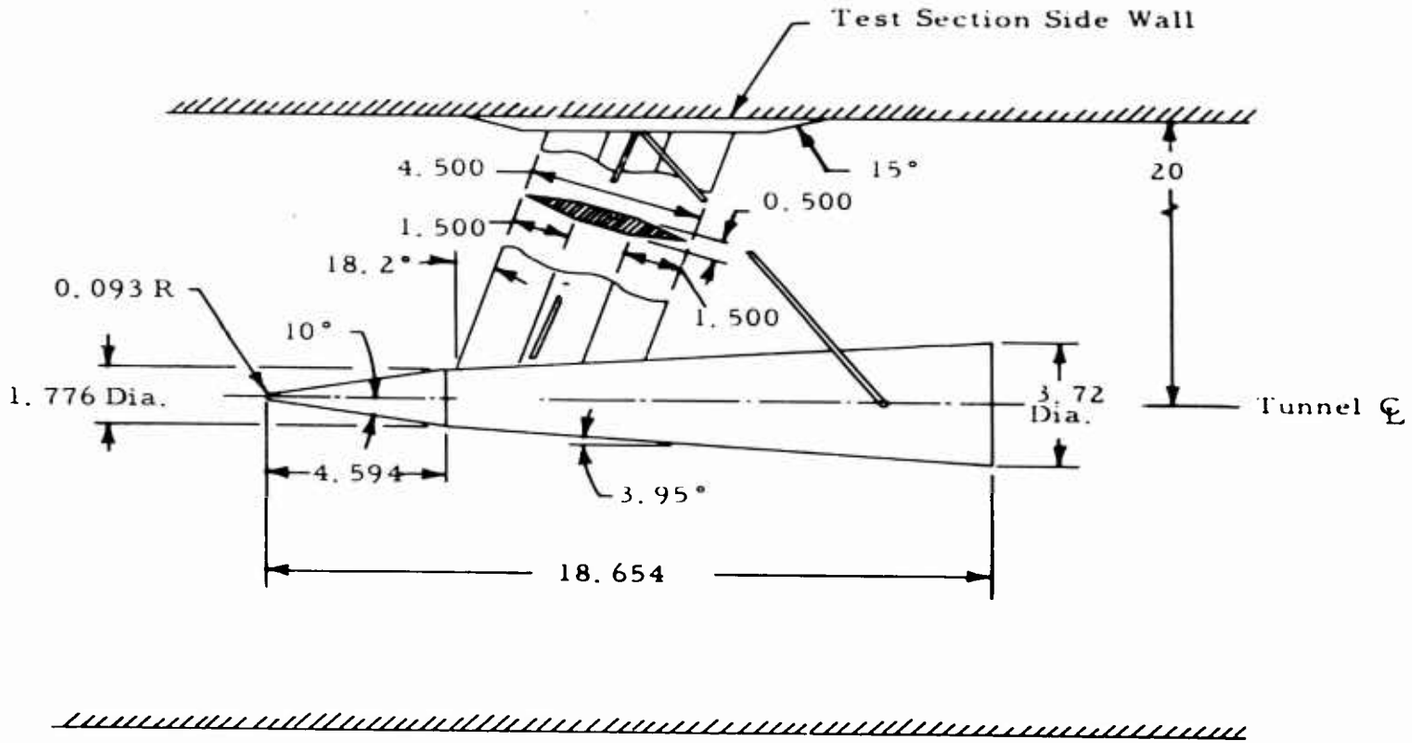

Figure II-5 Phase I Forebody, Parachute Tests

used to deploy the models when the desired tunnel flow conditions were attained. The deployment mechanism was actuated by an external mechanical pull-cable control. Provisions were also made for the possible deployment of two models during a tunnel run. One model (without provision for drag measurements) was to be stowed in a rip-cover on the trailing edge of the strut, and mounted to the forebody base by means of a yoke and ball release connection. An external pull cord was rigged so as to run from the rip-cover to outside the tunnel. By pulling this cord, the first parachute would be deployed upon removing the rip-cover.

Provision was made for the first parachute to be jettisoned downstream at the conclusion of the test by a release mechanism triggered by an initial displacement of the cable; further displacement of the cable actuated the deployment of the second parachute model stowed in the forebody. Due to possible complications to the tunnel operation caused by a jettisoned parachute, only the spring actuated deployment system was used. Drag measurements were provided by a strain gauge mounted drag link installed inside the forebody whose circuit was connected to the tunnel facility instrumentation equipment. Force measurements were recorded on Visicorder tape. Figure II-6 is a photograph of the parachute test installation used in the Phase I tests.

b. Test Model Descriptions

In the first series of parachute tests, a study was conducted involving five modified guide surface type canopies, five conical type canopies, a hemisflo canopy, and a flat circular ribbon canopy with the capability of remote variation of reefing area ratio. This selection conforms with the trends indicated in Section I-D and with contractual requirements. Variations in the basic gore designs of the guide surface types were accomplished in order to provide different inlet to maximum projected diameter ratios as well as inlet angles, the latter being based upon analyses similar to that discussed in Section I-D. Specifications for the various configurations tested in this program are shown in Table II-3. Sketches and material specifications of these configurations are shown in Figures II-7, II-8, and II-9, and Table II-4.

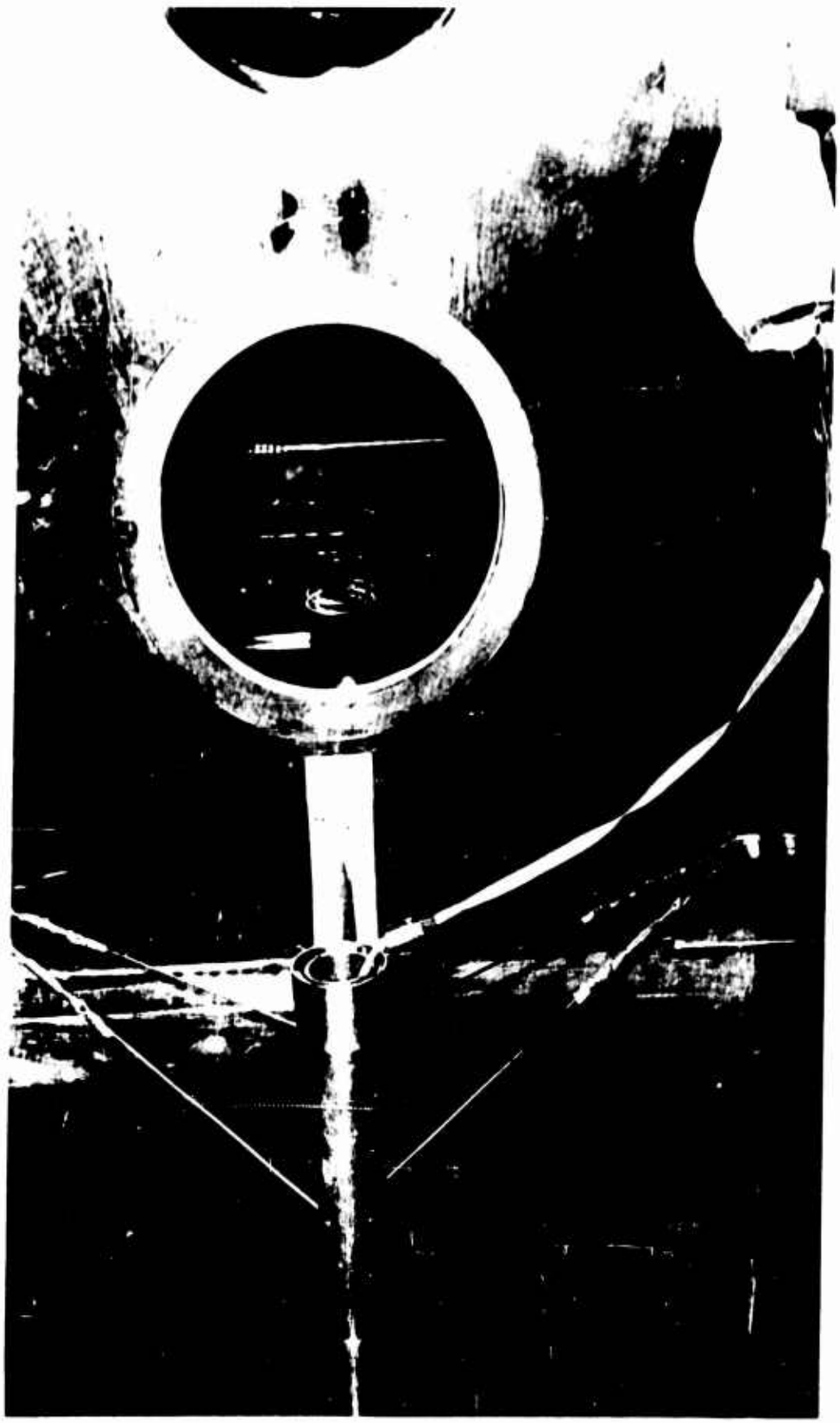

Figure II-6. Phase I Parachute Test Installation

TABLE II-3

PHASE I PARACHUTE TYPES AND SPECIFICATIONS

I Modified Guide Surface Ribless Types

Parachute Model	Suspension Line Length	θ_i (Deg.)	d_i/d_p	ℓ_i/d_p	Roof Type	S_o/S_p (2)
A	1 d_m	20	0.7	0.41	(1)	2.64
C	1 d_m	20	0.5	0.69	(1)	5.45
D	1 d_m	20	0.35	0.89	(1)	4.09
E	2 d_m	11	0.5	1.29	(1)	5.85

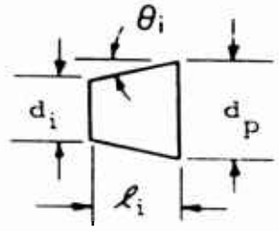

II Large Vent Bi-Conical Types

Parachute Model	Suspension Line	θ_i (Deg.)	d_i/d_p	ℓ_i/d_p	d_i/d_e	θ_R (Deg.)	S_o/S_p
F	1 d_m	20	0.7	0.41	1.14	20	3.3
G	1 d_m	20	0.5	0.69	1.14	20	4.57
H	2 d_m	11	0.5	1.29	1.14	20	6.27
I	1 d_m	20	0.5	0.69	1.14	30	3.83
J	1 d_m	20	0.5	0.69	1.21	30	3.87

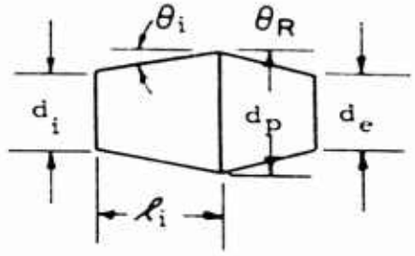

III Ribbon Type

Hemisflo - 25% porosity, 10% extension - S_o/S_p - 2.62

IV Ribbon Type

Ribbon - reefed - 28% porosity, 1% vent - S_o/S_p = 2.25

(1) Standard guide surface ribless

(2) Ratio of total cloth area to Maximum projected frontal area

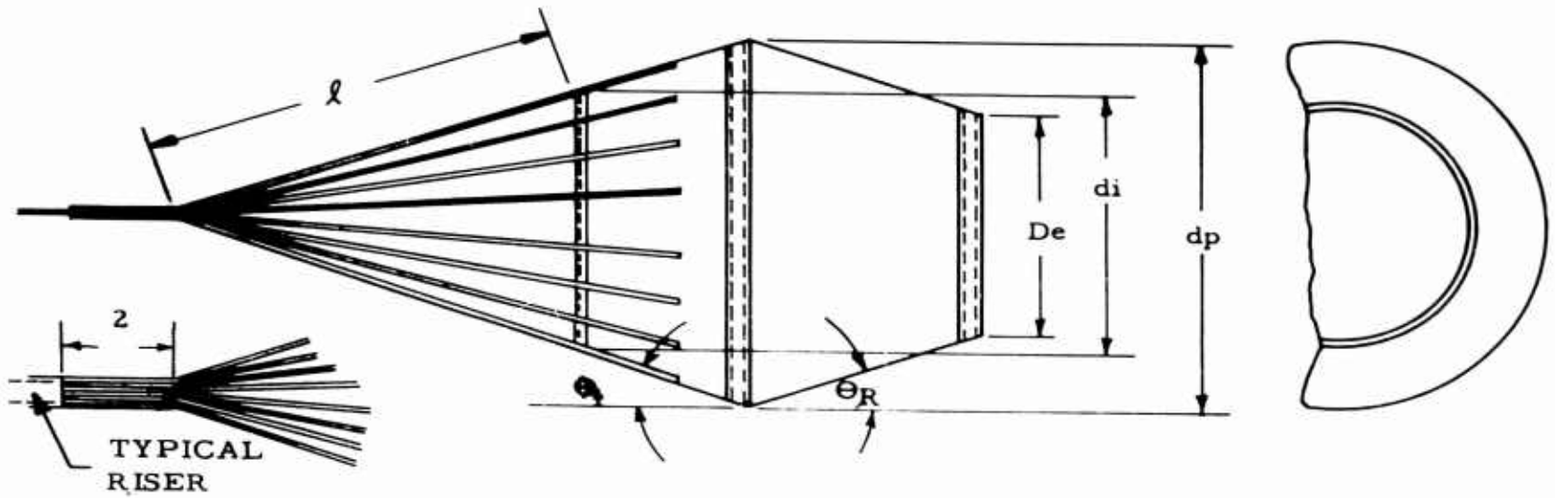

Type	De	di	dp	Θ_i	Θ_R	ℓ	MATERIAL			
							INLET CONE	EXIT CONE	S. L.	RISER
F	4.92	5.60	8	20°	20°	8	DANTEX, NEOPRENE COATED NYLON	SAME AS	CORD, NYLON CORELESS 90	WEBBING, NYLON MIL-W-4088 TYPE I
G	3.51	4.00	8	20°	20°	8	NO. 5678	INLET CONE	"	"
H	3.51	4.00	8	11°	20°	8	"	"	"	"
I	3.51	4.0	8	20°	30°	8	"	"	"	"
J	3.31	4.0	8	20°	30°	8	"	"	"	"

Figure II-7. Phase I Bi-Conic Parachute Test Models

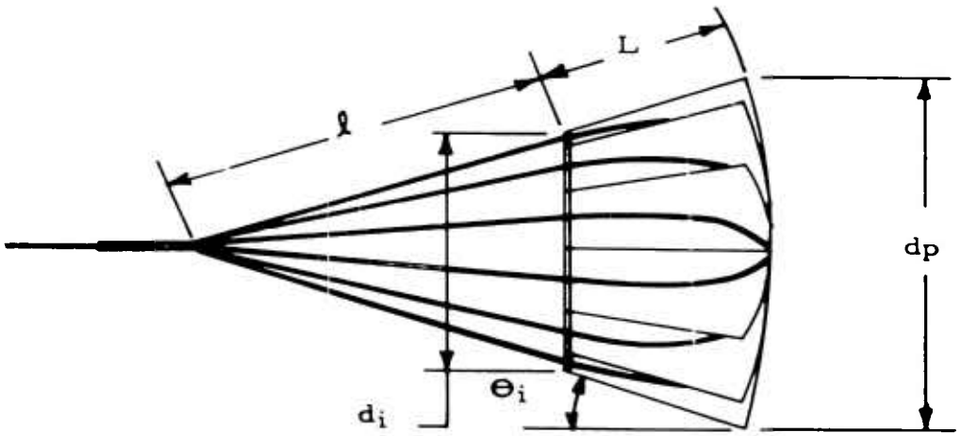

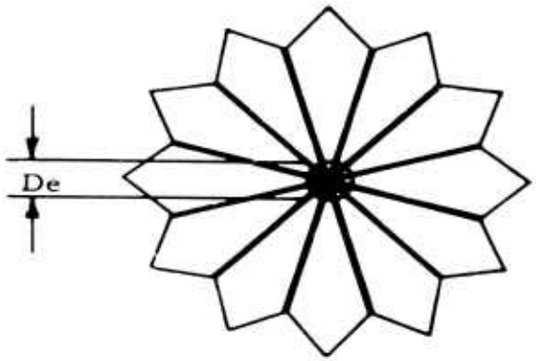

NOTE: 1. All dimensions in inches

2. Pattern dimensions do not include seam allowance.

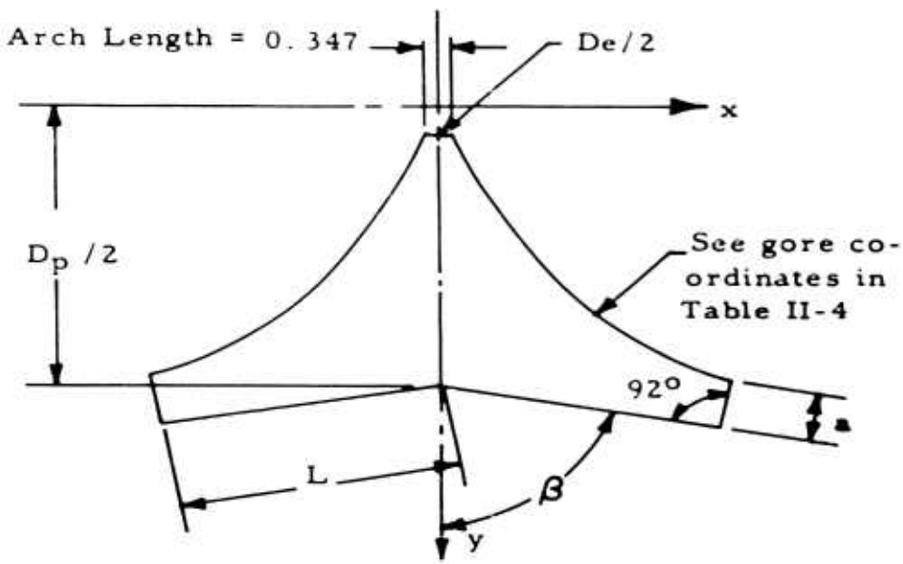

Figure II-8. Phase I Modified Guide Surface Models

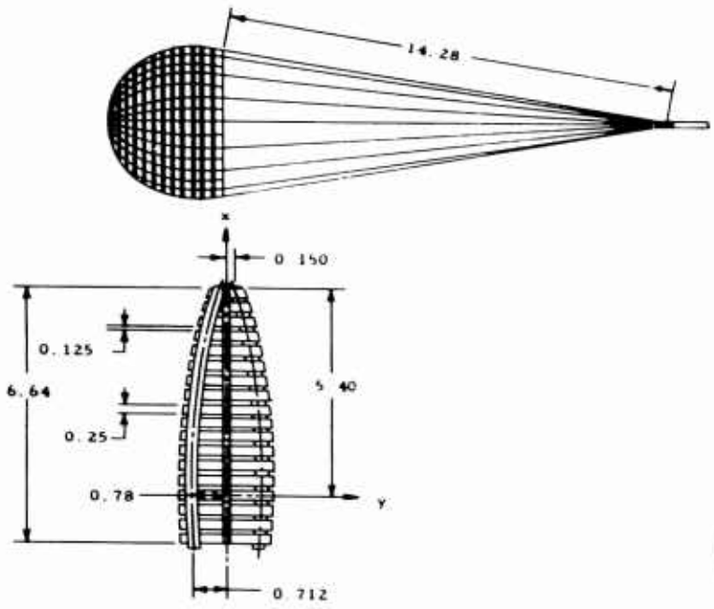

x	-1.25	0	1.54	2.06	3.08	4.11	5.14	6.16
y	0.71	0.78	0.75	0.67	0.54	0.39	0.20	0

16-GORE MEHISFLO MODEL

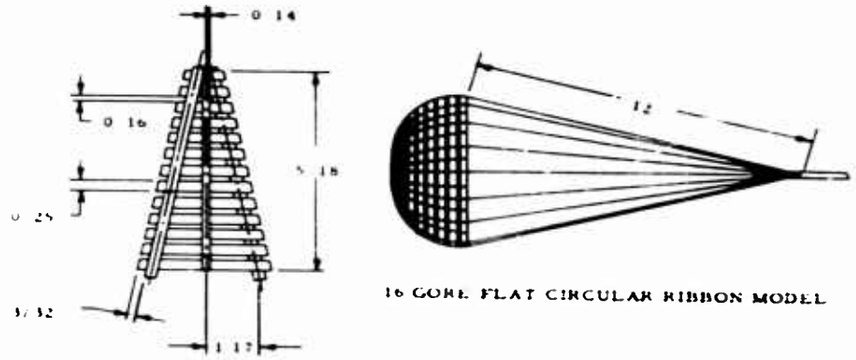

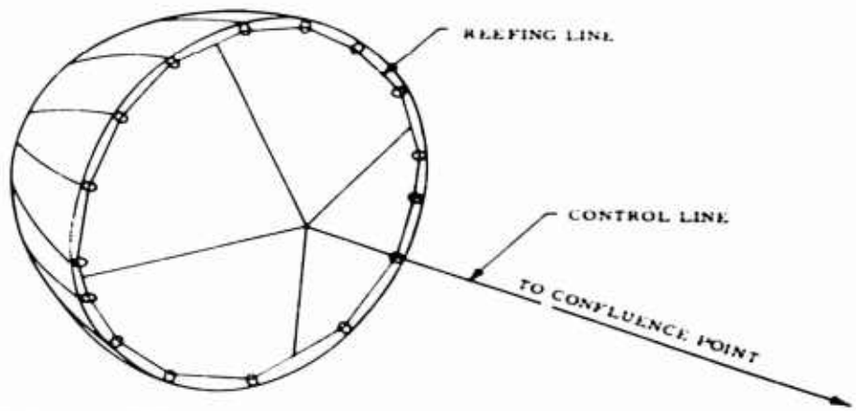

VARIABLE REEFING SYSTEM ON FLAT CIRCULAR RIBBON MODEL

Figure II-9. Phase I Hemisflo and Flat Circular Ribbon Models

TABLE II-4

PHASE I MODIFIED GUIDE SURFACE MODEL SPECIFICATIONS

TYPE	A&B		C		D		E		ALL CHUTES ARE MADE FROM FOLLOWING MATERIALS;
D_e	0.842		0.842		0.842		0.842		
D_i	5.89		4.21		2.95		4.21		
D_p	8.42		8.42		8.42		8.42		
O	23.7°		22.2°		21.7°		12.2°		
l	8		8		8		8		GORE: CLOTH, NYLON MIL-C-8021 TYPE I
L	3.51		5.85		7.6		10.5		
a	0.732		0.529		0.367		0.524		
β	80.5°		79.5°		79.5°		67°		
	x	y	x	y	x	y	x	y	
GORE CO-ORDINATES	0.16	0.57	0.24	0.47	0.53	0.80	0.29	0.66	SUSPENSION LINE: CORD, NYLON MIL-C-5040 TYPE I
	0.24	0.81	0.44	0.73	0.82	1.13	0.48	0.97	
	0.36	1.13	0.71	1.05	1.14	1.45	0.71	1.33	
	0.50	1.49	0.97	1.34	1.47	1.75	1.12	1.86	
	0.67	1.85	1.30	1.63	1.97	2.19	1.51	2.30	
	0.87	2.23	1.68	1.95	2.43	2.57	2.01	2.78	
	1.10	2.62	2.15	2.31	2.96	2.98	2.56	3.26	RISER: WEBBING NYLON MIL-W-4088 TYPE I
	1.38	3.00	2.59	2.63	3.35	3.27	3.12	3.70	
	1.61	3.23	3.02	2.93	3.89	3.65	3.86	4.21	
	1.90	3.46	3.51	3.26	4.74	4.21	4.53	4.65	
	2.38	3.73	3.95	3.53	5.35	4.54	5.24	5.11	
	2.81	3.91	4.53	3.90	6.20	4.89	5.93	5.53	
	3.61	4.08	5.03	4.21	7.55	5.25	6.68	5.98	
	-	-	5.88	4.71	-	-	7.48	6.41	
	-	-	-	-	-	-	9.92	7.79	

c. Results of Phase I Tests

In the conduction of this testing program, the basic instrumentation and equipment employed in the tests provided force measurements, direct motion photography, and Schlieren movies. Analysis of the force data recorded on Visicorder tape, as well as the motion pictures, resulted in both favorable and unfavorable performance characteristics of the test configurations. Since the direct movies (at 500 frames per second) and the Schlieren movies (at 1000 frames per second) made possible the analysis of various phenomena at short frame-time intervals, changes in inlet opening, amount of canopy inflation, steadiness of shock geometry and canopy stability characteristics were readily discernable. On the basis of this analysis Table II-5 was prepared which summarizes the essential performance parameters and characteristics of the test models.

In the accomplishment of this test program, indications of favorable canopy geometry were noted. In one instance (modified guide surface type D) an over-all indication of good performance prevailed, although the drag was low compared to types A and B. Since the suspension lines twisted due to model rotation within the first 0.5 second after deployment, a thorough study of this test canopy was not possible. During this time interval, however, direct photography indicated excellent inflation characteristics as seen in Figure II-10. Although the drag coefficient of 0.095 based upon constructed cloth area at a Mach number of 2.99, was not high, the important result of the Phase I test program was the attainment of favorable behavior of the canopy such as inflation and stability characteristics, and the steadiness of the shock wave. The latter was not observable in the case of configuration D since the line twist occurred prior to initiation of the Schlieren photography.

From the standpoint of drag, the modified guide surface type A canopy appeared best. This test canopy provided a drag coefficient of 1.24 based upon the design projected frontal area or 0.37 based upon the constructed cloth area at a Mach number of 1.99. This model was found to be somewhat unstable about its center of gravity.

Favorable characteristics of other canopies were observed in close examination of the high speed motion pictures. Although in most cases, other than the types A, B, and D, over-all canopy

TABLE II-5

PHASE I PARACHUTE TEST SUMMARY

Modified Guide Surface Types

Test Model	M	q p.s.i.	d_i Avg. and Deviation	d_m Avg. and Deviation (3)	$\frac{d_i \text{ Avg.}}{d_m \text{ Avg.}}$	Suspension Line Length In.	Average Projected Area Sq. In.	C_D (2) C_{D_p} C_{D_O}	Angle Relative to Point Attachment Deg.
A	1.99	2.254	6.9 ± 2.2%	9.3 ± 3%	.74	9.45	68.0	.915 1.24 .37	5
B	1.49	2.22	6. ± 10%	8.87 ± 1.5%	.68	9.00 ± .25	61.8	.64 .774 .232	2
(1)			3.56 ± 25%	6.25 ± 14%	.57	3.04 ± .8	30.6	.485 .291 .0870	0
C	2.99	1.09	5.05 ± 14%	9.35 ± 5%	.54	8.5 ± .23	68.5		0
(1)			3.9 ± 13%	7.95 ± 13%	.49	4.6 ± .10	49.5	.204 .201 .036	0
C	1.99	1.63	4.83 ± 4.6%	8.75 ± 5%	.55	8.8 ± .05	60.0	.266 .315 .0565	0
D	2.99	1.08	4.27 ± 0%	8.8 ± 2%	.485	9.2	61.0	.35 .424 .095	0
(1)			2.56 ± 23%	5.35 ± 10%	.47	2.1 ± .71	22.4	.495 .221 .05	0

Notes: (1) Suspension lines are twisted
(2) C_D based on average maximum inflated frontal area
(3) Constructed d_c = 8 inches

TABLE II-5 (CONT'D.)

PHASE I PARACHUTE TEST SUMMARY

Modified Guide Surface Types (cont'd.)

Test Model	M	q p.s.i.	d_i Avd. and Deviation	d_m Avg. and Deviation (3)	$\frac{d_i \text{ Avg.}}{d_m \text{ Avg.}}$	Suspension Line Length In.	Average Projected Area Sq. In.	C_D(2) C_{D_p} C_{D_o}	Angle Relative to point Attachment Deg.
D(1)	2.50	2.18	2.5 ± 42%	5.35 ± 28%	.467	2.6 ± 1.2	22.4	.615 .274	0
D(1)	1.99	2.21	2.85 ± 29%	5.1 ± 25%	.56	3.55 ± .48	20.40	.0613 .621 .252	0
E(1)	2.99	1.08	5.00 ± 14%	9.5 ± 24%	.525	18.2 ± .60 14.5 (1)	71	.0565 .56 .797	1.5
E	2.5	1.35	4.32 ± 33%	9.1 ± 23%	.473	17 ± .12	65.0	.104 .51 .663	1.5
E	1.99	1.89	3.56 ± 14%	8.4 ± 13%	.425	16.2 ± 2.38	55.3	.0865 .47 .523 .0682	1.5
				Conical Types					
F	2.99	.556	5.3 ± 28%	6.8 ± 20%	.78	9.6 ± .12	36.2	.65 .462	2
G	1.49	2.23	4.35 ± 41%	8.8 ± 20%	.425	10.2 ± .35	60.0	.14 .45 .782 .171	8

Notes: (1) Suspension lines are twisted.
(2) C_D based on average maximum inflated frontal area.
(3) Constructed d_c = 8 inches.

TABLE II-5 (CONT'd.)

PHASE I PARACHUTE TEST SUMMARY

Conical Types (Cont'd.)

Test Model	M	q p.s.i.	d_i Avg. and Deviation	d_m Avg. and Deviation (1)	$\frac{d_i \text{ Avg.}}{d_m \text{ Avg.}}$	Suspension Line Length In.	Average Projected Area Sq. In.	C_D (2) C_{D_P} C_{D_O}	Angle Relative to Point Attachment Deg.
H	2.99	.547	4.4 ± 35%	7.6 ± 35%	.58	10.7 ±1.2	45.3	.77 .69 .11	18
I	1.99	1.64	4.4 ±51%	6.6± 28%	.66	9.0± .48	34.7	.61 .73 .191	11
J	2.99	.554	4.5 ± 32%	7.6 ± 12%	.59	9.25±.24	47.2	.48 .43 .111	18.5

Notes: (1) Constructed d_c = 8 inches
(2) C_D based on average maximum inflated frontal area

TABLE II-5 (CONT'd.)

PHASE I PARACHUTE TEST SUMMARY

Ribbon Types — Flat Circular (28% Porosity) with Reefing

Test Model	M	q p.s.i.	d_i Avg. & Deviation	d_m Avg. & Deviation (3)	d_i Avg. / d_m Avg.	Suspension Line Length In.	Average Projected Area Sq. In.	C_D(2) C_{D_p} C_{D_O}	Angle Relative to Point Attachment Deg.	Reefing Ratio %(2)
10a	1.49	2.21	5.45±6%	6.35±7%	.86	13.6±.24	31.6	.9 .616	2.5	50
10b	1.49	2.21	4.95±1%	6.00±3%	.825	13.7±.28	28.3	.274 .45 .391	1.5	42
11	2.99	1.08	6.2±23%	6.76±12%	.92	13.3±.95	36.0	.174 .49 .380	1.5	100
11a	2.99	1.08	5.35±16%	6.2±7%	.86	15.2±.71	30.2	.169 .49 .320	3	49
11b	2.99	1.08	4.05±9%	5.4±5%	.75	14.7±.28	22.9	.142 .49 .241	0	28
11c	2.99	1.08	4.5±19%	5.6±13%	.80	16.4±.95	24.6	.107 .49 .261	2	35
11d	2.99	1.08	4.77±15%	5.6±8%	.85	14.7±.71	24.6	.116 .49 .261 .116	3	39

Notes: (2) C_D based on average maximum inflated frontal area
(3) Constructed d_c = 8 inches

TABLE II-5 (CONT'D.)

PHASE I PARACHUTE TEST SUMMARY

Ribbon Type - Hemisflo (25% Porosity - 10% Extension)

Test Model	M	q p.s.i.	d_m Avg. & Deviation	d_m Avg. & Deviation (3)	$\frac{d_i \text{ Avg}}{d_m \text{ Avg.}}$	Suspension Line Length In	Average Projected Area Sq. In.	C_D (2) C_{D_p} C_{D_O}	Angle Relative to Point Attachment Deg.	Reefing Ratio %(4)
15a	1.99	1.86	3.17±38%	4.46±21%	.71	11.7 8.2	16	.67 .193 .086	2	-
15b	2.99	1.09	3.76±25%	4.76±16%	.79	13±.12	17.8	.67 .216 .096	1.5	-

Notes: (2) C_D based on average maximum inflated frontal area
(3) Constructed d_c = 8 inches
(4) $(d_i / 2/3\ d_o)^2$

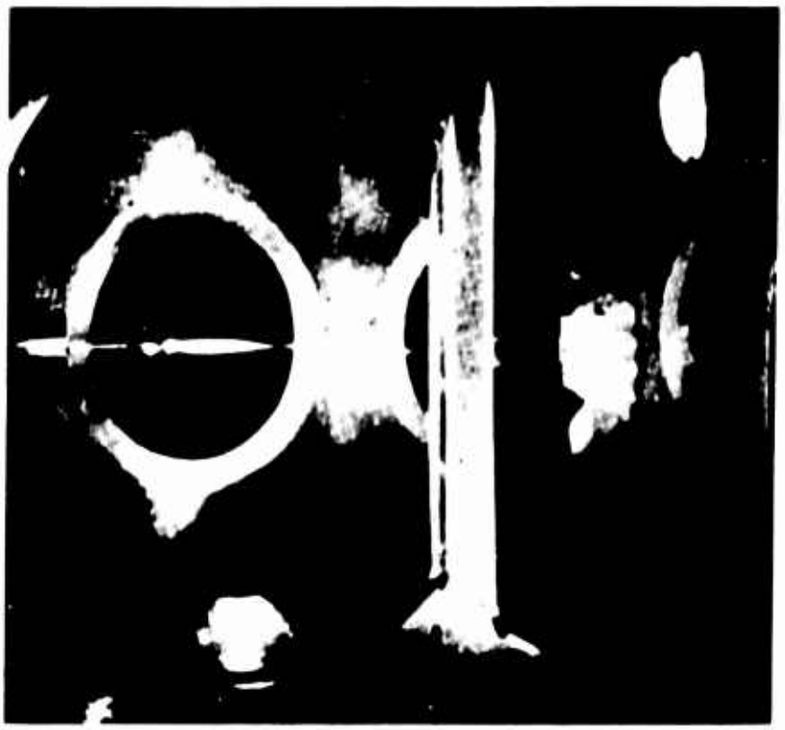

Figure II-10. Phase I Modified Guide Surface Model D. Film Speed:

500 fps, M = 2.99, q = 156 psf, x/d = 10

behavior was not outstanding. However, in several configurations there were indications of good inlet inflation, roof performance and shock wave steadiness. Outstanding among these is the type G conical canopy. The inlet geometry for this configuration may be seen (Fig. II-7) to be similar to the Type D guide surface model. The inlet of this model appeared to be very well inflated during its test when at near zero angle of attack. The Type F conical appeared best of all conical types from the standpoint of stability, although the canopy was underinflated. The conical type parachutes indicated (except for Type F) varying degrees of instability about the point of suspension. The reefed flat circular ribbon canopy exhibited very good stability and good roof inflation, particularly when reefed to 28 percent at a Mach number of 2.99.

In Table II-6 are listed the essential parachute components and associated geometry which indicated good component or over-all performance in the Phase I tests. The configurations with which these components or geometric properties are associated are also tabulated.

TABLE II-6

DEMONSTRATION OF FAVORABLE COMPONENT PERFORMANCE

PHASE I TEST MODELS

Component Performance	Associated Test Model Configuration
Inlet Inflation	A, B, C, D, E, G
Roof Inflation	A, B, D, RR*
Drag	A, B
Stability about point of suspension	A, B, C, D, E, F, RR* Hem.**
Stability about C. G.	C, D, E, F, RR*, Hem**

*Reefed circular flat ribbon
**Hemisflo

It may be noted also that the number of appearances which the various configurational types made in this tabulation directly indicate the number of favorable performance characteristics associated with a particular model configuration. Configurations A, B, and D each appear four of five times in this tabulation. Both A and B fail to appear in the category of good stability about the model center of gravity. The Type D configuration does not appear in the outstanding drag classification, which is expected since the inlet area of this model is much smaller than that for Types A and B, which exhibit very high drag.

The above mentioned results were utilized in selection of configurations for Phase Ia tests which are now described.

B. Phase Ia Parachute Test Program

1. General Configurational Considerations

This test program intervened between the first and second Government facility testing programs and was conducted in the Cook Technological Center wind tunnel facility. The objective of this program was to improve the Phase I configurations. The approach was to evaluate configurations which had geometric characteristics similar to those models which performed best in the Phase I program. As discussed in Part A, certain configurations tested in the Phase I program indicated either favorable inlet inflation characteristics, or over-all stability, or canopy roof inflation, or over-all inflation, or over-all inflation and stability. Since several configurations indicated favorable inlet inflation characteristics, these geometries were retained in future model designs, leaving the canopy roof study as the primary emphasis of this program. The non-porous bi-conical configurations, having indicated under-inflation characteristics, particularly in the roof regions, were modified in such a way as to decrease the exit to inlet area ratio. Since the type F conical canopy indicated good stability, and also represented the conical type with the smallest total surface area, it was considered for further study in this interim test program. Modifications were made in the roof geometry to improve the inflation characteristics.

The tests in the Phase I program involving the modified guide surface type canopies indicated excellent stability with reference to the point of suspension, and except for types A and B, they had excellent stability with reference to their center of gravity. Inflation characteristics were fair to good for some configurations (Types A,

B, C and D), and as previously mentioned, were best for the Type D. In some instances, involving tests of these configurations, some oscillation of the guide surface panels were noted. The tendency to rotate, resulting in suspension line wrap-up, was also indicated in those tests in which a swivel was not used. It was intuitively apparent that mal-alignments of the guide surface panels due to fabrication tolerances would tend to cause rotation. Tests indicated this to be true, particularly when the guide surface panels were well inflated (e.g., Type D). It was not apparent from the tests that the guide surface construction contributed significantly to the favorable performance of the guide surface models. Accordingly, part of the study in the interim program was aimed at evaluating the contribution of the guide surface panels. This was accomplished by constructing models with geometry similar to a particular guide surface model. Simultaneously, a study of canopy roof geometry was conducted.

The instability about the center of gravity which was characteristic of Types A and B was attributed to excess negative lift contributed by the flat roof. These configurations indicated excellent drag and exhibited good inflation and were also constructed with the smallest cloth area of the guide surface types (all having the same frontal area). Hence, they were considered particularly worthy of further study with modifications to improve their stability characteristics.

In the tests of the flat-circular ribbon model in the Phase I program, good inflation of the canopy roof was indicated when the model was in a reefed state. Flagging of the forward ribbons was apparent, and expected due to excess material in that area. Attention was given to the design of a model with a ribbon roof, and a shaped inlet. The inlet design was aimed at simulating the ribbon inlet in the best reefed condition (28% reefing ratio) of the Phase I tests.

As discussed above, the primary emphasis of the study performed in the interim test program was the application of favorable canopy geometry indicated by the Phase I test models. The interim test program was also to furnish data from which an evaluation may be made of the contribution to parachute performance of the guide surface panel construction.

2. Description of the Test Model Configurations

The models for the interim test program were designed in accordance with the conclusions drawn from the performance analysis of the Phase I test configurations and are described in Table II-7. The

TABLE II-7

PHASE Ia TEST MODEL SPECIFICATIONS

Test No.	Configuration	θ_i^o	d_i	d_c	θ_R^o	A_E/A_i	Object
1	C-1	20	4.2	1.68	45	0.16	Roof Modification of Type F
2	C-3	20	4.2	2.94	45	0.50	Roof Modification of Type F
3, 4, 12, 13	C-2	10	5.4	3.78	45	0.49	Inlet and Roof Modification of Type F
5	G.S.-1	10	5.4	-	90	0.22	Scaled Type A
6	C.R.-1	20	4.2	-	-	0.80	Simulation of Reefed Ribbon
7, 8, 9	G.S.-2	10	5.4	-	90	0.41	Modification of G. S. - 1, Annular Vent
10	C-4	20	4.2	-	90	0.41	Modification of Type F, Annular Vent
11	G.S.-4	10	5.4	-	90	0.41	Modification of G.S.-1 Center Vent
14	G.S.-5	10	5.4	-	90	0.41	Modification of G.S.-1, Annular Vent
15	C-5	20	4.2	-	90	0.50	Modification of Type F, Annular Vent
16	C-6a	10	5.4	-	90	0.21	Conical Equivalent of G.S.-5
17	C-9	20	3.2	-	90	0.26	Conical Equivalent of Type D
18	C-7b	10	5.4	-	90	0.46	Modification of C-6a - Mesh Roof
19	C-7a	10	5.4	-	90	0.42	Modification of C-6a - Mesh Roof
20	Cone Cup(2)	-	-	-	-	-	Test in wake of forebody

(1) All models in Tests 1 through 19 had maximum constructed diameter of 6 inches.

(2) This model was designed and constructed with a 4-inch maximum diameter, by the University of Minnesota.

(This page is unclassified.)

listing in the table corresponds generally to the order in which the models were tested. It is noted that the configurations C-1, C-3, C-2, C-4 and C-5 are modifications of the Phase I model, Type F. Model G.S.-1 is a scaled duplicate of the Phase I test model Type A. Since model Types A and B are quite similar, only one of these types (A) was employed, along with its modifications in the Phase Ia study. Test models G.S.-2, G.S.-4 and G.S.-5 are modifications (in roof configuration) of model G.S.-1. The test model C.R.-1 is a simulation of the reefed ribbon configuration which appeared to perform quite well in the Phase I tests. Test model C-6a was designed to duplicate the general geometry of model G. S.-5 with the purpose of evaluating the effectiveness of the guide surface panel construction employed in the model G.S.-5. The test model C-9 was designed to be the conical equivalent of the Phase I test model Type D for a similar evaluation. Models C-7a and C-7b were designed for further study of roof geometry and exit to inlet area ratio. These models are further modifications of test model C-6a. Photographs of test models C-7a and C-6a are shown in Figure II-11. Details of all Phase Ia models are given in Figures II-14, II-15, II-16, II-17, II-18, and Tables II-8 and II-9.

3. Wind Tunnel Test Installation and Deployment Methods

In the interim test program in the Cook Technological Center's wind tunnel facility, all parachute models were tested in the wake of a cone-cylinder forebody which was mounted in the test section as shown in Figure II-12. Test models employed risers which located the model skirt approximately ten forebody base diameters downstream. High speed (1000 fps) Schlieren photography data was obtained during each test. Force data were not obtained during this series of tests since the primary objective of the study was the evaluation of the behavior of the model from the standpoints of inflation, stability about the point of suspension, and characteristics of the shock geometry ahead of the model. The ratio of model diameter to forebody diameter (2, 18) employed in these tests approximate that used in the Phase I tests (2.13).

Parachute models were stowed in a bag secured by a break thread to the forward end of the riser (near the forebody base) during tunnel run-up. When flow conditions in the tunnel were established, the bag was pulled off by means of a line running from the bag to a downstream mechanism capable of axial translation by remote manual control.

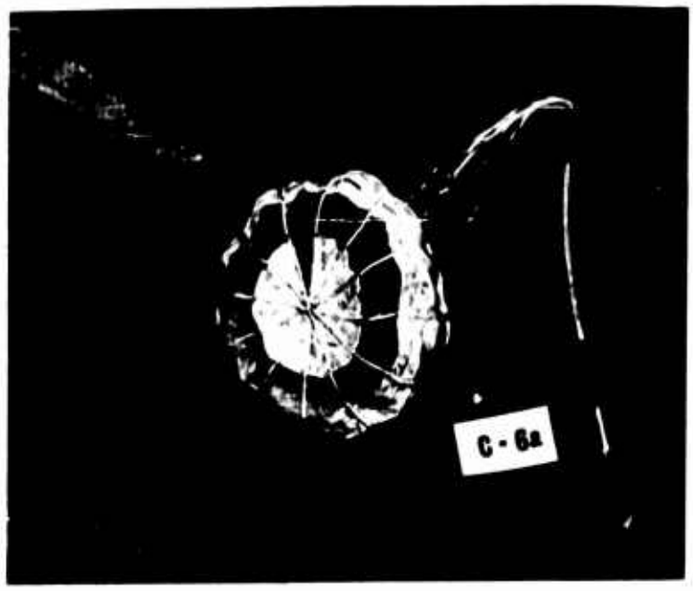

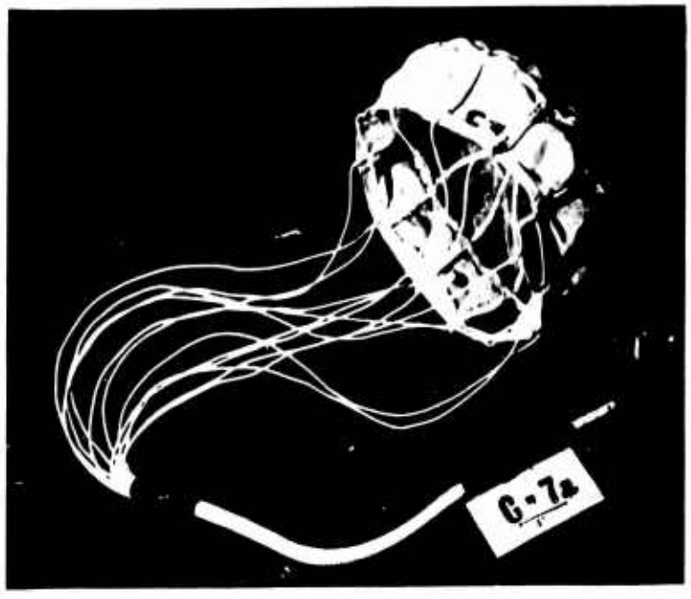

Figure II-11. Phase Ia Test Models C-6a and C-7a

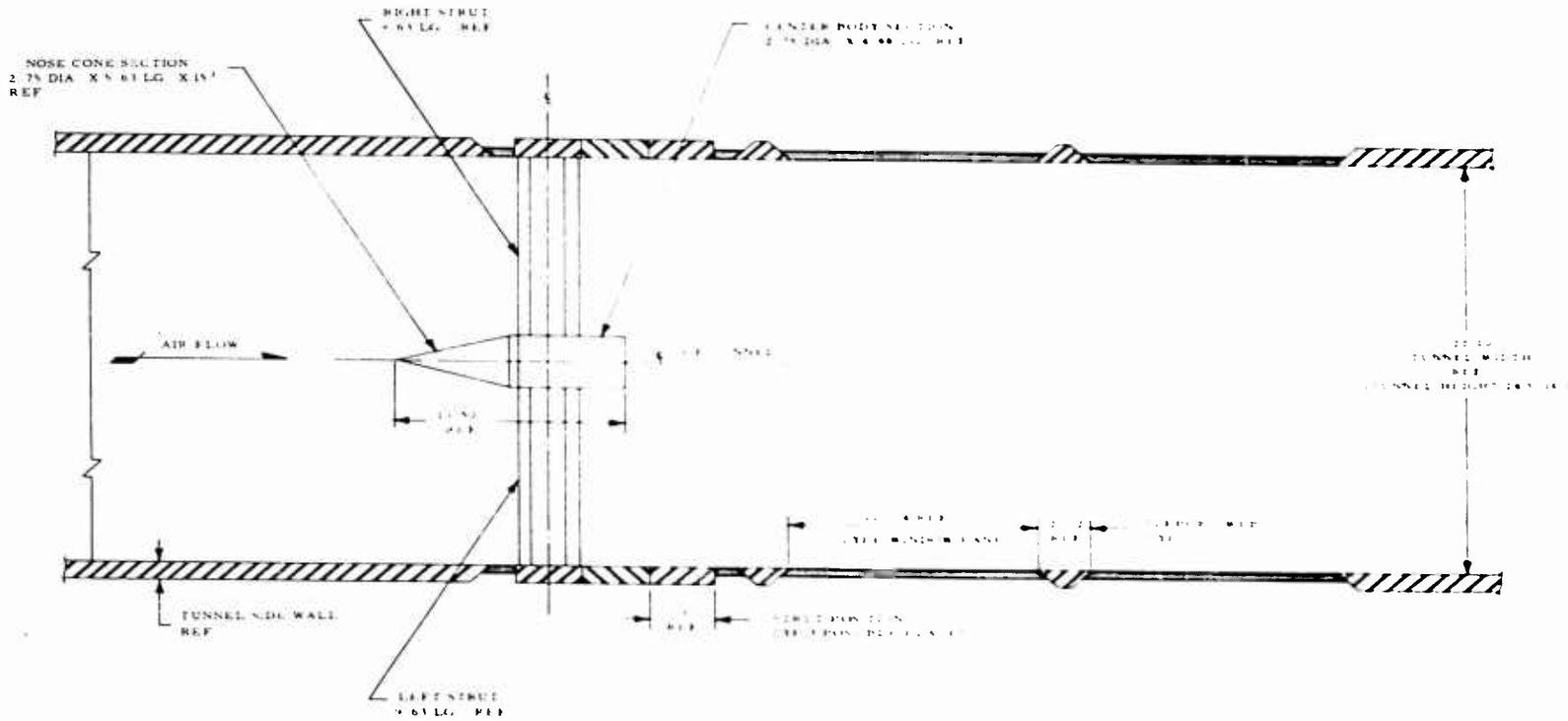

Figure II - 12 Phase I a Forebody, Parachute Tests

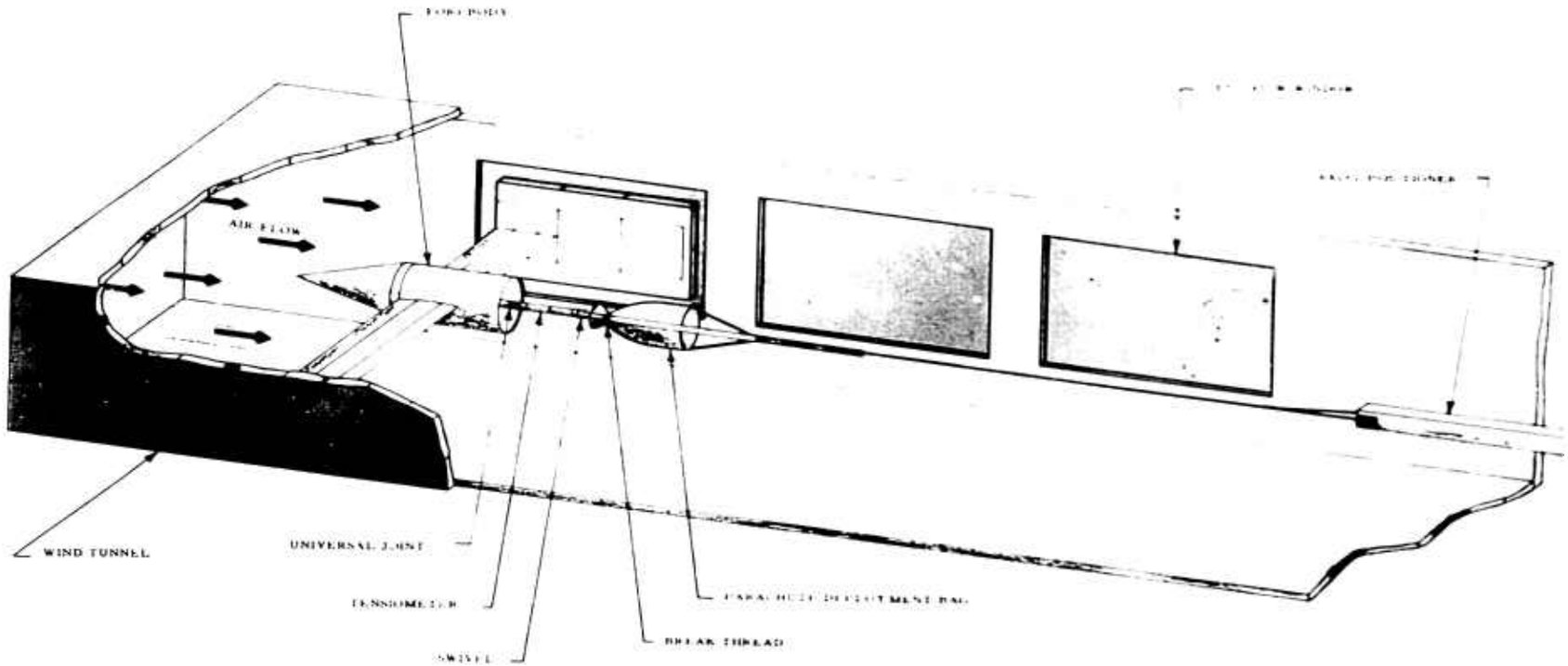

Figure II - 13. Phase Ia Parachute Test Installation

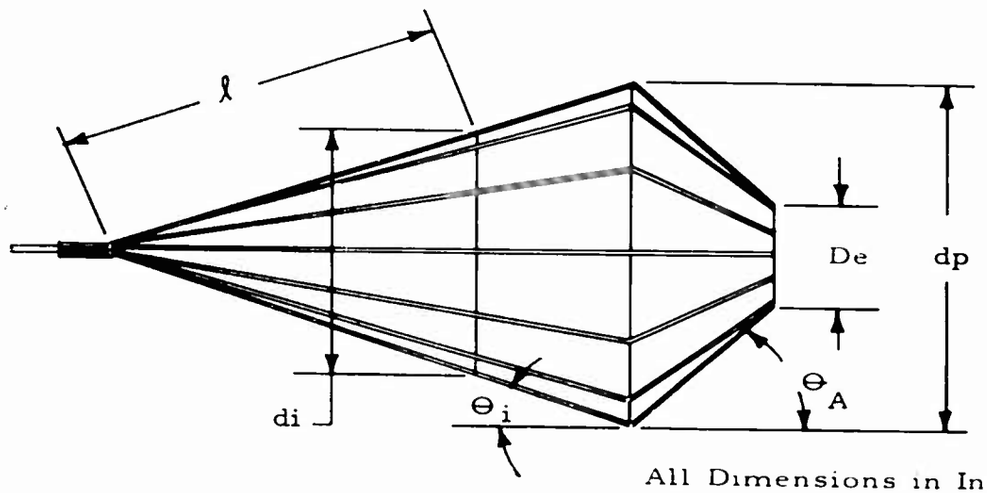

All Dimensions in Inches

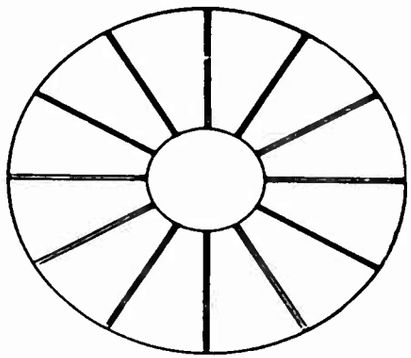

Typical Views of C-1, C-2, & C-3

TYPE	De	di	dp	Θ_i	Θ_A	ℓ	MATERIALS		
							CONES	S. L.	RISER BINDING
C-1	1.68	4.2	6	20°	45°	6	Dantex, Neoprene Coated Nylon	No. 90 Braided Nylon Line	Tape, Nylon MIL-T-5038 Type III
C-2	3.78	5.4	6	10°	45°	6	No. 5578 "	"	"
C-3	2.94	4.2	6	20°	45°	6	"	"	"

Figure II-14. **Phase Ia Bi-Conic Parachute Models**

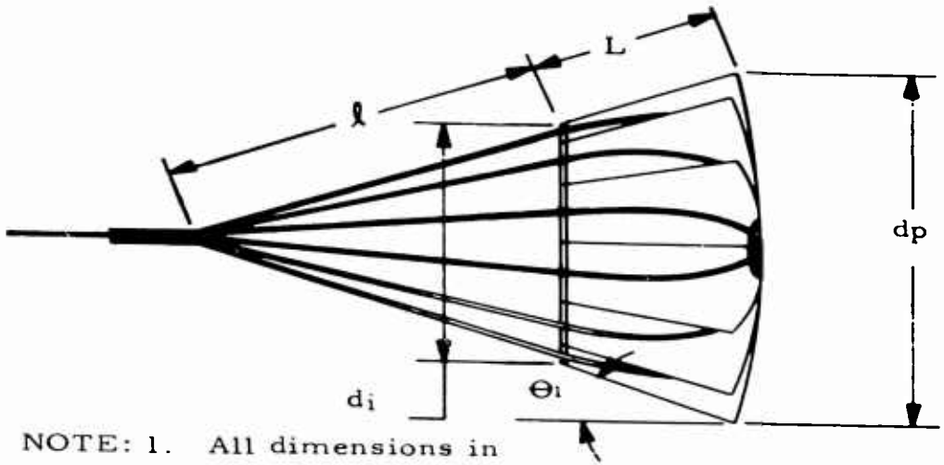

NOTE: 1. All dimensions in inches
2. Pattern dimensions do not include seam allowance.

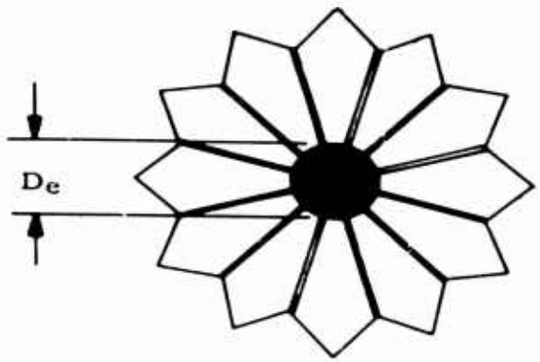

Conventional vent with nylon mesh is typical of GS-4. Types GS-1 and GS-3 have conventional vent, but no mesh.

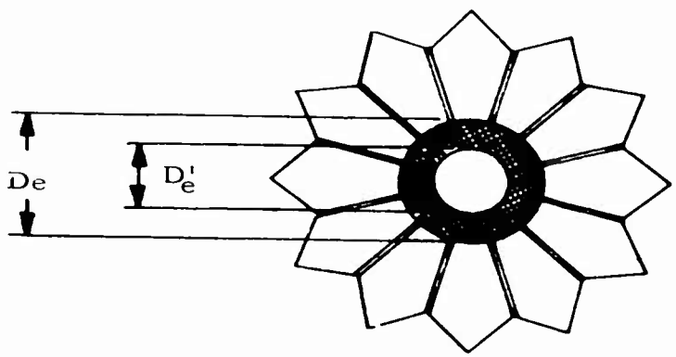

Annular vent with nylon mesh is typical of GS-2 and GS-5.

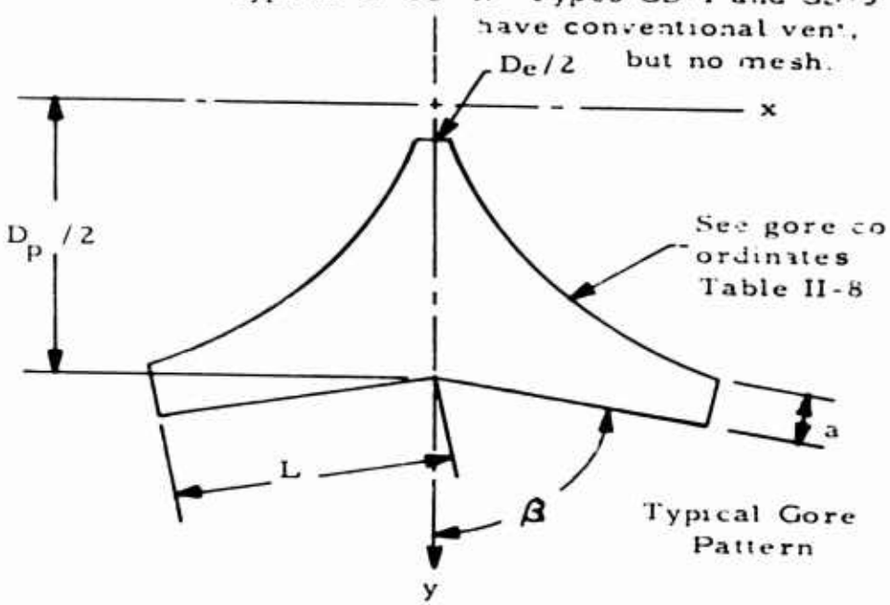

Figure II-15. Phase Ia Modified Guide Surface Models

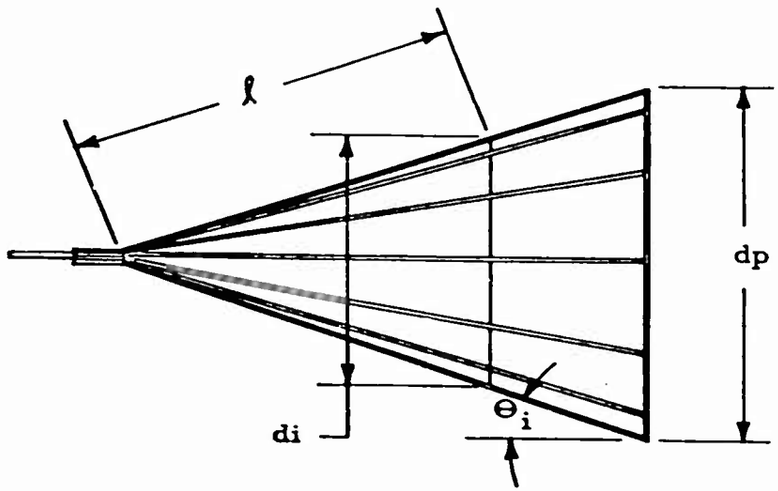

All Dimensions in Inches

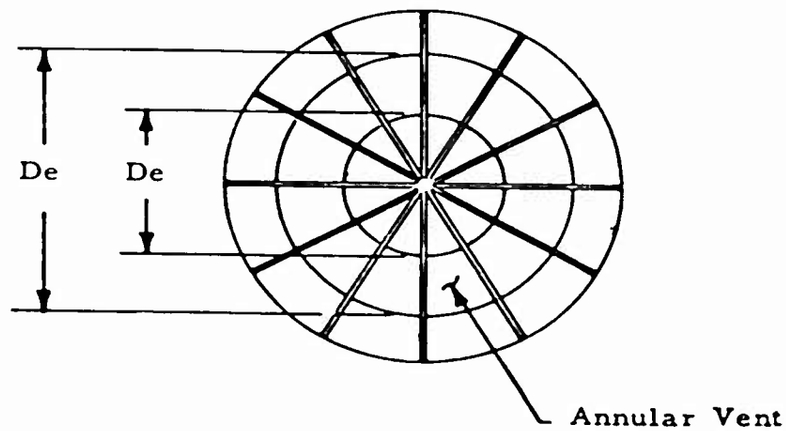

Typical Views of C-4 & C-5

TYPE	De	De'	di	dp	Θ_i	ℓ	MATERIALS		
							CONES	S. L.	RISER
C-4	4.1	3.20	4.2	6	20°	6	Dantex, Neoprene Coated Nylon No. 5678	No. 90 Braided Nylon Line	Tape, Nylon MIL-T-5038 Type 3
C-5	4.1	2.84	4.2	6	20°	6	"	"	"

Figure II-16. Phase Ia Conical Models C-4 and C-5

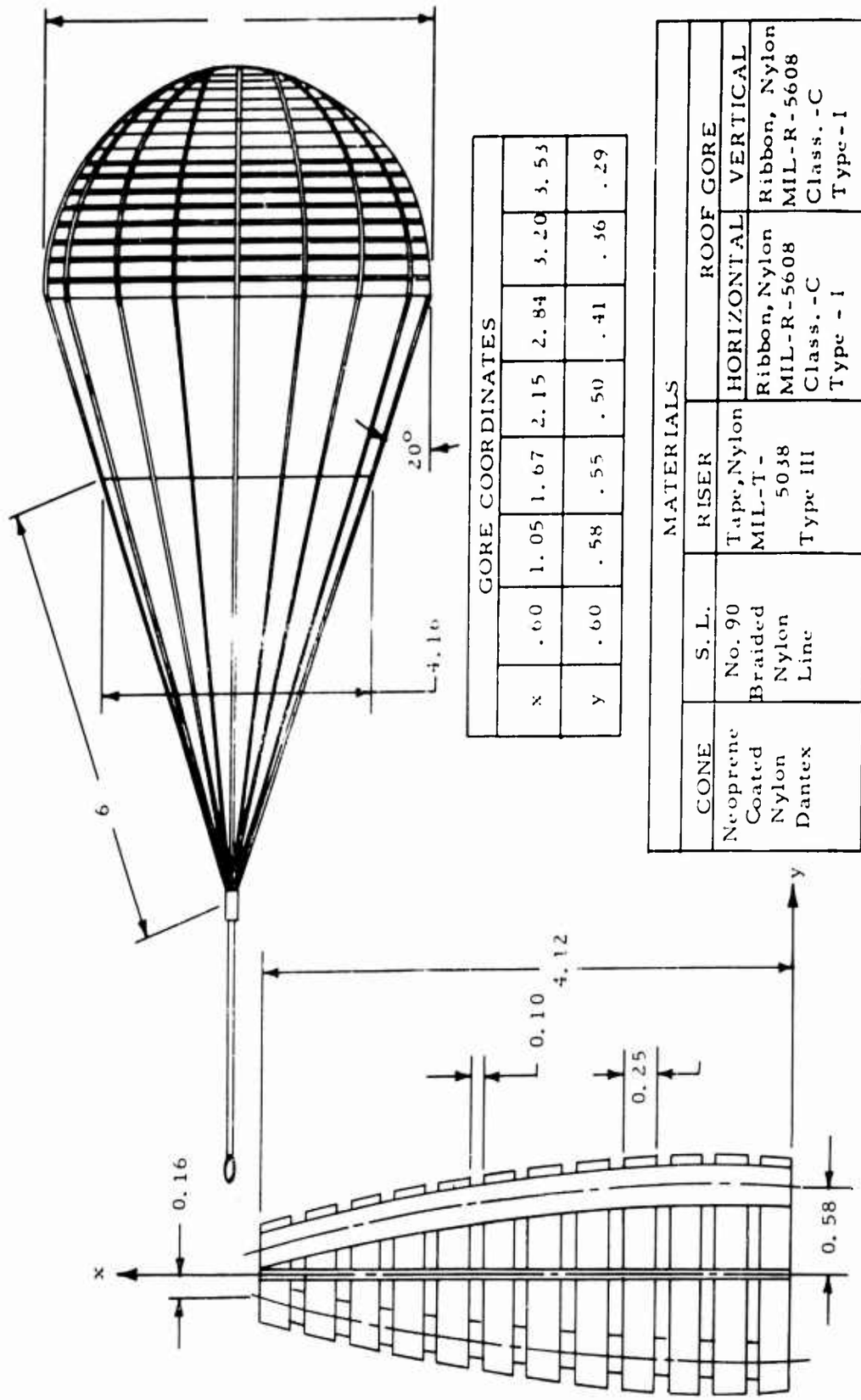

GORE COORDINATES

x	.00	1.05	1.67	2.15	2.84	3.20	3.53
y	.60	.58	.55	.50	.41	.36	.29

MATERIALS

CONE	S.L.	RISER	ROOF GORE	
			HORIZONTAL	VERTICAL
Neoprene Coated Nylon Dantex	No. 90 Braided Nylon Line	Tape, Nylon MIL-T-5038 Type III	Ribbon, Nylon MIL-R-5608 Class. -C Type - 1	Ribbon, Nylon MIL-R-5608 Class. -C Type - 1

Figure II - 17. Phase Ia Ribbon Roof Model C. R. - 1

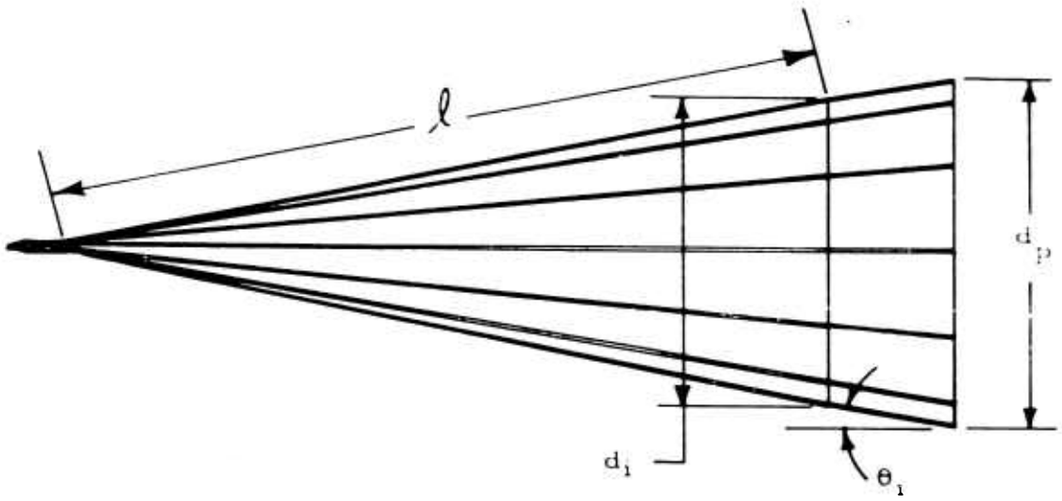

Note: Refer to Table II-9 for detailed specifications

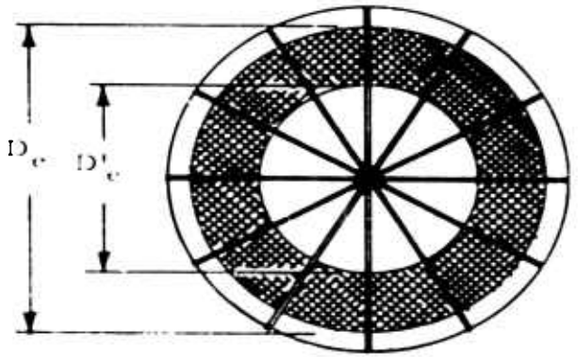

Typical Roof of C-6a

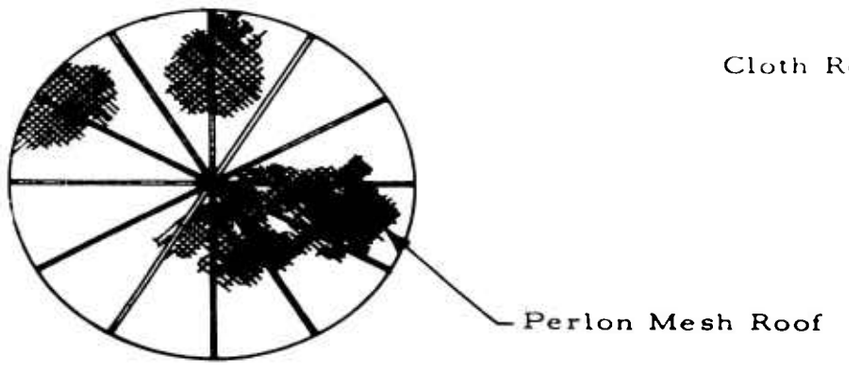

Typical Roof of C-7a
The suspension lines of C-7b do not cross roof

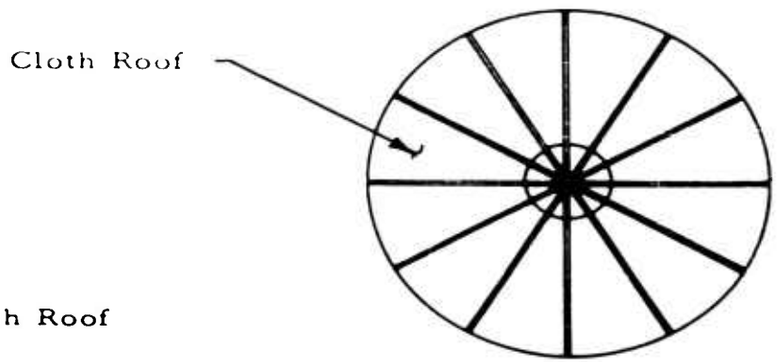

Typical Roof of C-9

Figure II-18. Phase Ia Conical Models C-6a, C-7a, C-7b and C-9

TABLE II-8
PHASE Ia MODIFIED GUIDE SURFACE MODEL SPECIFICATIONS

TYPE	VENT	D_e	D_e'	d_i	d_p	θ_i	ℓ	L	a	β
GS-1	Conv*	0.60	N.A.	5.4	6.0	10°	12	1.68	0.706	64.5
GS-2	Annular with mesh	4.1	3.2	"	"	"	"	"	"	"
GS-3	Conv*	2.56	N.A.	"	"	"	"	"	"	"
GS-4	Conv* with mesh	4.1	N.A.	"	"	"	"	"	"	"
GS-5	Annular with mesh	5.2	3.2	"	"	"	"	"	"	"

*Conventional

COMMON GORE CO-ORDINATES														
	x	.68	1.00	1.34	1.81	2.00	2.12	2.25	2.37	2.50	2.62	2.87	3.00	3.15
	y	.18	.28	.37	.50	.56	.59	.65	.71	.81	1.00	1.37	1.56	1.84

GORES:	S.L. :	MESH:	RISER BINDING:
Cloth, Nylon MIL-C-8021 TYPE I	Cord, Nylon MIL-C-5040 TYPE I	Nylon Mesh 40% Porosity	Tape, Nylon MIL-T-5038 TYPE III

TABLE II-9

TEST Ia CONICAL TEST MODEL SPECIFICATIONS

Type	d_i	d_p	D_e	D_e'	ℓ	θ	Materials			Remarks
							Cone	S.L.	Roof	
C-62	5.4	6	4.8	3.0	12	10°	Cloth, Nylon MIL-C-8021 Type I	Cloth, Nylon MIL-C-5040 Type I	Cloth, Nylon MIL-C-8021 Type I	Annular vent is filled with Perlon mesh. Perfab No. 250/25
C-7a	5.4	6	6.0	N.A.	12	10°	Cloth, Nylon MIL-C-8021 Type I	Cloth, Nylon MIL-C-5040 Type I	Mesh, Perlon Perfab No. 250/25	Entire roof is filled with Perlon mesh
C-7b	5.4	6	6.0	N.A.	12	10°	Cloth, Nylon MIL-C-8021 Type I	Cloth, Nylon MIL-C-5040 Type I	Mesh, Perlon Perfab No. 250/25	Same as C-7a except the S.L. do not cross over the roof
C-9	3.2	6	0.6	N.A.	6	20°	Cloth, Nylon MIL-C-8021 Type I	Cloth, Nylon MIL-C-5040 Type I	Cloth, Nylon MIL-C-8021 Type I	Entire roof is made of nylon cloth with a standard vent.

N.A. Not Applicable
All dimensions in inches

This system is illustrated in Figure II-13. When sufficient tension in the pull line was applied, failure of the parachute deployment bag breakline resulted in deployment of the model. The mechanism used to deploy the model is part of the installation used in the Cook Technological Center's Basic Test Program, discussed in Section I.

4. Results of the Test Program and Data Analysis

In the conduct of this test series, initial model designs were performed in accordance with general modifications as indicated by the analysis of the Phase I test program and discussed previously. However, structural and fabrication problems developed as the test series progressed, requiring construction modifications as indicated by test model performance analysis, and as required for test model survival throughout the testing period. The high dynamic pressure (700 psf) environment of these tests imposed quite severe requirements on the materials employed, as well as the fabrication techniques. However, minimum weight, strength and stiffness materials were employed where possible in the fabrication of the models in order to maintain as limp a construction as possible. In all tests, the model canopies were deployed from a tightly packed initial condition, requiring that they self-inflate after deployment.

In Table II-10 the tests conducted in this series are listed chronologically. Stability about the point of suspension ($\Delta\alpha^{o}$) and inflation characteristics are tabulated. It may be noted that successive tests do not necessarily fully explore a given configuration along with modifications indicated by the previous test. This occurs because study of the data derived from a given test was not conducted before testing of a modification of this canopy. During this study period, different configurational types were tested.

Tests of canopies which were constructed of non-porous materials were found, as in the Phase I tests, to suffer structural damage either early in the test period or before wind tunnel shutdown. Model canopies in the Phase I tests as well as models C-1, C-2, C-3, and C-4 in the Phase Ia tests were constructed of Dantex , a neoprene coated nylon fabric. A heavier material, Vulcan, was also considered for the construction of the non-porous canopies, and was employed for one of the later (C-5) tests. However, as indicated previously, it was desired to construct canopies in as limp a form as possible, and resort to this heavier material was not made until conclusive evidence of its need was shown by tests. It may be appropriate to point out at this time that static loadings are not critical since even the use of lightweight materials in model canopy construction result in high static factors of

TABLE II-10

PHASE Ia PARACHUTE TEST SUMMARY

Configuration	M_∞	Δa^o	Inflation
C-3a	2.10	2.5	Good
G.S.-1	2.08	15.0	Good
C.R.-1	2.11	0.0	Poor
G.S.-2	2.12	8.0	Good
C-4	Subs	-	Good subsonic
G.S.-4	2.09	10.0	Good
G.S.-5	2.10	9.0	Good
C-5	2.03	7.0	Good
C-6a	2.13	5.0	Good
C-9	2.06	1.5	Fair
C-7b	2.06	3.0	Good to Poor
C-7a	2.09	5.0	Good to Poor

safety. Instead, dynamic loadings caused by high frequency oscillations appear to be critical, and since these are difficult to predict, material requirements must be based upon test results.

The first test in the Phase Ia series involved the model canopy C-1 which was designed to consist of a roof modification of the Phase I Type F conical. The roof angle was increased (to keep the total constructed area low) and the vent area decreased in order to decrease the exit to inlet area ratio. The reduction in exit to inlet area ratio was aimed at improving the inflation characteristics of the Type F canopy which indicated under-inflation in the Phase I tests. Although the C-1 model deployed prematurely, it indicated good inflation in the

subsonic flow conditions prevailing during tunnel shutdown. Examination of the canopy after the test revealed initiation of structural failure, and it was decided that the canopy with this low (0.16) exit to inlet area ratio would not survive supersonic test.

The model C-3a test followed. With an exit to inlet area ratio of 0.50, very good inflation was indicated (Figure II-19), although a very low frequency breathing was evident. The model was highly stable, with oscillation limits about the point of suspension of $\pm 2.5^{\circ}$. The low frequency inflation and collapse of this model is considered to indicate marginal inflation characteristics for the Mach number (M = 2.1) of this test. The canopy type C-2 test indicated fair stability and good inflation although examination of the Schlieren film indicated canopy damage shortly after deployment. This canopy had approximately the same exit to inlet area ratio as the type C-3, but with high inlet to maximum diameter ratio (0.9 compared to 0.7).

Test model G.S.-1 was designed to duplicate the Phase I test model modified guide surface Type A, which indicated excellent inflation in the Phase I tests. Since modifications of the roof geometry were contemplated in order to improve stability characteristics about the canopy center of gravity, this configuration was scaled to the Phase Ia model size and tested for comparative purposes. As in the Phase I tests, the canopy inflation proved to be excellent with instability about the point of suspension of $\pm 15^{\circ}$. Instability about the canopy center of gravity was not apparent in this test, due possibly to differences in canopy suspension system mass distributions as compared to the Phase I test.

Test model C.R.-1 was constructed with a non-porous inlet, and a hemispherical ribbon roof. The gore patterns for the roof were constructed from a 16-gore, 22.5 percent geometric porosity hemisflo design. This configurational study was suggested by the Phase I test performance of the reefed circular flat ribbon canopies, where good inflation and stability were shown at M = 3. The shaped conical inlet was employed to eliminate the excess skirt region material normally associated with a reefed parachute. In the test of this model, very poor inflation and severe breathing were evidenced. The poor inflation may be attributed to the high (0.80) exit to inlet area ratio.

Model G.S.-2 was designed to provide a reduction in the flat plate lift associated with model G.S.-1, by employing an annular vent. This canopy proved to be very well inflated, and exhibited a reduction in instability about the point of suspension (8°) as compared to model

Figure II-19. Schlieren Photograph of Phase 1a Model C-3a
Film Speed: 1,000 fps, M = 2.10, q = 705 psf,
x/d = 10

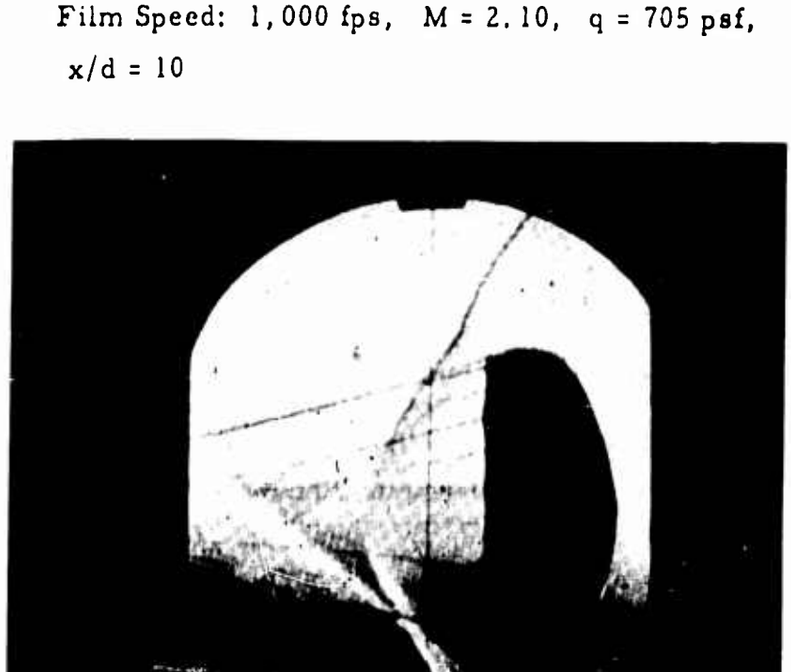

Figure II-20. Schlieren Photograph of Phase Ia Model C-6a. Film Speed:
1,000 fps, M = 2.13, q = 695 psf, x/d = 10

G.S. -1 (15°). Analysis of the Schlieren films for this test indicated a considerable amount of relative motion of the roof center disc with respect to the main canopy. Relative motion of this type could result in an unsymmetrical vent area distribution, hence, a further reduction in canopy oscillation about the point of suspension should result by providing a fixed vent area. It was decided to retest this configuration, giving some attention to improving the roof disc support.

The test model C-9 (roof modification of Type F) was studied next in the test series. This model has a similar vent construction to the model G.S. -2. Although premature deployment resulted in this test, the instability of the roof disc was marked, as in the case of test model G.S. -2. The use of a porous mesh material or a geodetic type of line suspension from the canopy to the disc to provide a uniform exit geometry was considered in succeeding canopy designs employing an annular vent.

In order to test the capability of a non "mil-spec" mesh material and also, the merits of a central vent, the test model G.S. -4 was designed. In this model, a 40 percent porosity nylon mesh was used. The mesh material filled nearly the entire roof, providing a central vent. In the test of this model, very good inflation was realized, and oscillation angles about the point of suspension (10°) indicated better stability than the G. S. -1 (15°) but poorer than the model G.S. - 2 (8°). The exit to inlet area ratio of this configuration is approximately the same as that for the model G.S. -2.

Canopy model G.S. -5 was designed to have the same exit to inlet area ratio as model G.S. -4, but with an annular vent filled with 40 percent porosity mesh to secure the roof center disc and maintain a fixed vent geometry. Analysis of the Schlieren films indicated that a reduced oscillation (9°) about the point of suspension resulted with this configuration as compared to canopy models G.S. -1 and G.S. -4. Excellent inflation of the canopy was realized, and the use of the mesh material appeared to provide a more uniform vent geometry.

Configuration C-5 was designed to represent a modification of the type F conical model. A flat roof with an annular vent providing an exit to inlet area ratio of 0.50 was used. This model was constructed of non-porous Vulcan material. A different means of securing the roof center disc was attempted in this model by employing a bicycle spoke arrangement of lines from the canopy to the disc. Schlieren film analysis indicated small (7°) canopy oscillations about the point of suspension. Rapid breathing and considerable relative

motion of the roof disc with respect to the main canopy were observed. The disc motion resulted in attachment line failure and ultimate destruction of the model prior to tunnel shutdown.

Model canopy C-6a was designed in order to evaluate the relative performances of a conical type canopy with the guide surface type construction. The model was designed to duplicate the geometry of the model G.S.-5 in inlet to maximum diameter ratio, inlet angle, roof geometry, exit to inlet area ratio and construction material. The model was constructed with a lower exit to inlet area ratio than that of G.S.-5, however. A much lower oscillation angle (5^{o}) resulted in the test, with excellent inflation (Figure II-20). This appeared to indicate that there is no specific contribution of the guide surface construction, except perhaps the unfavorable rotation tendency of this type of construction caused by asymmetries introduced in fabrication.

The model canopy C-9 was next tested in the Phase Ia series. This canopy was designed to be the conical equivalent of the design geometry of the Phase I modified guide surface model D. The Type D model was described in Section I, and as indicated in that section, proved to be the best performing configuration in the Phase I tests from the standpoint of inflation and stability characteristics. In the Phase Ia test of the model C-9, the canopy was not well inflated, although highly stable (1.5^{o} oscillation).

It was decided to design two model canopies with moderately high exit to inlet area ratios (0.5 and 0.6) to determine, if possible, the limiting area ratio for good inflation at the M = 2 condition. Test models C-7a and C-7b were designed with this in view. Model C-7b was designed with the same inlet geometry as models G.S.-1, G.S.-2, G.S.-4, G.S.-5 and C-6a. The roof is flat and consists of a 35 percent porosity mesh (Perlon) monofilament. The suspension lines are not carried over the roof, as in the case of C-7a. Examination of the Schlieren films of the C-7b test reveals a strong shock in front of the canopy when fully inflated with indications of severe shock wave suspension line boundary layer interaction. This type of shock wave structure appears to indicate unstable flow conditions ahead of the canopy. This was also observed in the test of Model C-3 previously described. A very low frequency canopy inflation and collapse (breathing) appeared to exist in the C-7b model test.

Schlieren films of the Model C-7a canopy test revealed a delayed opening of the canopy followed by a period of excellent inflation, stability (5^{o}) and shock wave structure (Figure II-21). Upon an angular

Figure II-21. Schlieren Photograph of Phase Ia Model C-7a.

Film Speed: 1,000 fps, M= 2.09. q = 704 psf, x/d = 10

excursion of approximately 5^{o} about the point of suspension, which brings the canopy in close proximity to the shock wave, the canopy collapsed and remained so for the remainder of the test film. It appears tha. the inflation characteristics of this configuration are marginal (for M = 2), causing it to be extremely sensitive to small disturbances. In contrast with this, examples of strong inflation characteristics are represented by the model C-6a which remained well-inflated and was insensitive to disturbances even up to 10^{o} of angular oscillation, and model G.S.-1 which remained well-inflated throughout angular excursions of 15^{o}.

A significant increase in the effective exit to inlet area ratio of several configurations was revealed by calculating this ratio on the basis of the inflated geometry of the canopy as revealed by the Schlieren photographs. For example, the model C-7b was constructed with an exit (open) to inlet area ratio of 0.46. During test, calculations based on surface area increase reveal the effective exit to inlet area ratio to be 0.53. Similarly, the model C-7a which was constructed with an exit - inlet area ratio of 0.42 had an effective exit - inlet area ratio of 0.52. The high dynamic pressure encountered during these tests (the order of 700 psf) was responsible for this material stretch.

The effect of exit - inlet area ratio on stability is shown in Figure II-22 where the stability appears generally to vary directly with this ratio for a given Mach number, as indicated by early tests. Also shown on this figure are several effective exit - inlet area ratios which are based upon the inflated geometry. An analytical treatment of supersonic parachute stability is beyond the scope of the present study.

In addition to the exploratory tests conducted in this program which led to the final configurational designs of high performance parachutes, a parachute which represented a parallel program of development at the University of Minnesota under the direction of Prof. Helmut G. Heinrich, was tested. This configuration (Figure II-23) consists of a solid cone to which a large vent flexible canopy is attached. Successful tests of this configuration have been conducted by the University of Minnesota at Mach 2 and Mach 3. Such tests have been normally conducted without a significant forebody, and have resulted in a stable shock configuration with an attached shock at the cone vertex. The test in the Cook Technological Center wind tunnel of a 4 inch maximum diameter model in the wake (x/d = 10) of a 2.75 inch cone-cylinder forebody (Figure II-12), provided a parachute diameter to forebody diameter ratio of 1.45. In this test, the canopy

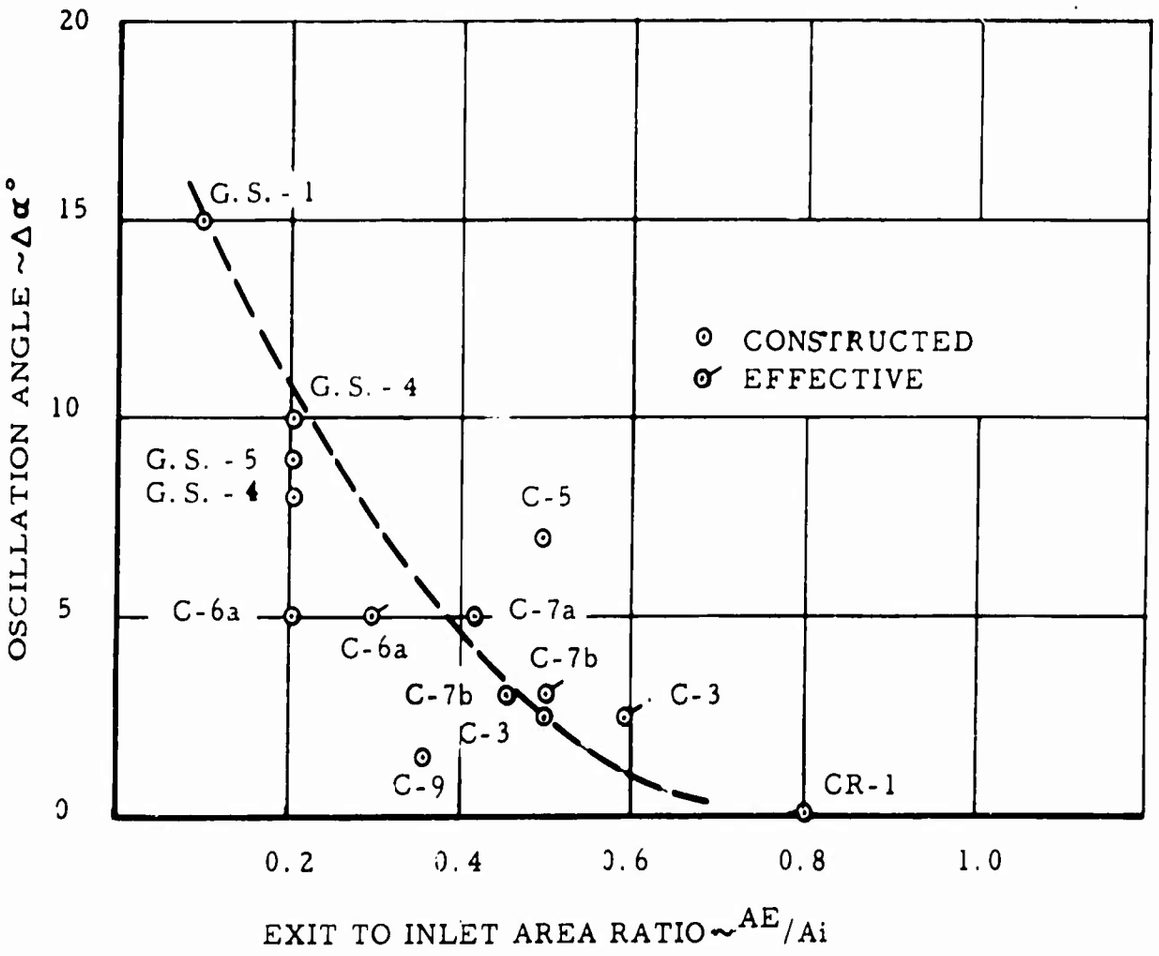

Figure II-22. Stability of Phase Ia Test Models vs. Exit to Inlet Area Ratio M_∞ = 2.0 x/d = 10

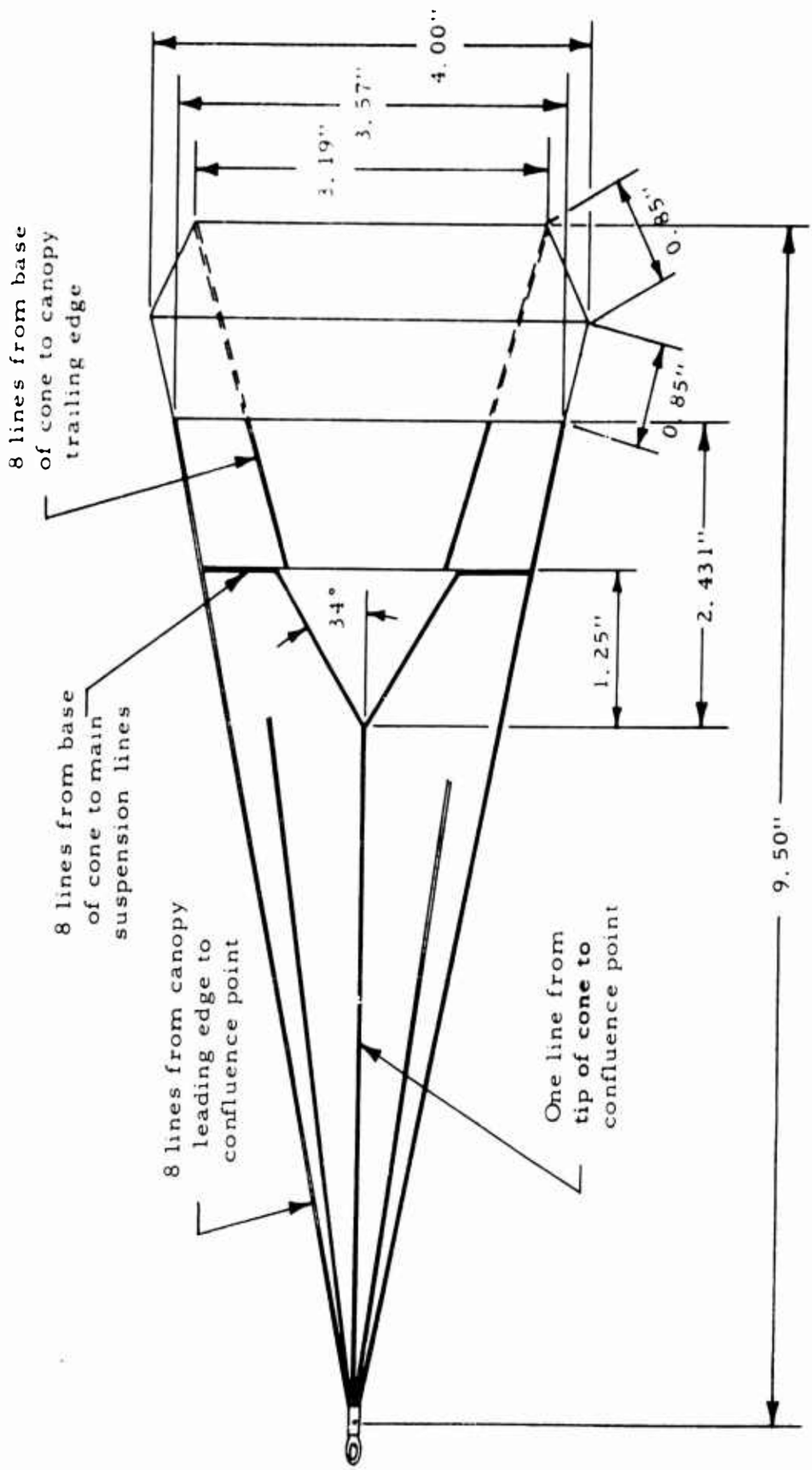

Figure II-23. Phase Ia Spiked Parachute Model

did not inflate properly, although it appeared that a proper selection of cone angle and cone position would provide the necessary geometry for a stable shock pattern if the wake flow properties for the x/d position at which the cone and canopy are positioned are considered. The primary advantage of this configuration consists of the application of a parachute-like decelerator of large diameter to forebody diameter ratio at supersonic speeds. As will be discussed later, the favorable effects of a forebody wake are essential to the satisfactory performance of a trailing parachute decelerator at supersonic speeds. The use of the cone is intended to provide the necessary favorable flow conditions ahead of the canopy for satisfactory operation. It may be noted (Figure II-23) that a distinct similarity exists between this canopy inlet shape and that of configurations C-6a and C-7a.

For parachute configurations which are constructed without a conical appendage such as is used in the "spiked parachute or cone-cup" configuration described above, satisfactory wake conditions may be provided, for example, by means of a small parachute in the wake of which a larger parachute is deployed.

Analysis of the Phase Ia tests indicated that the general use of a low porosity material in the canopy inlet region provides the necessary high inflation characteristics if the maximum inlet angle which is employed is limited to that which corresponds to the local flow direction ahead of the canopy. The length of the stabilizing inlet conical surface need not be large to provide stability for the low total canopy porosities tested. The conical extension used, however, is greater (even for models C-6 and C-7) than that previously employed on conventional extended skirt parachutes. The use of the flat roof of high relative porosity minimizes the area of the roof region and results in a low ratio of total cloth area to projected frontal area. The need for shaping a canopy in the direction of the expected inflated configuration appears unnecessary, since configurations such as C-6 and C-7 appear to adapt readily to a near-hemispherical shape when inflated.

The ratio of inlet diameter to maximum diameter may be large, resulting in correspondingly high drag coefficients.

The contribution of porosity distribution in the roof area was not clearly apparent as to its effect on over-all performance at the conclusion of the Phase Ia test program.

C. Phase II Parachute Test Program

1. Phase II Test Facility

This test phase was conducted in the Langley Research Center, large supersonic tunnel facility. The test section employed was the 4 foot x 4 foot Section 2 which is capable of a Mach number range of 2.3 to 4.65. A description of this test facility is given in Appendix III.

2. Selection of the Phase II Test Configurations

The results of the performance analysis of the various configurations in the Phase I and Phase Ia test programs provided the basic canopy shapes which were selected for the Phase II test program. In order to further evaluate the effects of the forebody wake on the parachute performance, model parachutes with inflated diameters of six inches in some models were selected to provide a comparison with the eight inch models. An inflated diameter of eight inches provides a parachute to forebody diameter ratio of approximately 3.33 and a parachute inflated diameter of six inches provides a 2.5 ratio of parachute diameter to forebody diameter. Although the model C-9 did not perform to expectations in the Phase Ia tests, it was decided to test this configuration in the Phase II program because of its superior performance in the Phase I tests. Also, in these latter tests, Schlieren movies were not obtained since the suspension lines of model D twisted due to rotation of the model before Schlieren coverage was initiated.

It was also decided that a ribbon roof configuration be tested in the Phase II program. The model C.R.-1 had not inflated, as discussed previously, due to the high exit to inlet area ratio. Furthermore, the use of the hemisflo roof design contributed considerable bulk to this portion of the canopy. In increasing the inlet area, by using a 0.9 inlet to maximum diameter ratio, and constructing a flat circular ribbon roof of porosity 16 percent, where the constructed diameter is the same as the inflated canopy diameter, an exit to inlet area ratio of 0.32 resulted. Except for the roof porosity distribution, the geometric characteristics of this configuration are similar to the model C-6a. This type of roof construction would be readily applicable to full scale applications if found satisfactory.

The model C-6a, which had superior performance in the Phase Ia tests, along with a modified (higher porosity vent) model (C-6b) were selected for the Phase II test program in order to evaluate the

performance of this model up to Mach 4. Model C-7a was selected, due to its marginal inflation characteristics at Mach 2, in order to evaluate the effects on its performance with increasing Mach number. This model was adaptable to a reduction in exit to inlet area ratio, due to its mesh roof construction, if the high Mach number tests indicate a requirement for this trend, although it was realized that testing under lower dynamic pressure conditions would result in a lower effective exit to inlet area ratio. By the addition of a non-porous central roof disc the maximum diameter of which is limited only by the diameter of the model, a wide range of exit - inlet area ratios could be provided. The model C-3 was selected because of its good performance in the Phase Ia tests, and also because of the good performance of the conical Type F of which it is a modification, in the Phase I tests. The model C-3a was further altered (C-3b) for the Phase II tests by the addition of a 45 percent porosity mesh which fills the vent, and the vent diameter was increased so as to provide the original exit to inlet area ratio. Figure II-24 is a photograph of the Phase II test models.

The design parameters of the Phase II test models are shown in Table II-11 and sketches and specifications of these configurations are shown in Figure II-25 and Table II-12. In addition to the models resulting from the Phase Ia tests, a conventional hemisflo type parachute was also tested. This is the same model used in the Phase I tests, and was retested to substantiate the results of that program.

The model C-6a was tested employing both the normal $2d_p$ C-6a (1) suspension lines as well as $1\ d_p$ lines C-6a (VIII). This configuration was also tested with both 8 inch and 6 inch maximum diameters. Test model C. R.-2 was tested employing both 8 inch (C.R.-2b) and 6 inch (C.R.-2a) models. Configurations C-3b, C-6b and C-9 were tested employing only 8 inch maximum diameter models and configuration C-7a was tested by employing a 6 inch maximum diameter model.

The canopy shapes, along with indicated modifications, which were considered for final testing in this program do not necessarily prescribe specific limitations to the geometric parameters for satisfactory performance over the range of Mach numbers considered. The optimum geometry for a decelerator application must necessarily represent a compromise in drag effectiveness, acceptable stability criteria, and system weight. In anticipation of attaining maximum drag effectiveness with low canopy weight, the general trend in the

TABLE II-11
PHASE II TEST MODEL DESIGN PARAMETERS

Test Model	Inlet Angle (Deg.)	Roof Angle (Deg.)	Maximum Diameter (In.)	Inlet Diameter (In.)	Inlet Porosity (%)	Roof Porosity (%)	Total Porosity (%)	Exit to Inlet Area Ratio	S/S_o p (4)
C-6a (I)	10	90	8	7.2	2.0	18.0	10.5	0.27	2.09
C-6b (II)	10	90	8	7.2	2.0	25.2	13.0	0.34	2.09
C-9 (III)	20	90	8	4.25	2.0	3.0	2.3	0.25	3.0
C-3b (IV)	20	45	8	5.6	0.0	20.6	9.2	0.50	2.53
C-6a (V) (1)	10	90	6	5.4	2.0	14.8	8.1	0.21	2.09
C-7a (VI) (1)	10	90	6	5.4	2.0	32.2	18.0	0.42	2.09
CR-2a (VII)	10	90	6	5.4	2.0	16.0	9.0	0.32	2.09
C-6a (VIII) (2)	10	90	8	7.2	2.0	18.0	10.5	0.27	2.09
CR-2b (IX)	10	90	8	7.2	2.0	20.0	11.0	0.36	2.09
Hemisflo (X)	N.A. (3)	N.A.	8	N.A.	N.A.	N.A.	25.0	0.72	2.62

(1) Phase Ia test models
(2) Same as C-6a (I) except with Id_p lines.
(3) Not applicable to this configuration
(4) Ratio of total surface area to frontal area.

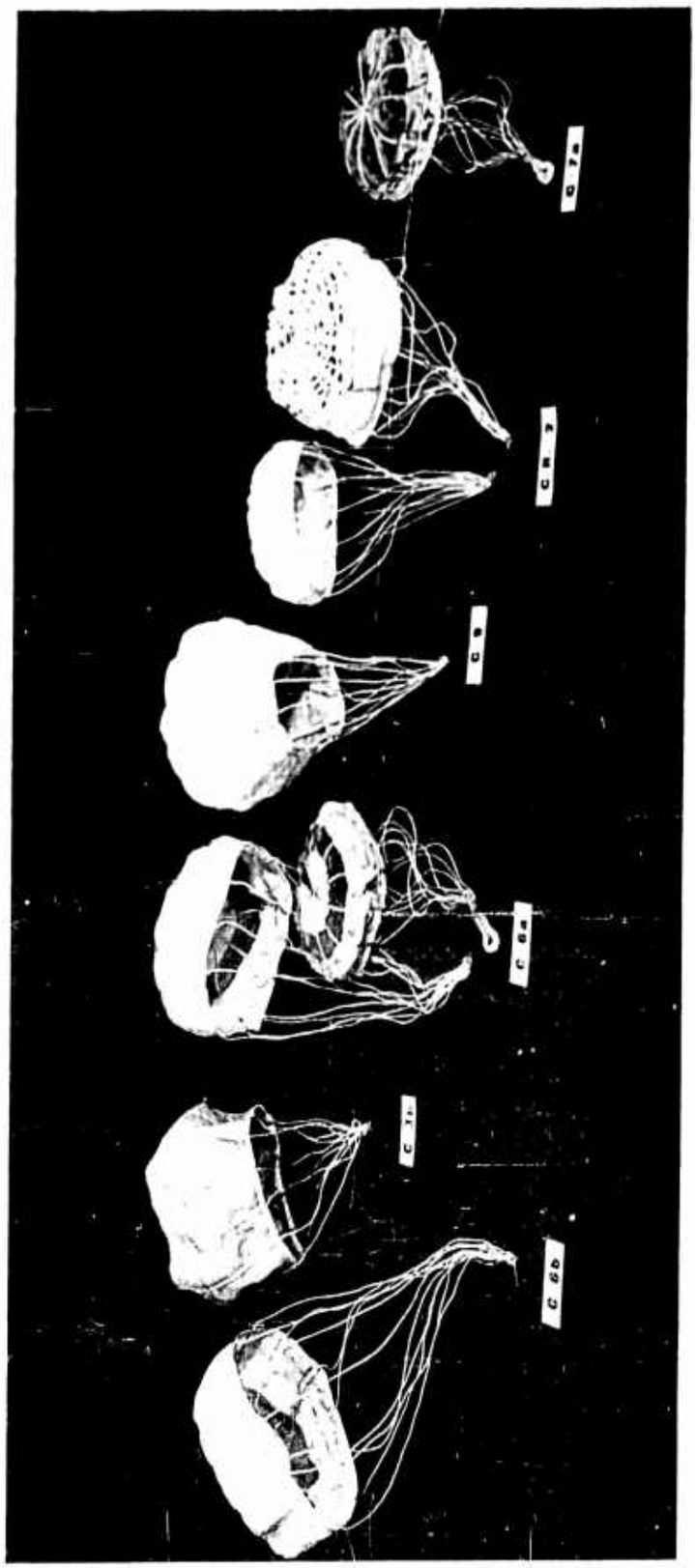

Figure II-24. Phase II Test Models

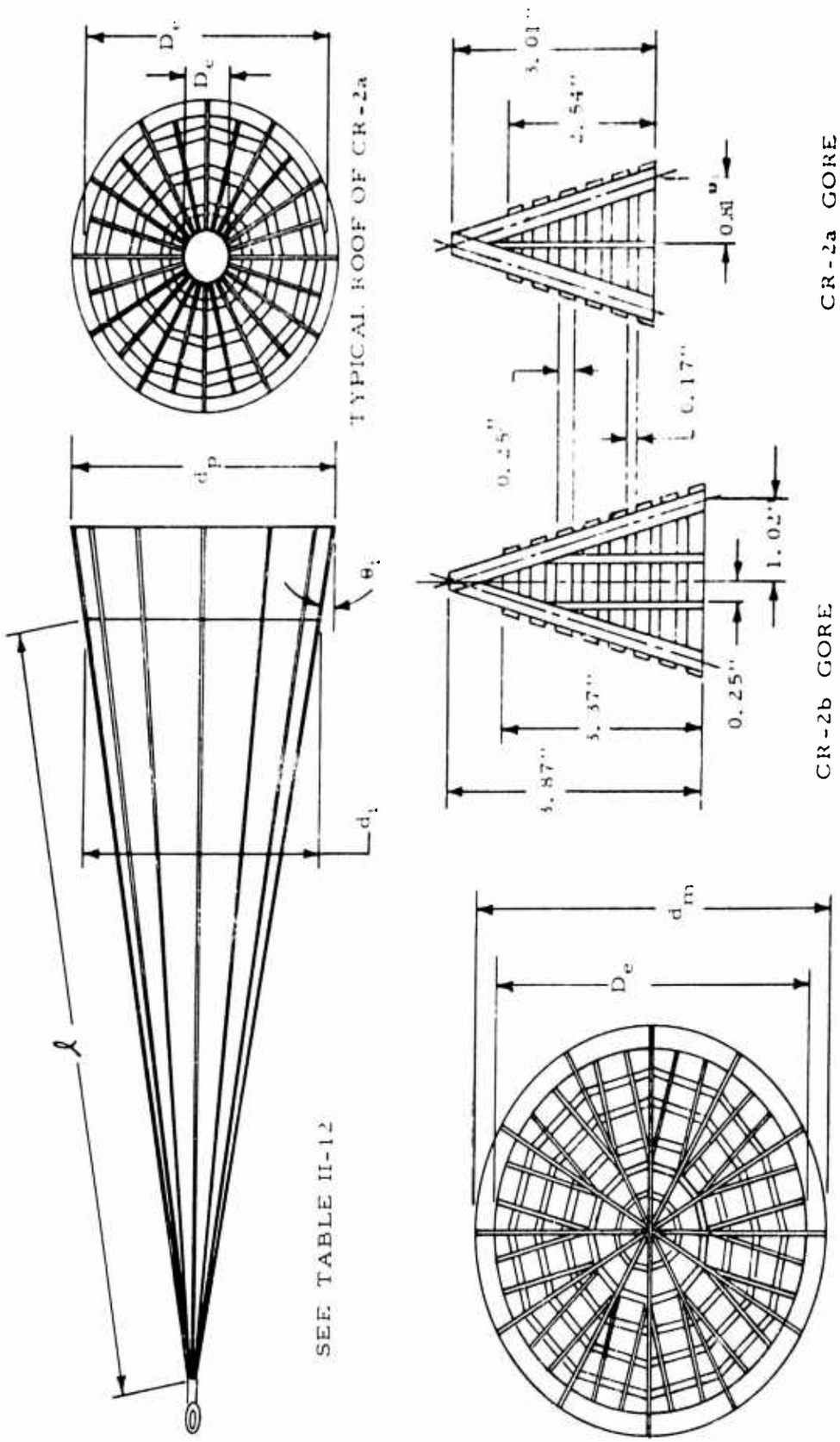

Figure II - 25. Phase II Conical Models C. R: - 2a and C.R. - 2b

TABLE II-12

PHASE II TEST MODEL SPECIFICATIONS

Type	d_p	d_i	D_c	D_e'	θ_1	θ_c	ℓ	Materials: Cone	Materials: S.L.	Materials: Roof	Notes	Refer to Figure
C-6a (I)	8	7.2	7.25	4.5	10^0		16	Cloth, Nylon MIL-C-8021 Type I	Cord, Nylon MIL-C-5040 Type I	Cloth, Nylon MIL-C-8021 Type II Mesh, Perlon Perfab No. 250/25	Annular vent filled with Perlon mesh.	II-18
C-6b (II)	8	7.2	7.25	4.5	10^0	-	16	Cloth, Nylon MIL-C-8021 Type I	Cord, Nylon MIL-C-5040 Type I	Cloth, Nylon MIL-C-8021 Type II Mesh, Nylon PA No. 5	Same as above except Nylon mesh is used in roof.	II-18
C-9 (III)	8	4.2	1.6	-	20^0	-	8	Cloth, Nylon MIL-C-8021 Type I	Cord, Nylon MIL-C-5040 Type I	Cloth, Nylon MIL-C-8021 Type II Mesh, Perlon No. 250/25	Cloth roof with mesh in standard vent	II-18
C-3b (IV)	8	5.6	5.9	-	20^0	45^0	8	Nylon, New prene coated No. 5809	Cord, Nylon MIL-C-5040 Type I	Mesh, Nylon PA No. 5	Nylon mesh roof	II-14
C-6a (V)	6	5.4	4.8	4.0	10^0	-	12	Cloth, Nylon MIL-C-8021 Type I	Cord, Nylon MIL-C-5040 Type I	Cloth, Nylon MIL-C-8021 Type I Mesh, Perlon Perfab No. 250/25	-	II-16
C-7a (VI)	6	5.4	6.0	-	10^0	-	12	Cloth, Nylon MIL-C-8021 Type I	Cord, Nylon MIL-C-5040 Type I	Mesh, Perlon Perfab No. 250/25	All mesh roof	II-16
CR-2a (VII)	6	5.4	5.2	1.0	10^0	-	12	Cloth, Nylon MIL-C-8021 Type II	Cord, Nylon MIL-C-5040 Type I	Ribbon, Nylon MIL-R-5608 Class C, Type I Cloth, Nylon MIL-C-8021 Type II	Ribbon roof	II-24
C-6a (VIII)	8	7.2	7.25	4.5	10^0	-	8	Cloth, Nylon MIL-C-8021 Type I	Cord, Nylon MIL-C-040 Type I	Mesh, Perlon Perfab No. 250/25 Cloth, Nylon MIL-C-8021 Type I	Annular vent filled with Perlon mesh	II-18
CR-2b (IX)	8	7.2	7.2	-	10^0	-	16	Cloth, Nylon MIL-C-8021 Type II	Cord, Nylon MIL-C-5040 Type I	Ribbon, Nylon MIL-R-5608 Class C, Type I Cloth, Nylon MIL-C-8021 Type II	Ribbon Roof	II-24
Hemis-flo (X)	-	-	-	-	-	-	16	--	--	--	Line length changed to $2\ d_p$	II-9

(This page is unclassified.)

selection of test model shapes for the Phase II test program was to explore those canopies which have high inlet to maximum diameter ratios, and low ratios of constructed to frontal areas.

3. Wind Tunnel Installation and Deployment Method

Test models were deployed in the wake of a cone-cylinder forebody (Figure II-26). In order to provide for the maximum use of wind tunnel time during a given tunnel run-up, use was made of a remotely controlled motor driven winch which, with the double strut mounted forebody, was equipment of the NASA Langley Large Supersonic Tunnel. This equipment made possible the rapid location of the test model at a selected distance aft of the forebody base.

Before deployment, models were stowed in a deployment bag which was secured near the forebody base with a break thread. The bag was connected by a line to a downstream tunnel strut which is capable of axial movement, (Figure II-27). To deploy the model, the externally controlled strut was moved downstream until the break line failed, allowing the parachute suspension lines to pay out and the bag to go downstream, deploying the parachute. This same general method of deployment had proved successful in the Phase Ia tests in the Cook Technological Center wind tunnel described in Part B.

4. The Phase II Parachute Test Program

The completed Phase II test schedule is shown in Table II-13. At each test Mach number, data was taken at either two or three canopy positions aft of the forebody base. Both force measurements and high speed (1000 fps) Schlieren movies were performed at each condition. The listing in this table is not in the chronological order of tests as performed. In general, models were deployed at the high Mach number which was successively reduced with the model deployed. In the high Mach number range (M = 4 to 4.65) test models were deployed at Mach 4. Although the large supersonic tunnel of the Langley Research Center is capable of a Mach number range of 2.3 to 4.65, three modes or compressor arrangements are necessary to accomplish this range. After deploying and testing a model in a given mode (e.g., M = 2.3 to 2.75), rather than accepting the loss of time associated with the tunnel shutdown and redeployment of the model in the next higher mode (M = 3.0 to 3.75), the model was left in the tunnel requiring it to survive the shock excursion through the test section during the mode change. This was accomplished successfully without model damage in all but two cases in the entire test program, and

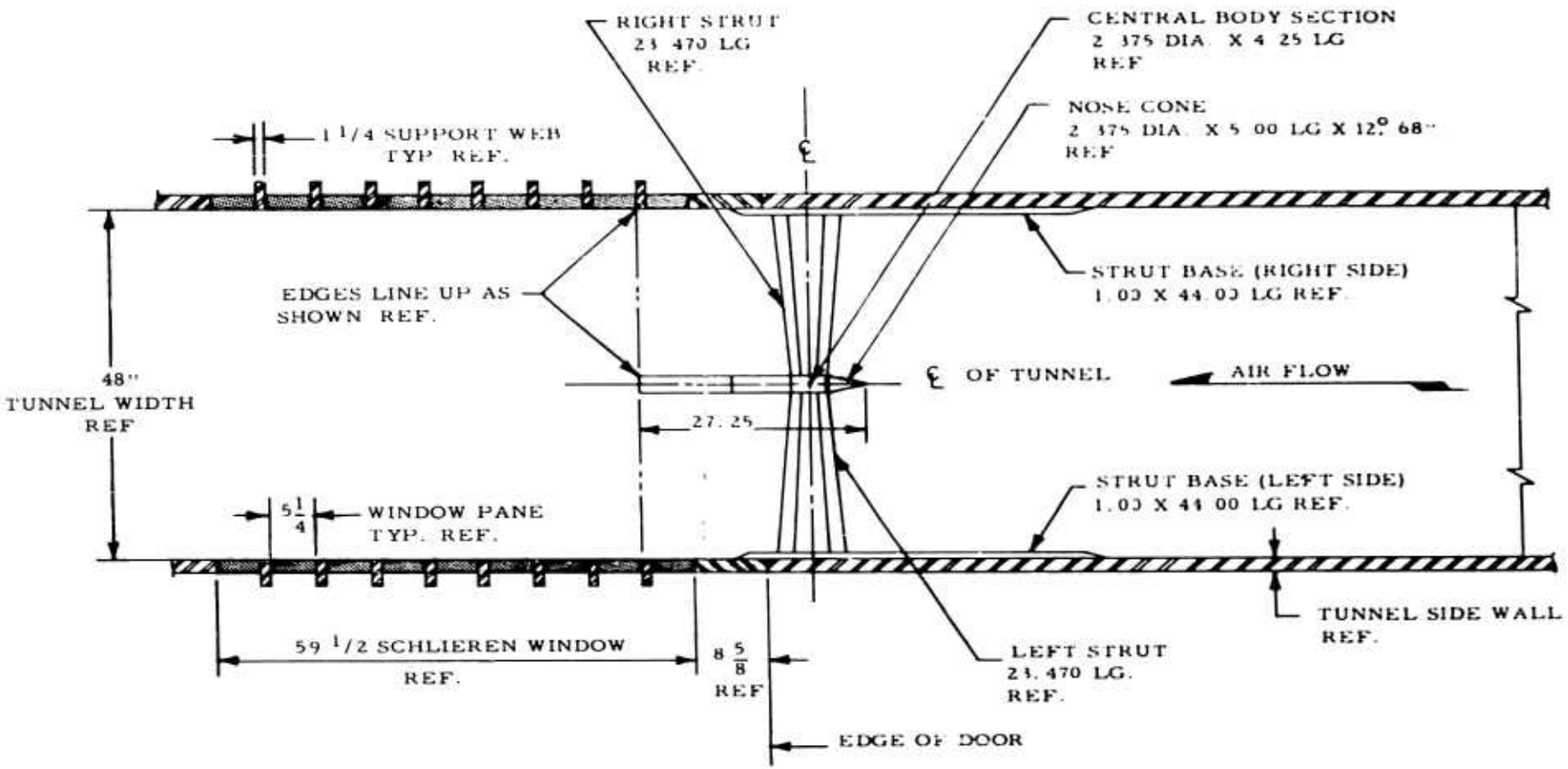

Figure II - 26 Phase II Forebody, Parachute Tests

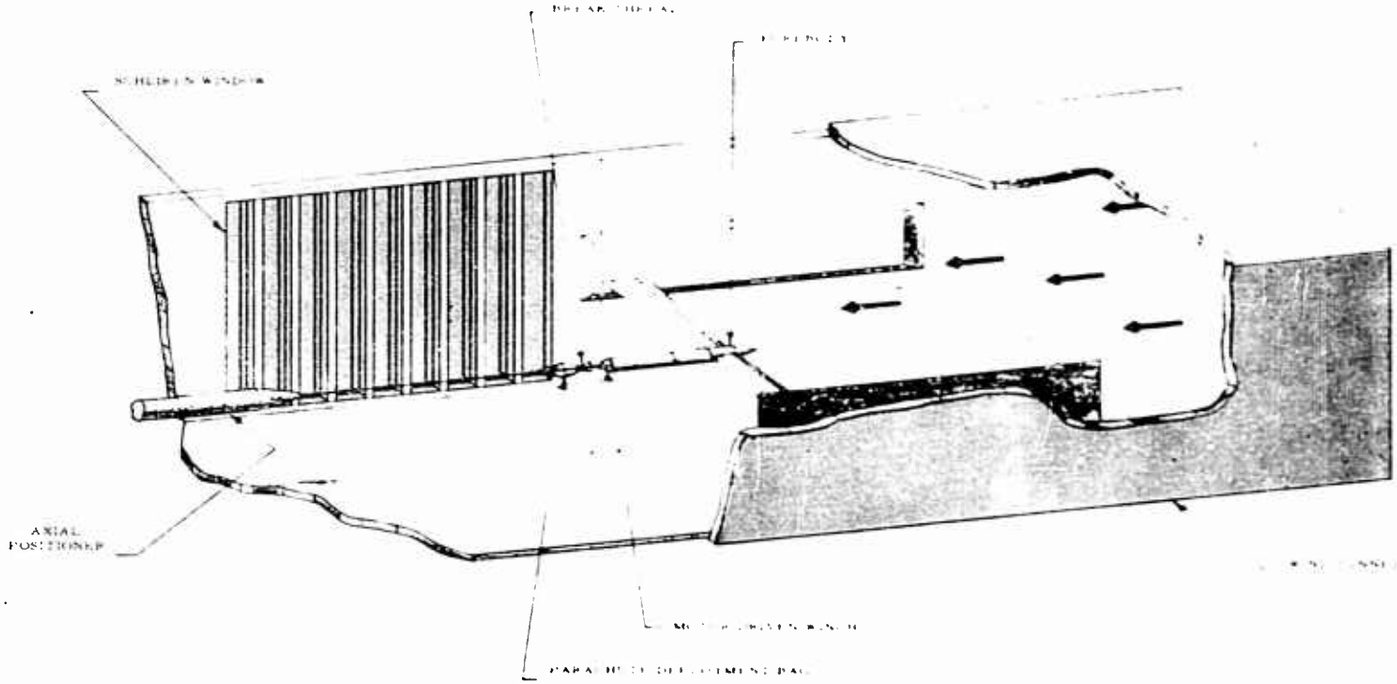

Figure II - 27 Phase II Parachute Test Installation

TABLE II-13

PHASE II - PARACHUTE TEST SUMMARY

Configuration	Max. Dia. (In.)	Mach No.	x/d	q_∞ (psf)
C-6a (I)	8	2.3	8	197
			10	
		2.75	9	136
			10	
			13	
		3.0	9	123
			10	
		3.2	9	103
			10	
		3.5	9	81
			10	
		3.75	8	65
			10	
		4.0	8	159
			10	
C-6b(II)	8	2.75	9	152
			10	
		3.00	9	123
			10	
		3.20	9	105
			10	
		3.5	9	81
			10	
		3.75	8	66
			10	

TABLE II-13 (CONT'D)

PHASE II - PARACHUTE TEST SUMMARY

Configuration	Max. Dia. (In.)	Mach No.	x/d	q_∞ (psf)
C.R.-2a (VII)	6	2.3	7	214
			10	
			12	
		2.75	7	152
			10	
			12	
		3.0	7	123
			10	
			13	
		3.2	7	105
			10	
			12	
		3.5	7	81
			10	
			12	
		3.75	7	66
			10	
			13	
C-6a (V)	6	2.5	7	220
			10	
			13	
			7	117
			10	
			13	
		2.75	7	96
			7	158
			10	
			13	

TABLE II-13 (CONT'D)

PHASE II - PARACHUTE TEST SUMMARY

Configuration	Max. Dia. (In.)	Mach No.	x/d	q_∞ (psf)
C-6a(V) (cont'd.)	6	3.0	7	124
			10	
			13	
		3.2	7	105
			10	
			13	
		3.5	7	81
			10	
			12	
		3.75	7	66
			10	
			13	
			10	79
		4.0	7	159
			10	
		4.3	7	149
			9	
			12	
		4.65	7	156
			9	
			12	
C-7a (VI)	6	2.3	7	214
			10	
			13	
		2.5	7	185
			10	
			13	
		2.75	7	152
			10	
			13	

TABLE II-13 (CONT'D)

PHASE II - PARACHUTE TEST SUMMARY

Configuration	Max. Dia. (In.)	Mach No.	x/d	q_∞ (psf)
C-7a (VI) (cont'd.)	6	2.9	7	134
		2.98	7	125
			10	
			13	
		3.2	7	105
			10	
			13	
		3.5	7	81
			10	
		3.75	7	66
			10	
			12	
		4.0	7	158
			10	
		4.3	7	149
		4.65	7	157
			10	
C-9 (III)	8	3.0	5	123
			7	
			10	
		3.2	4	105
			7	
			10	
		3.5	4	81
			7	
			10	
		3.75	5	66
			7	
			10	

TABLE II-13 (CONT'D)

PHASE II - PARACHUTE TEST SUMMARY

Configuration	Max. Dia. (In.)	Mach No.	x/d	q_∞ (psf)
C-3b (IV)	8	3.0	10	123
		3.2	6	105
			9	
			10	
		3.5	7	81
			10	
		3.75	7	74
			10	
C-6a (VIII)	8	2.5	7	185
			8	
		2.75	6	152
			7	
			9	
		3.0	6	123
			7	
			9	
		3.2	6	105
			7	
		3.5	6	81
			8	
		3.75	5	66
			8	
C.R. -2b (IX)		3.75	8	79
			10	
			12	
			10	143

TABLE II-13 (CONT'D)

PHASE II - PARACHUTE TEST SUMMARY

Configuration	Max. Dia. (In.)	Mach No.	x/d	q_∞ (psf)
Hemisflo (X)	8	2.3	8	214
			10	
			13	
		2.75	8	152
			10	
			13	
		3.0	8	124
			10	
			12	
		3.2	8	104
			10	
			13	
		3.5	8	81
			10	
			13	

contributed to the attainment of the large amount of data gathered in this program. The greatest contribution, however, was due to the favorable performance characteristics of the model canopies, since oscillations caused by improper design lead to rapid failure of model components. For example, one model canopy (C-7a) survived, with no apparent damage, four hours of operation in the Mach number range from M = 2.3 to M = 4.65 in this program, after having been used in the M = 2 high dynamic pressure tests in the Phase Ia test program conducted in the Cook Technological wind tunnel facility.

Several other models were subjected to several hours of tunnel operation with either little or no damage.

5. Results of Test Program and Data Analysis

a. Parachute Drag

As shown in Table II-13, three model configurations, namely C-6a (I), C-6a (V) and C-7a (VI), were tested from Mach 2.3 to 4.0, with the latter two models tested to M = 4.65. Most other models were tested only to Mach 3.75 due to limitation in available tunnel testing time. Drag coefficients based upon design dimensions are plotted versus Mach number in Figure II-28 for several configurations, and canopy positions. In this figure, it may be noted that drag coefficients for most configurations, reach a peak at M = 3.75 drop rapidly after this Mach number, and level off at Mach numbers above 4.0. A similarity to these data may be noted in Figure II-29 for the case of a solid cone with 45 degree half angle tested in the wake of a forebody. Figure II-29 is based on data from References 4 and 5.

It may be suspected in the parachute cases, that this effect is a reflection of either Reynolds number or dynamic pressure effects. This is strongly evidenced by comparing the tunnel dynamic pressures versus Mach number during the conduction of the Phase II program with the associated drag coefficients of two model configurations, shown in Figure II-30, where maximum drag coefficients for model configurations C-6a (V) and C-7a (VI) correspond to the minimum dynamic pressure at M = 3.75. The inflated diameters of these models, however, as measured from the Schlieren movies do not appear to vary significantly at M = 3.75 from those measured at other Mach numbers. For example, the average inflated to constructed diameter ratio for test model C-7a (VI) at Mach 3.75 is 0.89

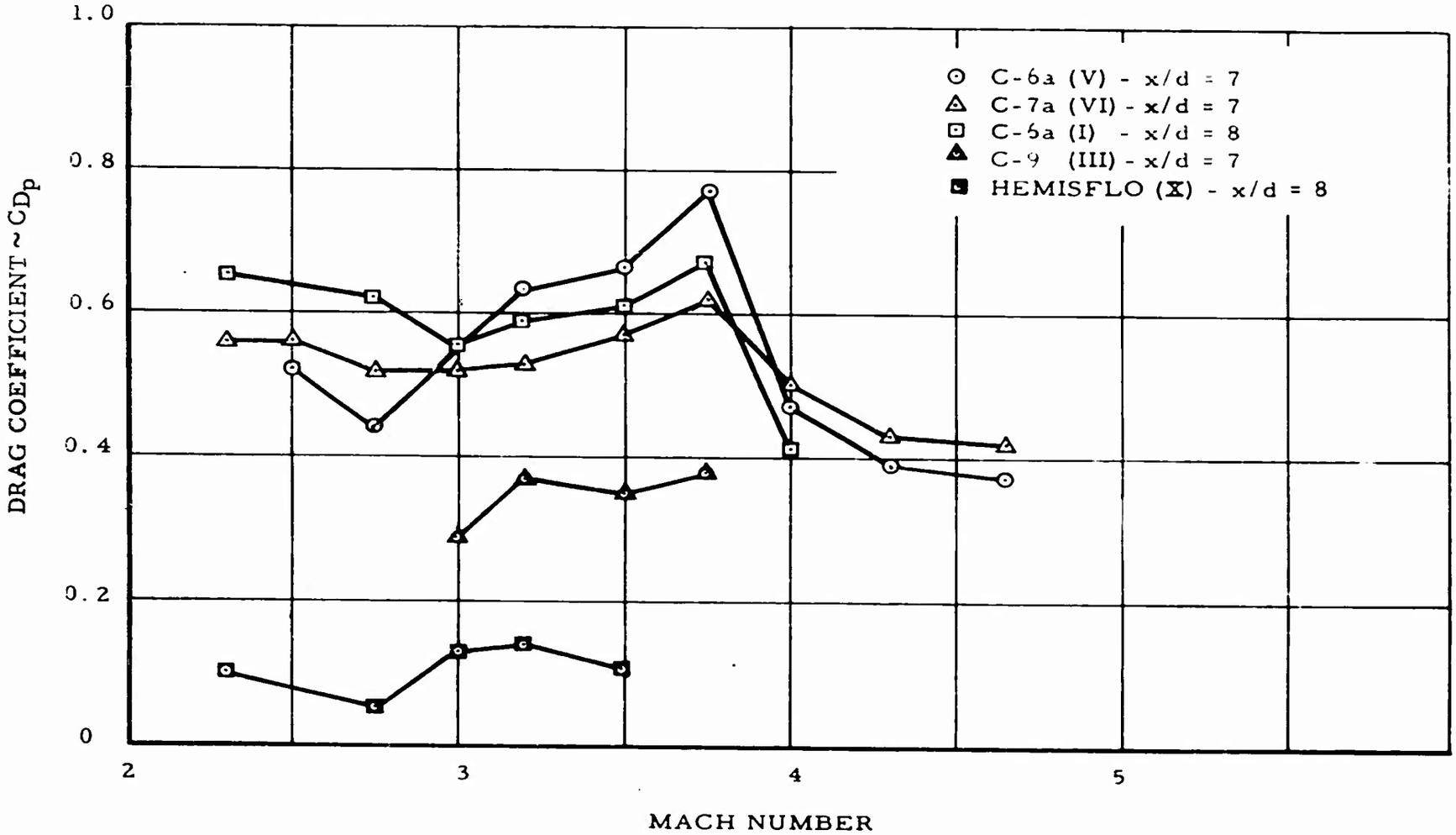

Figure II-28. Drag Coefficient vs. Mach Number, Several Phase II Models

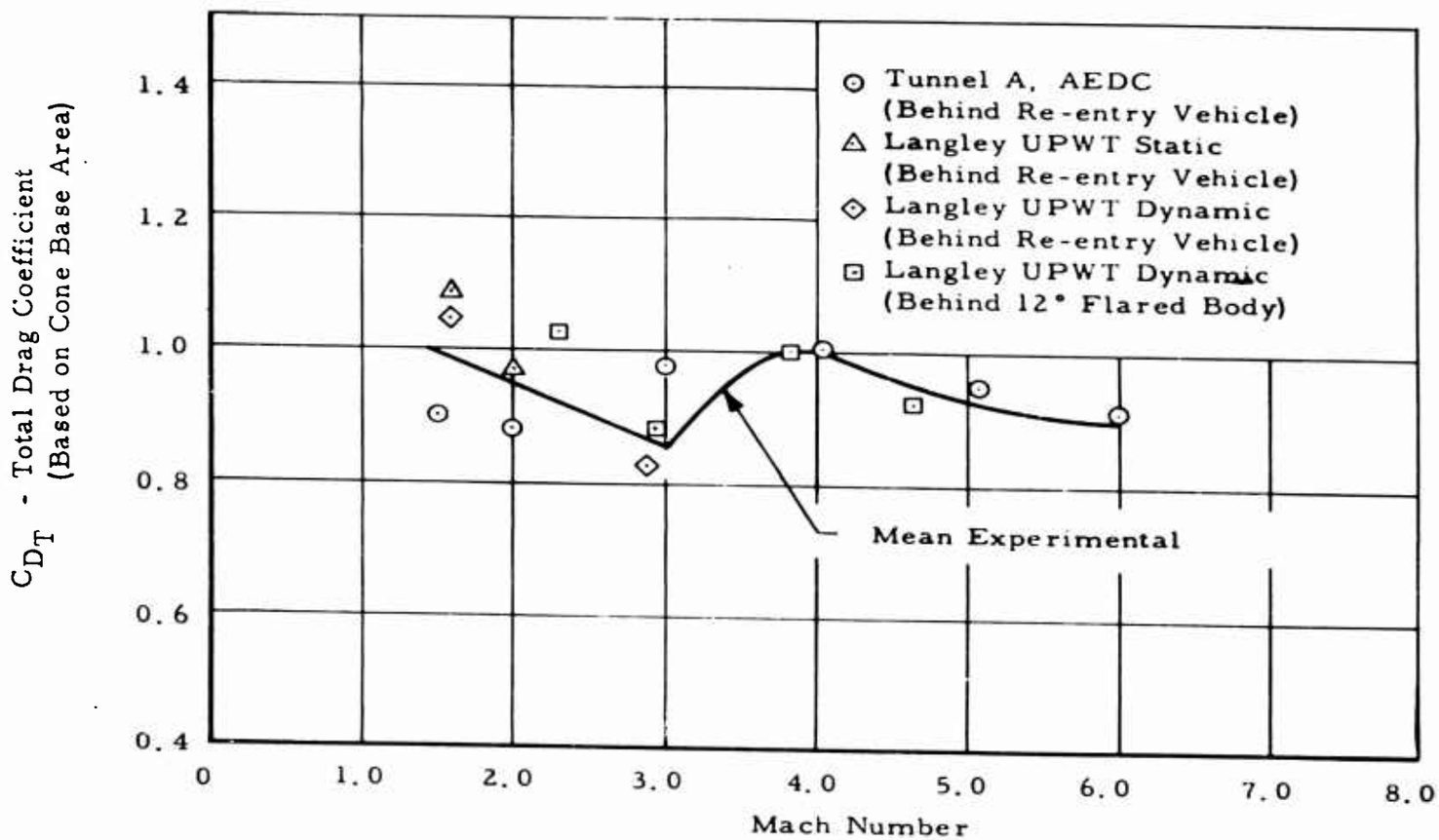

Figure II-29. Drag Coefficient vs. Mach Number of Solid 45° Half Angle Cone in Wake of Forebody

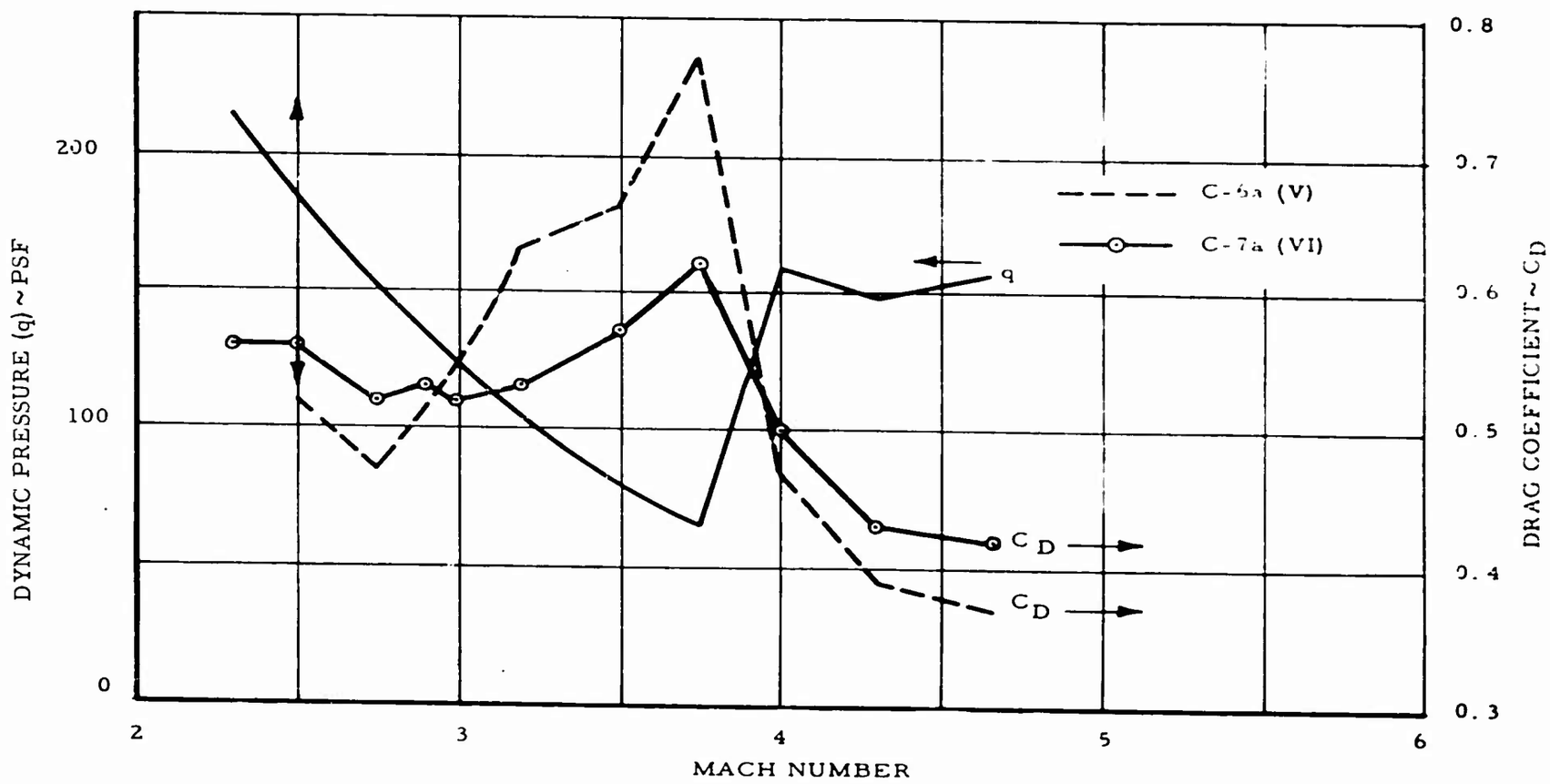

Figure II-30. Tunnel Dynamic Pressure and Drag Coefficient Vs. Mach Number for Two Phase II Test Models at x/d = 7

and the value of this ratio at Mach 4.0 is 0.90. A significant reduction in drag coefficient would normally be expected to be associated with a reduction in inflated area. The effect of Reynolds number on supersonic parachute performance has not generally been found to be significant in previous test programs. The tests involving solid cones referred to above were all conducted with Reynolds numbers per foot in excess of 2×10^6, which would be expected to represent turbulent flow conditions in these tests. Further study and testing is required to define the nature of the flow conditions in the Mach number range from 3 to 4 and above.

As stated in Reference 6, the qualitative characteristics of turbulent boundary layers in supersonic flows up to Mach 4 are similar to those in incompressible flow. At speeds above this value, new effects due to the coupling of turbulent velocity or vorticity field with the fluctuations in state variables become significant. Since the characteristics of the wake of a body are governed by the boundary layer properties of the body, these effects may correspondingly become significant in the performance of a trailing decelerator which is submerged, or partly submerged in the wake at high supersonic speeds.

In considering the drag effectiveness of the tested model canopies, reference may be made to Figure I-3. Flow deviation through the canopy shock was shown to result in the spreading of the wake after the shock into a conical region which extends to the canopy inlet. Within this region, an essentially constant pressure region exists which satisfies pressure boundary requirements across the normal portion of the shock on the wake centerline, and on the diverging flow boundary.

It may be expected that the drag of the canopy under these conditions is equivalent to the drag on a cone having the same half angle as that represented by conical diverged flow region. In Figure II-31 is shown the average conical shock wave angle as measured from Schlieren photographs of Model C-7a (VI) tests. Also shown is the half angle cone which would produce the equivalent drag to that measured in the tests, and the corresponding shock wave angles. Figure II-31 represents a canopy location of seven forebody diameters, and Figure II-32 is shown to represent similar characteristics at 9.5 forebody diameters aft of the forebody base. Corresponding measured and calculated shock wave angles are shown for the model configuration C-6a (I) in

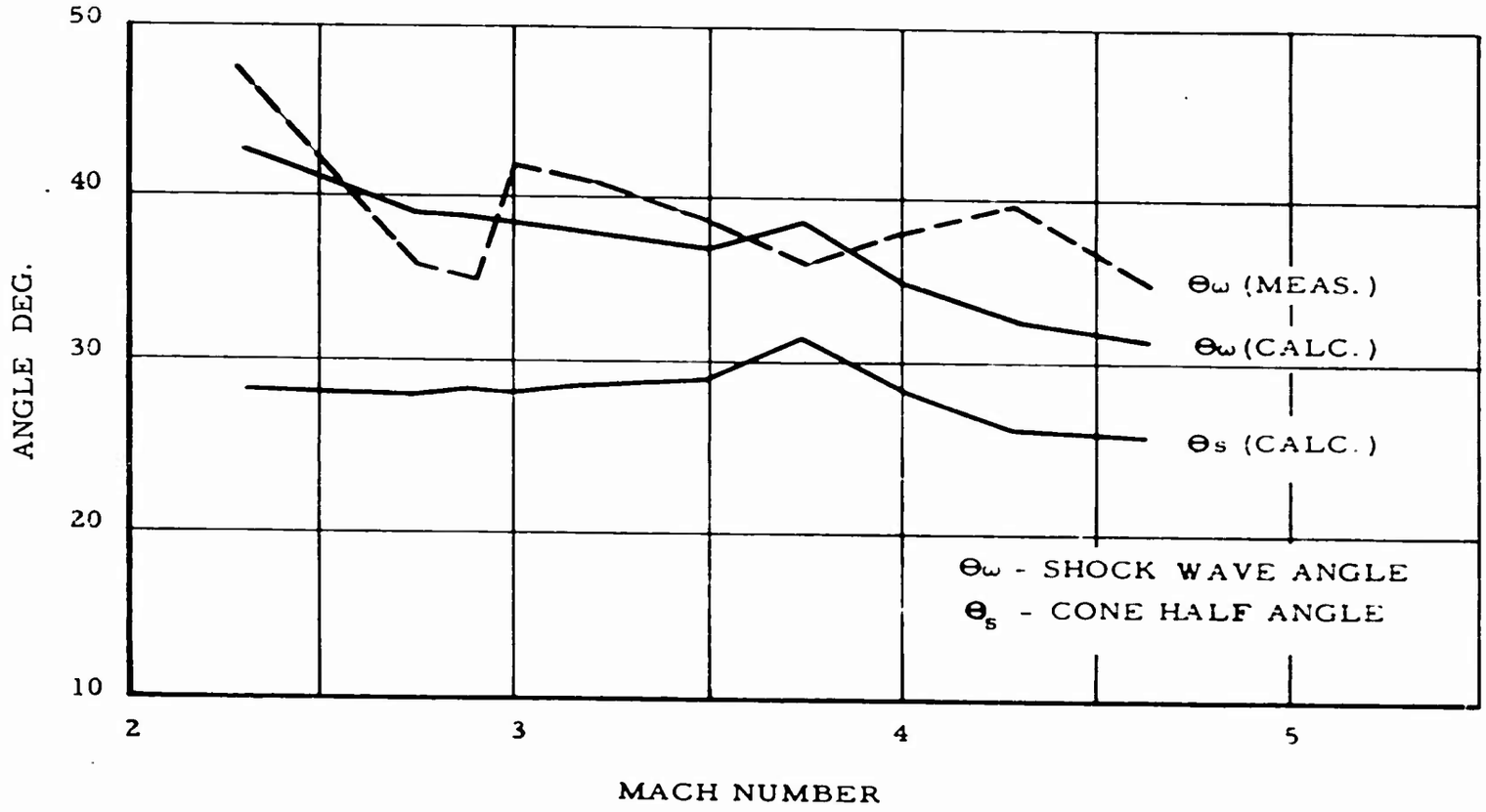

Figure II-31. Comparison of Measured and Calculated Shock Wave Angles Based Upon Drag Measurements Phase II Tests, Model c-7a (VI), x/d = 7

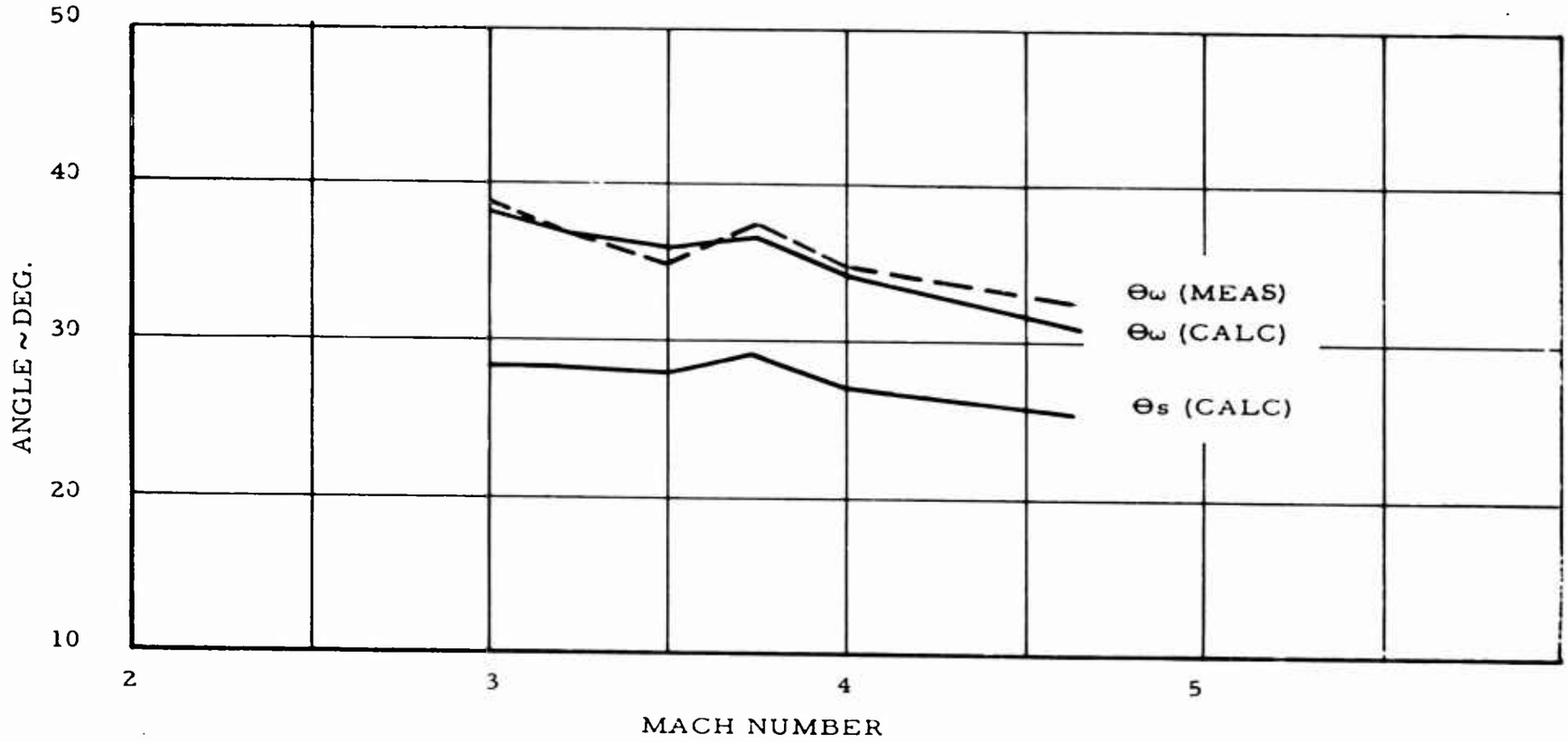

Figure II-32. Comparison of Measured and Calculated Shock Wave Angles Based Upon Drag Measurements Phase II Tests, Model C-7a(VI) x/d = 9.5

Figures II-33 and II-34.

That a stable flow condition may be maintained which satisfies pressure boundary requirements will now be discussed. By the employment of the methods to determine wake flow characteristics discussed in Section I-D, the pressure ratios across the normal portion of the canopy shock wave on the wake centerline are determined for various x/d locations aft of the forebody. These were determined by the procedure described in Section I for various free stream Mach numbers. Examples of these calculations are shown in Figures II-35, II-36, II-37, II-38. Conical surface pressure coefficients for various cone half angles at the corresponding free stream Mach numbers are also shown. The agreement of the above calculated data with the performance of configuration C-7a is shown in Table II-14 and illustrated in Figures II-35, II-36, II-37 and II-38. In Table II-14, equilibrium conditions (examples of which are shown in Figures II-35, II-36, II-37, and II-38.) are tabulated and corresponding half cone angles as determined by drag for configuration C-7a are shown. Close agreement of the calculated data is apparent. During the conduct of the Phase II tests, it was found that the canopy location had a very marked effect on the performance of all configurations tested, and optimum canopy locations appeared generally to be in region of 8 calibers or less aft of the forebody.

TABLE II-14

CORRELATION OF CALCULATED SHOCK VERTEX POSITION AND EQUILIBRIUM DIVERGED CONICAL REGION WITH PARACHUTE DRAG MEASUREMENTS FOR MODEL C-7a (VI)

M	Shock Vertex x/d	Equilibrium Half Cone Angle (Deg.)	Equivalent Drag Half Cone Angle (Deg.)
2.75	7.0	28.0	-
3.0	7.2	28.4	28.2
3.2	7.0	28.0	28.2
3.5	7.3	27.7	28.0
3.75	7.3	27.2	29.3
4.00	7.1	26.5	27.4
4.30	7.0	25.6	-
4.65	6.4	24.5	25.2

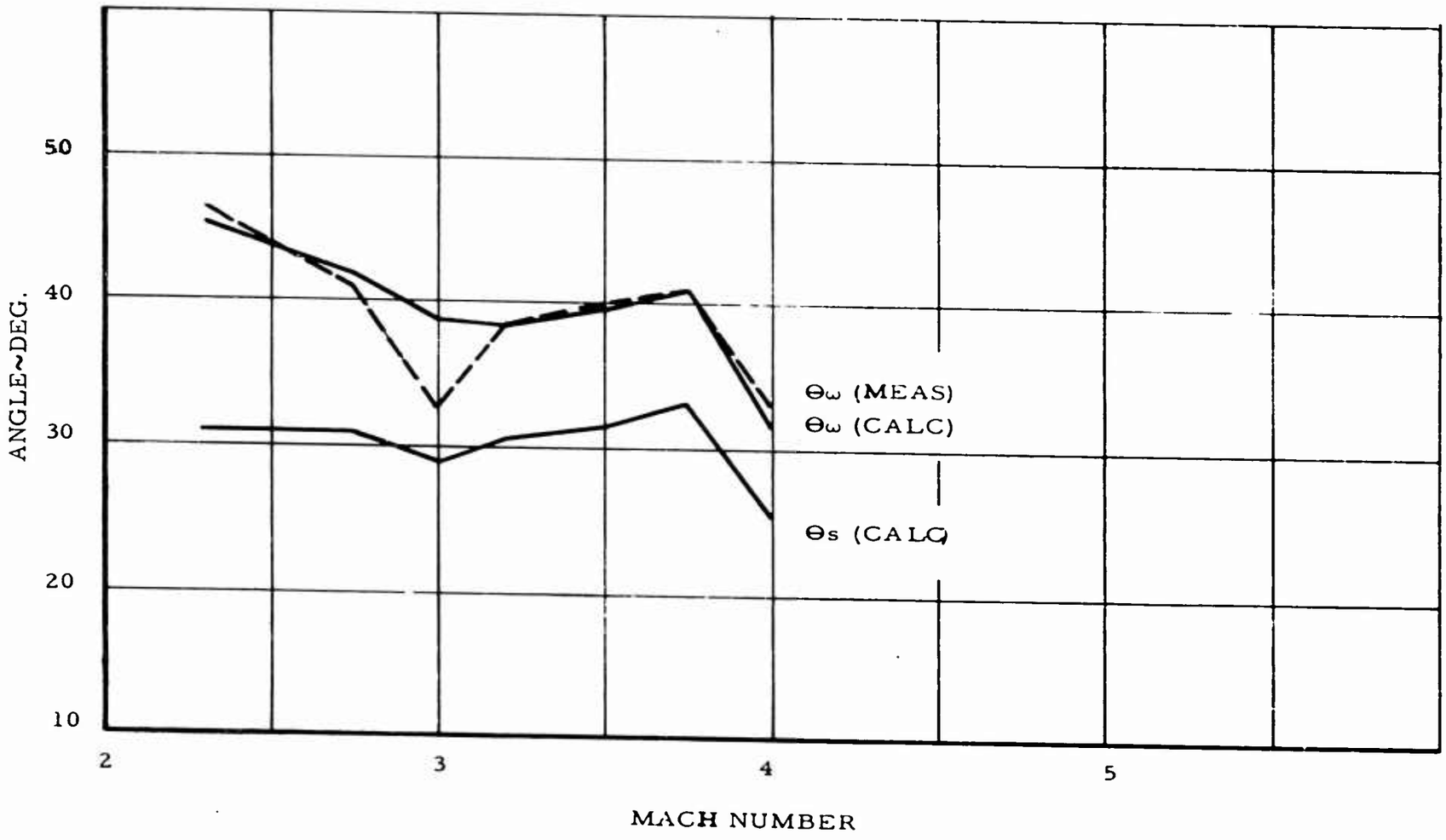

Figure II-33. Comparison of Measured and Calculated Shock Wave Angles Based Upon Drag Measurements Phase II Tests, Model C-6a(I) x/d = 8

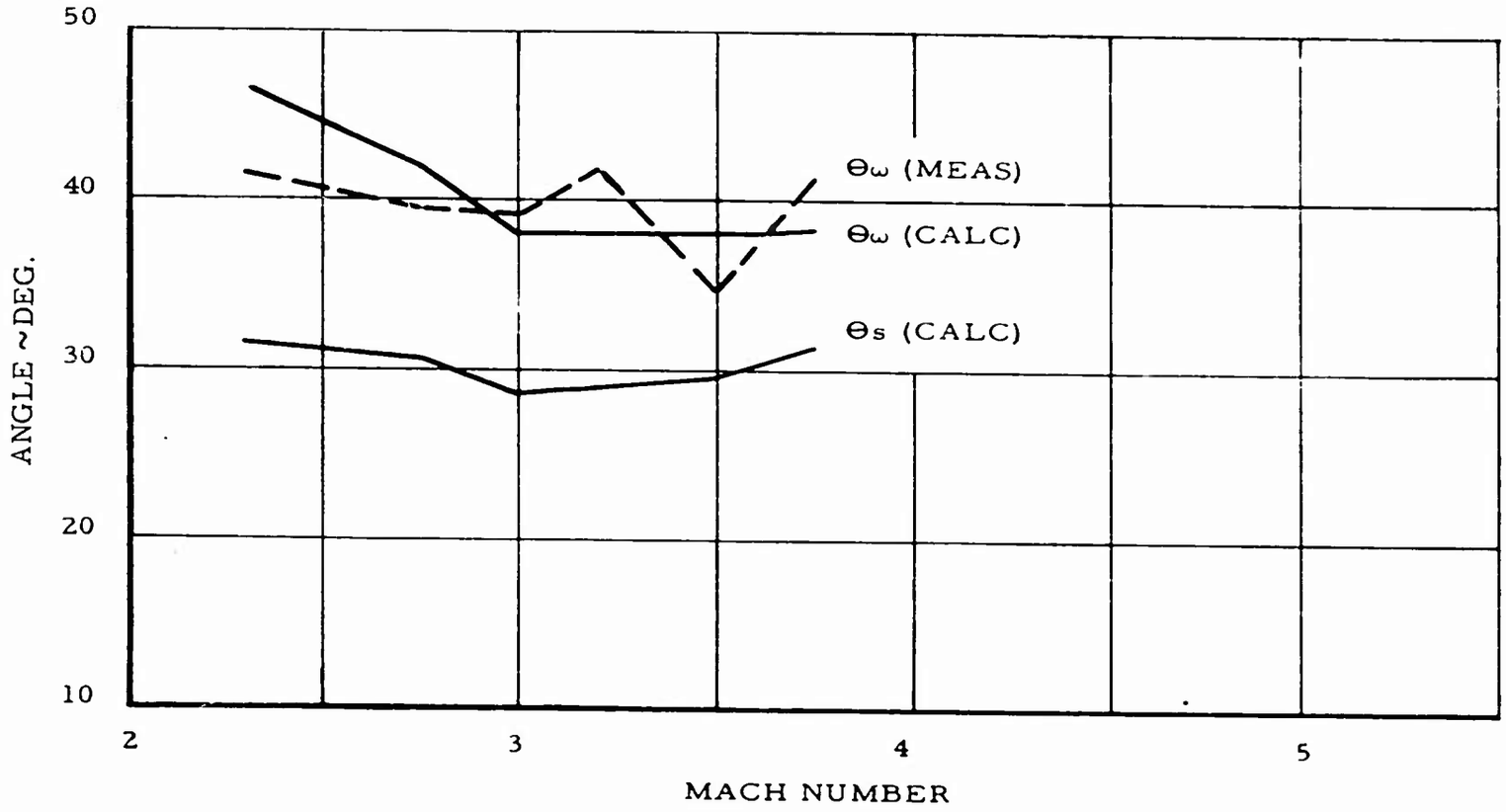

Figure II-34. Comparison of Measured and Calculated Shock Wave Angles Based Upon Drag Measurements Phase II Tests, Model C-6a(I) x/d = 9.5

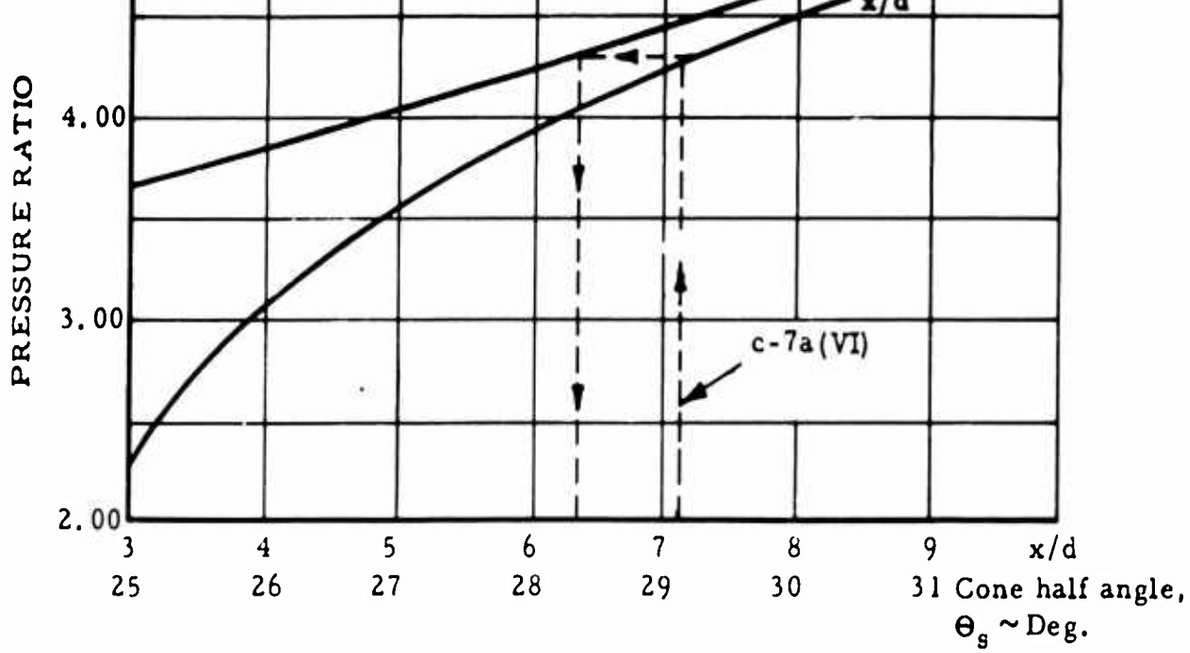

Figure II-35. Wake Centerline Normal Shock (Vertex) Pressure Ratio Vs. x/d, and Cone Surface Pressure Ratio Vs. Cone Half Angle at $M\infty$ = 3.00

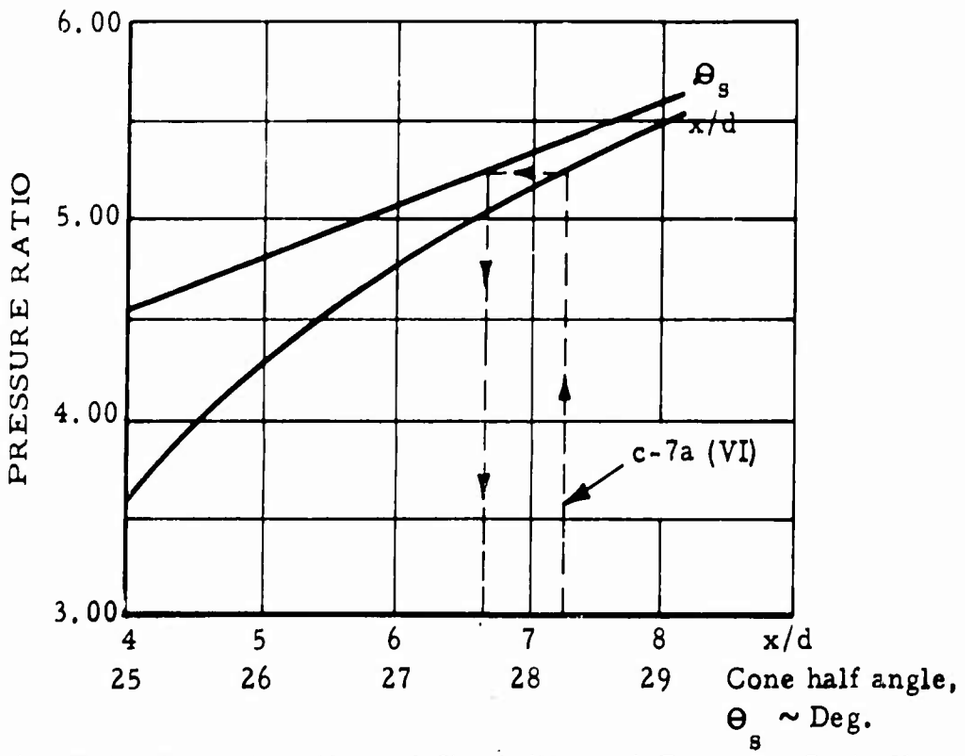

Figure II-36. Wake Centerline Normal Shock (Vertex) Pressure Ratio Vs. x/d, and Cone Surface Pressure Ratio Vs. Cone Half Angle at $M\infty$ = 3.50

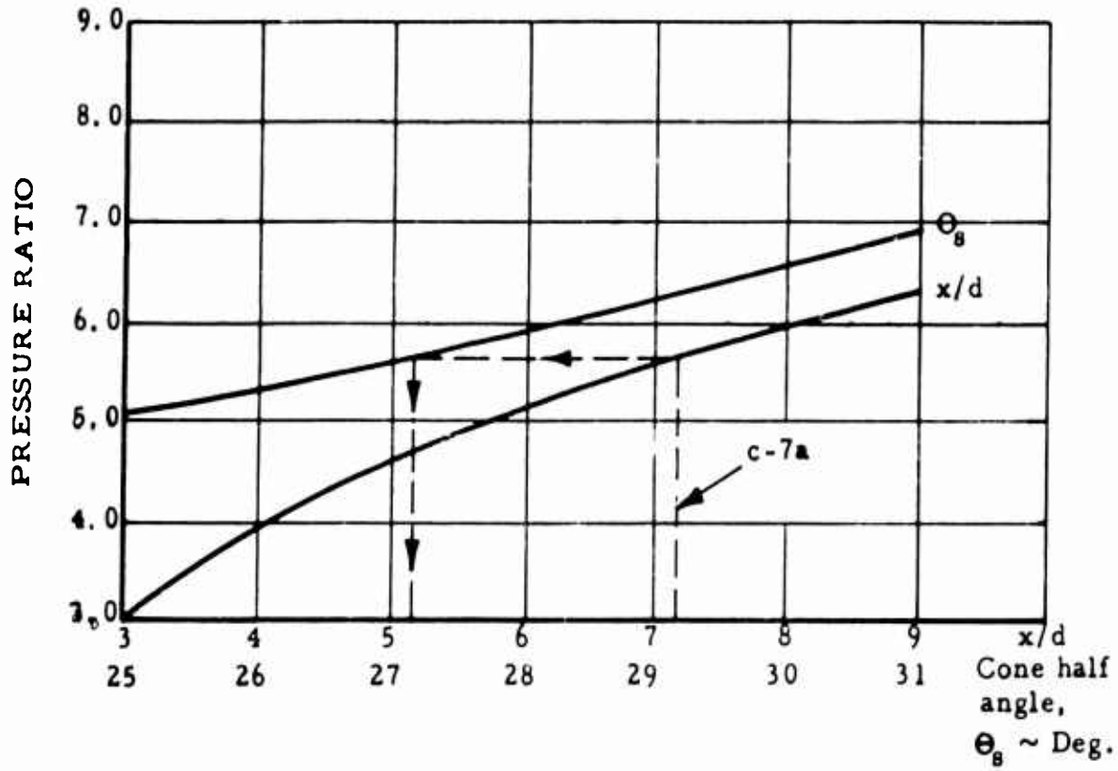

Figure II-37. Wake Centerline Normal Shock (Vertex) Pressure Ratio Vs. x/d, and Cone Surface Pressure Ratio Vs. Cone Half Angle at $M\infty = 3.75$

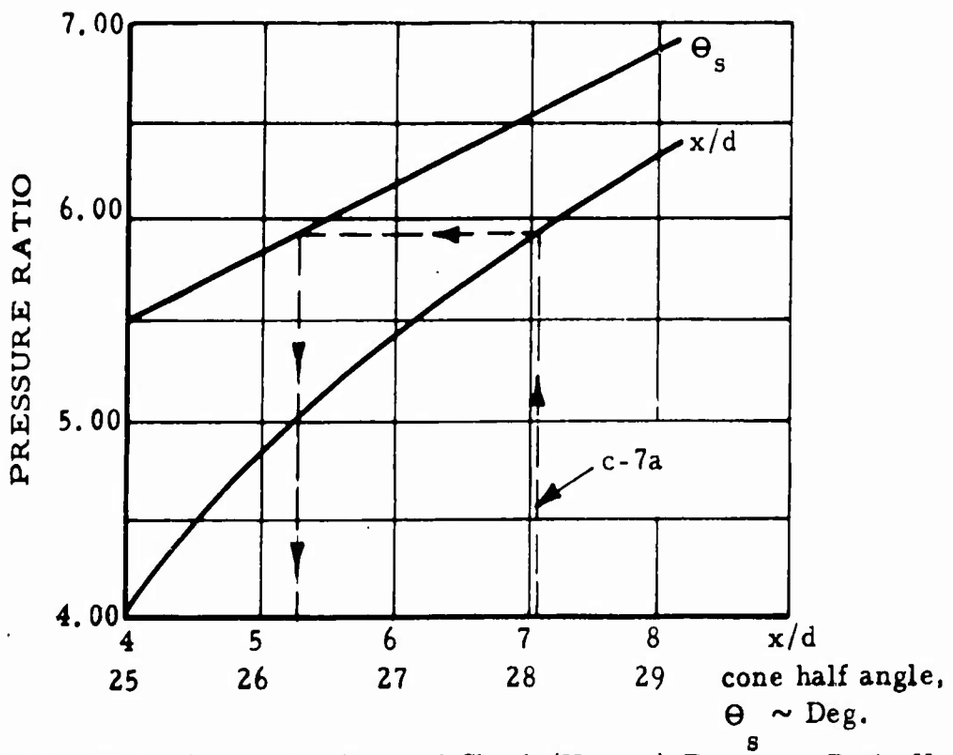

Figure II-38. Wake Centerline Normal Shock (Vertex) Pressure Ratio Vs. x/d, and Cone Surface Pressure Ratio Vs. Cone Half Angle at $M_\infty = 4.00$

Upon examination of Figures II-35 through II-38, it may be noted that as x/d is increased, the cone angle for equilibrium conditions also increases. Although the apparent deflection angles realized in the examined cases are greater than those through an oblique shock, the high pressures (near stagnation) existing within the canopy cause the flow to deviate further. It may be anticipated that there will be a limiting downstream canopy location for which stable flow conditions will prevail. This is premised on the assumption that the flow conditions described earlier are responsible for the excellent canopy performances realized, particularly at low x/d canopy positions.

A summary of performance data for the Phase II test program is given in Table II-15. Drag coefficients are based upon the actual constructed frontal area in all cases.

b. Parachute Stability

In general, the models tested in this program were highly stable with respect to the point of suspension. A definite trend, however, was noted in the stability of the canopy as a function of canopy location aft of the forebody. This was discussed previously in the subsection on parachute drag. One notable exception to the generally stable performance characteristics of the test models was configuration C-3b (IV) which exhibited quite violent instability about the point of suspension. Upon examination of the model after test, considerable damage was evident to the roof mesh material at one point near the mesh attachment point. Close examination of the Schlieren movies also indicated signs of failure in this area, but it is impossible to determine whether this damage occurred early in the tests, causing a destabilizing assymmetry to the vent. This model configuration was a slightly modified version of the Phase Ia Model C-3a, which exhibited high stability in the Phase Ia tests.

Measurement of oscillation angles for the test canopies was found to be complicated, particularly at large x/d canopy positions, by the introduction of secondary oscillations of a swivel which was used in the tests. Since the weight of the swivel (located at the confluence point) was comparable to the model canopy and suspension line weights, alternate oscillations of the two masses resulted. As a consequence, accurate quantitative measurements of oscillation angles of the model canopies about the point of suspension were not possible, except for the

TABLE II-15

PERFORMANCE SUMMARY OF THE PHASE II TEST MODELS

Test Model	Mach No.	x/d	Δa^o	d_m/d_c (averaged$_m$)	C_{D_c}
C-6a (I)	2.3	8.0	2.1	0.89	0.67
(d_c = 7.9 in.)		9.7	0.5	0.87	0.70
	2.75	8.5	4.2	0.87	0.64
		9.5	1.5	0.82	0.63
		12.5	5.0	0.85	0.57
	3.0	8.0	6.5	0.67	0.56
		9.5	7.5	0.81	0.54
	3.2	8.0	10.3	0.91	0.61
		9.5	7.5	0.87	0.55
	3.5	8.0	3.0	0.79	0.63
		9.5	8.0	0.85	0.57
	3.75	8.0	7.4	0.82	0.69
		9.0	6.6	0.81	0.62
	4.0	8.0	3.9	0.78	0.42
C-6b (II)	2.75	8.5	8.1	0.84	0.54
(d_c = 8.0 in.)		9.9	7.2	0.84	0.53
	3.00	8.2	3.2	0.83	0.53
		10.0	9.7	0.82	0.51
	3.20	8.5	8.4	0.83	0.56
		10.0	2.4	0.89	0.51
	3.50	8.5	10.0	0.87	0.60
		9.6	5.0	0.86	0.55
	3.75	8.4	5.7	0.88	0.67
		9.8	7.8	0.90	0.59
C.R.-2a (VII)	2.3	7.0	0.0	0.93	0.64
(d_c = 5.40 in.)		10.0	4.8	0.93	0.79
		11.8	2.4	1.05	0.79
	2.75	6.9	5.0	1.02	0.69
		9.7	4.9	1.04	0.77
		11.9	4.0	0.94	0.75

TABLE II-15 (CONT'D)

PERFORMANCE SUMMARY OF THE PHASE II TEST MODELS

Test Model	Mach No.	x/d	$\Delta\alpha^{o}$	d_m/d_c (average d_m)	C_{D_c}
C.R.-2a (VII)	3.00	6.7	2.9	0.94	0.67
(d_c = 5.40 in.)		9.3	4.1	0.96	0.70
(cont'd.)		12.2	5.1	0.97	0.73
	3.2	6.7	15.3	0.87	0.80
		9.8	10.0	0.92	0.69
		11.5	9.5	0.87	0.73
	3.50	6.8	12.1	0.96	0.83
		9.5	5.0	0.96	0.70
		11.5	2.7	1.00	0.64
	3.75	6.6	15.5	1.00	0.89
		9.7	4.7	1.00	0.74
		12.4	4.8	1.00	0.69
C-6a (v)	2.50	7.0	0.0	0.92	0.58
(d_c = 5.7 in.)		9.9	2.7	0.98	0.71
		12.8	5.0	0.97	0.70
	Low q	7.0	0.0	0.88	0.58
		9.3	2.3	0.91	0.73
		12.0	4.6	0.97	0.72
	2.75	7.0	0.0	0.89	0.49
		9.9	2.4	0.88	0.64
		12.5	3.8	0.93	0.64
	3.00	7.0	5.1	0.96	0.61
		9.7	3.0	1.00	0.60
		12.6	2.8	0.93	0.62
	3.20	6.5	9.2	0.93	0.70
		9.5	6.0	0.90	0.61
		12.0	6.0	0.95	0.61
	3.50	7.0	7.5	0.91	0.73
		10.0	2.9	0.90	0.61
		12.0	2.4	0.91	0.56

TABLE II-15 (CONT'D)

PERFORMANCE SUMMARY OF THE PHASE II TEST MODELS

Test Model	Mach No.	x/d	$\Delta\alpha^{o}$	d_m/d_c (average d_m)	C_{D_c}
C-6a (V)	3.75	7.0	2.7	0.93	0.85
(d_c = 5.7 in.)		10.0	4.1	0.97	0.71
(cont'd.)		12.0	1.4	0.97	0.61
	4.0	7.0	2.4	0.90	0.52
		10.0	3.8	0.91	0.55
	4.3	7.0	6.1	0.83	0.43
		9.1	4.5	0.93	0.48
		11.7	4.1	0.88	0.51
	4.65	7.3	3.9	0.88	0.41
		9.0	4.8	0.84	0.41
		11.7	0.61	0.86	0.44
C-7a (VI)	2.3	6.7	0.0	0.91	0.58
(d_c = 5.9 in.)	2.75	6.8	0.0	0.92	0.54
	2.90	6.8	0.0	0.88	0.55
	2.98	6.7	0.0	0.95	0.54
		9.5	4.5	0.90	0.54
		12.0	5.0	0.92	0.53
	3.2	6.8	2.5	0.92	0.55
		9.3	3.9	0.87	0.53
		12.5	0.4	0.88	0.53
	3.5	6.7	1.8	0.88	0.59
		9.5	2.8	0.87	0.52
	3.75	6.7	3.6	0.89	0.64
		9.5	1.8	0.90	0.56
		12.0	6.0	0.92	0.53
	4.0	6.8	0.0	0.90	0.52
		9.5	3.8	0.90	0.49
	4.3	7.0	3.4	0.80	0.45
	4.65	7.0	3.4	0.92	0.44
		9.0	4.8	0.83	0.41

TABLE II-15 (CONT'D)

PERFORMANCE SUMMARY OF THE PHASE II TEST MODELS

Test Models	Mach No.	x/d	$\Delta\alpha^{o}$	d_m/d_c (average d_m)	C_{D_c}
C-9 (III)	3.00	4.5	0	0.66	0.21
(d_c = 8.0 in.)		6.6	0	0.68	0.29
		9.6	0	0.68	0.27
	3.20	4.5	0	0.75	0.36
		6.5	0	0.77	0.37
		9.5	0	0.75	0.26
	3.50	4.5	0	0.70	-
		6.7	0	0.79	0.35
		9.6	0	0.77	0.27
	3.75	4.5	0	0.67	-
		6.8	0	0.74	0.38
		10.0	0	0.78	0.32
C-3b (IV)	3.0	9.8	Model Damaged		0.32
(d_c = 7.7 in.)	3.2	5.8	Model Damaged		0.40
		7.0	Model Damaged		0.38
		10.0	Model Damaged		0.38
	3.5	7.0	3.4	0.78	0.40
		10.0	7.1	0.74	0.37
	3.75	7.0	3.4	0.80	0.40
		9.5	-	-	0.34
C-6a(VIII)	2.5	7.0	11.8	0.68	0.39
(d_c = 7.9 in.)		7.5	1.3	0.67	0.37
	2.75	7.0	0.7	0.63	0.24
		7.5	8.5	0.56	0.25
		9.8	6.1	0.71	0.30
	3.0	6.9	0.0	0.71	0.23
		7.5	0.0	0.60	0.22
		10.1	1.7	0.68	0.24
	3.2	6.7	5.3	0.69	0.27
	3.5	6.1	0.0	0.81	0.32
		7.9	9.0	0.81	0.28

TABLE II-15 (CONT'D)

SPERFORMANCE SUMMARY OF THE PHASE II TEST MODELS

Test Models	Mach No.	x/d	$\Delta\alpha^o$	d_m/d_c (average d_m)	C_{D_c}
C-6a (VIII)	3.75	4.7	0.0	0.69	0.18
(d_c = 7.9 in.)		6.6	1.8	0.69	0.28
(cont'd.)					
C.R.-2b (IX)	3.75	8.0	7.0	0.88	0.69
(d_c = 8.0 in.)		10.0	4.8	0.83	0.54
		12.0	4.0	0.81	0.52
Hemisflo (X)	2.3	8.5	0	0.43	0.10
(d_c = 8.0 in.)		10.0	0	0.43	0.13
		12.7	1.5	0.43	0.14
	2.75	8.3	0	0.27	0.05
		9.7	0	0.34	0.06
		12.8	3.0	0.39	0.11
	3.0	8.3	1.2	0.46	0.13
		9.8	1.2	0.43	0.12
		12.7	0.9	0.45	0.13
	3.20	8.3	0	0.48	0.14
		9.8	1.0	0.47	0.15
		12.6	0	0.48	0.16
	3.50	8.3	0	0.48	0.11
		9.7	0	0.44	0.12
		12..7	0.9	0.48	0.12

minimum x/d positions where the swivel location was close to the base of the forebody. As pointed out previously, observations made at the time of the tests and also from the Schlieren movies indicated the general trend of increased stability with decreasing x/d canopy positions from an x/d of near 13 to an x/d of 7. For the six inch inflated diameter models with 12 inch suspension lines, the minimum x/d position which could be accomplished was slightly less than x/d = 7. For the 8 inch inflated diameter models with 16 inch suspension lines, the minimum distance was x/d = 4. However, in this latter case, configuration C-6a (VIII), violent instabilities were evidenced at x/d locations both greater and less than the range from x/d = 5.5 to 8. The proximity of the large diameter canopy to the wake trailing shock apparently caused the instability at x/d locations less than 5.5. Since the suspension line angle for this configuration is approximately 20° and the inlet cone angle is 10°, the suspension line inward load component is apparently greater than the net outward pressure differential at the canopy inlet, leading to indentations of some of the conical inlet panels. This was visually apparent during the tests of this configuration. For this short line length configuration, the wake conditions of the suspension line confluence point may also upset the equilibrium conditions described in the previous subsection. Large excursions of the shock wave were noted for this configuration with the most upstream position of the shock wave forward of the confluence point. Interaction of the canopy shock wave with the suspension line boundary layer could induce a pressure ratio across the shock which is sufficient (Reference 2) to separate a turbulent two dimensional boundary layer, resulting in a separated low energy flow region extending to the canopy inlet. In Table II-15, are listed oscillation angles about the point of suspension at the low x/d canopy positions, for Phase II test configurations.

c. Parachute Inflation

Inflation characteristics, except for test models C-9 and Hemisflo, were in general good. In particular, the 6 inch maximum diameter models were outstanding. In Figure II-39 are shown Schlieren photographs of test model C-7a (VI) at various Mach numbers, and in Figure II-40 are shown Schlieren photographs of test model C-6a (V). In Table II-15 are listed average inflated diameter to constructed diameter ratios for Phase II configurations. It may be noted that average inflated to constructed diameter ratios of the 6 inch diameter models are in general

M = 2.3, x/d = 7

M = 2.98, x/d = 10

M = 3.75, x/d = 7

M = 4.65, x/d = 7

Figure II-39. Schlieren Photographs of Phase II Model C-7a(VI) at Several Mach Numbers. Film Speed: 1,000 fps

M = 2.5, x/d = 7

M = 3.0, x/d = 7

M =3.75, x/d = 7

M = 4.65, x/d = 9

Figure II-40. Schlieren Photographs of Phase Model C-6a (V) At Several Mach Numbers: Film Speed 1,000 fps

greater than those for the 8 inch models. Also, the percentage of inflation of the 8 inch models with 16 inch lines are greater than those for the 8 inch model with 8 inch lines (C-6a (VIII)).

D. Summary of Test Model Performance

Those configurations which were characterized by a high ratio of conical inlet diameter to maximum diameter, a low cone inlet angle, a flat roof, with low inlet cone porosities and relatively high roof porosities were outstanding in performance characteristics in the Phase Ia and Phase II wind tunnel test programs. These configurations (such as models C-6a, C-6b, C-7a, C-7b, CR-2a and CF-2b) also represent the lowest ratio of total cloth area to projected frontal area (2.0). of all models tested. This ratio is also lower than conventional circular flat canopies which normally have a ratio of 2.25 in the speed ranges where they perform satisfactorily.

In the design of the models listed above, a wide range of flat roof constructions was employed. Total porosity ranges of these models were from 8 to 18 percent. Corresponding roof porosities ranged from 14 to 34 percent, and inlet porosities for all of the aforementioned models were low (2 percent).

Very little difference was noted in the relative performance of these configurations, although in general, those which exhibited the highest stability about the point of suspension were constructed with the highest total porosity (e.g., C-7a). This appears to confirm early data with respect to the effect of total porosity on stability. As pointed out previously, however, these differences were small even though a relatively wide range of total porosities was employed in the model designs.

The configurations C-6, C-7, and CR-2 resulted from a series of modifications of the Phase I test models A and B.

Although the model C-9, which evolved from the Phase I model D, did not perform outstandingly in the Phase Ia and Phase II test programs, it is felt that a considerable improvement in the inflation characteristics of this configuration would result if the ratio of inlet diameter to maximum diameter were increased. This particular configuration in such a modified version would be particularly adaptable to those applications where extreme stability of the trailing device is essential. Since the drag of a parachute is proportional to the inlet area, a compromise of required drag and stability could be attained with this configuration by an appropriate selection of the ratio of inlet diameter to projected diameter.

The Hemisflo configuration which was tested in the Phase I and Phase II test programs failed to inflate properly at any time in the speed range from M = 2.3 to 3.75. Since the high inflation characteristics of the Models C-6, C-7 and CR-2 were primarily attributed to the low porosities employed in the inlet region, as well as the low total porosities used, it is not surprising that this configuration did not inflate well. This is particularly striking since hemisflo parachutes, like most conventional ribbon constructions, are designed with the maximum localized porosities in the inlet and skirt regions and are generally constructed with relatively high total porosity. It is not expected that a mere reduction in total porosity of this canopy would result in its satisfactory performance, since a porosity distribution such as to provide low values in the inlet area have been demonstrated in this program to be desirable.

SECTION III

SYMBOLS AND NOTATION

A	Wake parameter
a	Speed of sound
a, b, c	Constants for streamline fitting in Section III-E
B	Wake parameter
C_p, C_V	Specific heats at constant pressure and constant volume, respectively
d	Diameter of body
f	Function representing entire streamline
K	Correction factor for boundary conditions at shock wave
k, l, m	Constants for normal fitting in Section III, E
ℓ	Reference length
M	Mach number
n	Arc length of normal
P	Point in flow field
p	Pressure
Q	Infinitesimal quantity
R	Gas constant
r	Number of points used in least squares fit
S	Entropy
s	Arc length on streamline

SYMBOLS AND NOTATION (CONT'D)

T	Temperature
V	Velocity
x, y	Cartesian coordinates
α, β	Orthogonal curvlinear coordinates
γ	Ratio of specific heats
δ	Deflection angle of streamline through shock wave
ϵ	Constant
ζ	Infinitesimal quantity
η	Function representing entire normal
θ	Angle of flow direction
ρ	Density
ψ	Stream function
ω	Shock wave angle

SUBSCRIPTS

i	Streamline index
j	Normal index
s	Quantities immediately behind the shock wave
o	Total flow conditions of undisturbed flow
∞	Freestream conditions
1, 2	Quantities before and behind shock wave, respectively

SUPERSCRIPTS

h	Level of iteration

SECTION III

ANALYTICAL STUDY

The purpose of the theoretical phase of this program was the establishment of a procedure whereby feasible parachute shapes could be predicted analytically.

In order to accomplish the above, it was necessary to decide upon a technique or techniques for solving the flow equation for all regions downstream of the bow shock wave. One approach would have treated each of the subsonic, transonic, and supersonic regions individually, thereby requiring three different analytical techniques. A second approach was one whereby one technique would treat all three regions. In addition, this approach would correct the shock shape and shock standoff distance. Because of the provision rendered for shock adjustment and the obvious advantage of one rather than three different analytical techniques, the second approach was adopted.

The approach adopted is the method of flux analysis due to Uchida and Yasuhara. This is a method for finding exact numerical solutions for the direct problem in which the shape of a blunt body in a uniform supersonic flow is given and the shape and location of the detached bow shock and field behind it are unknown.

The method was modified appreciably so that it would provide the initial approximation to the flow field as well as successive corrections to it. In the modification, some features of the inverse problem were utilized. The inverse problem is one whereby the shape of the shock wave is given and the shape of the body and details of the flow are unknown.

The approach was entirely mechanized, however, it was found to present certain difficulties impractical to circumvent within the time of this program. No reasonable way was found to make compatible elements of the inverse and direct approaches.

Consequently, recourse was taken to a semigraphical method paralleling that indicated in Reference 7, which is described below.

A. Shock and Compressible Flow Relations

1. Uniform Upstream Field

For the case of the uniform upstream flow the shock conditions

necessary in the field and shock calculations are obtained from the standard shock and flow relations as follows:

For a given environment and vehicle Mach number the following parameters are known:

$$M_1,\ T_1,\ p_1,\ \rho_1$$

Using these, the remaining parameters can be calculated:

$$T_o = T_1\ (1 + 0.2M_1^2) \qquad \text{III-1}$$

$$V_1/a_o = M_1\ (1 + 0.2M_1^2)^{-1/2} \qquad \text{III-2}$$

$$p_2/p_1 = (7M_1^2 \sin^2\omega - 1)/6 \qquad \text{III-3}$$

$$p_2 = p_1\ (p_2/p_1) \qquad \text{III-4}$$

$$\rho_2/\rho_1 = 6M_1^2 \sin^2\omega/(M_1^2 \sin^2\omega + 5) \qquad \text{III-5}$$

$$\rho_2 = \rho_1\ (\rho_2/\rho_1) \qquad \text{III-6}$$

$$M_2^2 = \left[36M_1^4 \sin^2\omega - 5(M_1^2 \sin^2\omega - 1)(7M_1^2 \sin^2\omega + 5)\right] / \qquad \text{III-7}$$

$$\left[(7M_1^2 \sin^2\omega - 1)\ (M_1^2 \sin^2\omega + 5)\right]$$

$$T_2/T_1 = (7M_1^2 \sin^2\omega - 1)(M_1^2 \sin^2\omega + 5)/36M_1^2 \sin^2\omega \qquad \text{III-8}$$

$$V_2/a_o = \left[M_2^2\ (T_2/T_1)\ (T_1/T_o)\right]^{1/2} \qquad \text{III-9}$$

$$1/\tan\delta = \tan\omega\left\{\left[1.2\,M_1^2/(M_1^2\sin^2\omega - 1)\right] - 1\right\} \qquad \text{III-10}$$

2. Non-Uniform Upstream Flow

In the case of the analysis of the flow field around a parachute, a portion of the upstream flow will necessarily be non-uniform due to the presence of the vehicle wake. Therefore, the analysis of the previous section must be modified and extended in order to accommodate this type of upstream field.

The equation for the velocity distribution in the wake at a given caliber distance aft of the vehicle, as discussed in Section I, is rewritten for convenience in this analysis and expressed as follows:

$$V_1/a_0 = V_\infty/a_0\left\{1 - A\left[B - (y/\ell)^{3/2}\right]^2\right\} \qquad \text{III-11}$$

where

$$V_\infty/a_0 = M_\infty(1 + 0.2\,M_\infty^2)^{-1/2}$$

and A and B are wake parameters

The resulting Mach number distribution is:

$$M_1 = (V_1/a_0)\left[1 - 0.2\,(V_1/a)^2\right]^{-1/2} \qquad \text{III-12}$$

The assumption is now made that the static pressure in the wake after the wake throat is constant and equal to the free stream static pressure.

With pressure and velocity distributions known, it remains only to determine the distribution of density. Since this method of flux analysis requires the field have constant total energy, the density distribution will be calculated using this criterion. Physically, this criterion is applicable since the presence of a vehicle and vehicle bow shock do not appreciably alter the total constant energy possessed by

the uniform flow upstream of the vehicle bow shock. For a perfect gas, this condition of total constant energy is satisfied by requiring the total temperature, T_o, to be constant.

Thus:

$$\rho_o = p_o / RT_o \qquad \text{III-13}$$

where

$$p_o = p_1 (1 + 0.2\, M_1^2)^{3.5} \qquad \text{III-14}$$

Finally

$$\rho_1 = \rho_0 / (1 + 0.2\, M_1^2)^{2.5} \qquad \text{III-15}$$

The shock conditions are now obtained from equation III-3 through III-10.

B. Field and Shock Calculations

1. Field Calculations

The over-all scheme of this analysis is similar to many numerical techniques, that is, to set down an initial approximate solution to the downstream field and shock and then correct both by successive iterations.

With the field nomenclature as shown in Figure III-1, the procedure for correcting the initial field is as follows. Isolate the j and j + 1 normals: (See Figure III-2).

On the j normal boundary conditions to be satisfied are

$$\psi_{\mathcal{C}_L} = 0 \qquad \text{at} \beta = 0 \qquad \text{III-16}$$

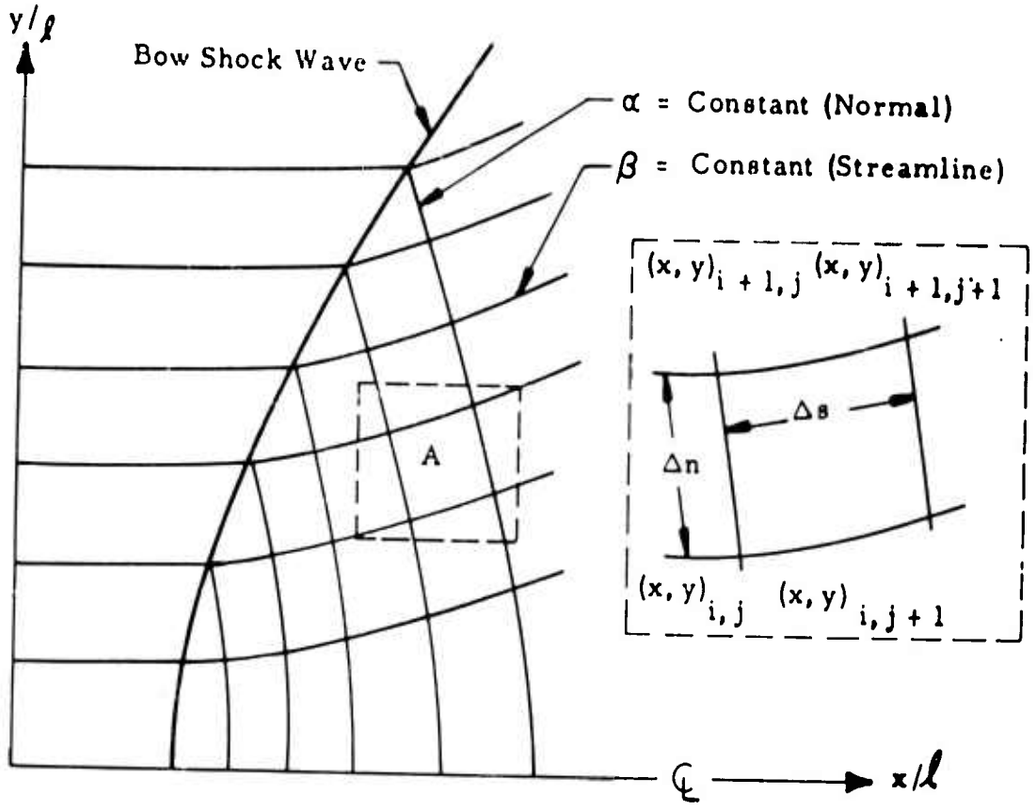

Figure III-1 Field Coordinates

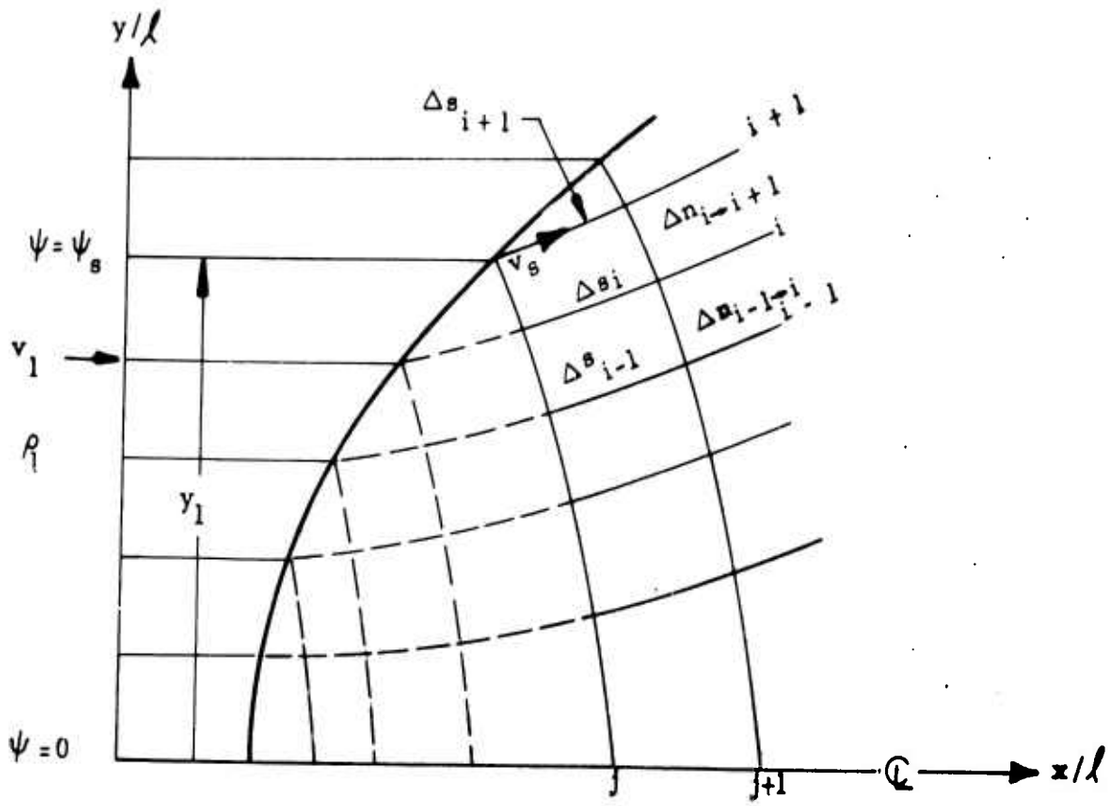

Figure III-2 Flow Field Illustration

$$\psi_s = \rho_1 V_1 (y_1/2)^{\epsilon} y_1 \qquad \text{at } \beta = \beta_s \qquad \text{III-17}$$

or in non-dimensional form

$$\frac{\psi_s}{\rho_o a_o \ell\, (\ell/2)} = \frac{\rho_1 V_1 y_1}{\rho_o a_o \ell} \quad (y_1/\ell)^{\epsilon} \qquad \text{III-18}$$

where $\epsilon = 0$ in two dimensional flow and

$\epsilon = 1$ in axially symmetric flow

The condition of momentum conservation through the shock is temporarily relaxed although all conditions are to be satisfied in the final solution.

For a given field pattern and distribution of entropy, it is possible to determine the velocity distribution along a normal by the following equation:

$$\left(\frac{V_{i,j}}{a_o}\right)^2 = e^{(S_i - S_{i+1})/C_P}\left\{\left(\frac{V_{i+1,j}}{a_o}\right)^2\left(\frac{\Delta s_{i+1}}{\Delta s_i}\right)^2 - \frac{1}{\gamma-1}\left[1+\left(\frac{\Delta s_{i+1}}{\Delta s_i}\right)^2\right]\right\}+\frac{1}{\gamma-1}\left[1+\left(\frac{\Delta s_{i+1}}{\Delta s_i}\right)^2\right] \qquad \text{III-19}$$

where:

Δs = distance between two successive normals (j and j+1) measured along a streamline

$(S_i - S_{i+1})$ = entropy change between the i and i + 1 streamlines

The change in entropy between streamlines is calculated from the assumed shape of the shock in the following manner:

$$e^{(S_i - S_{i+1})/C_p} = \left(P_i/P_{i+1}\right)_2^{1/\gamma} \Big/ \left(\rho i/\rho i+1\right)_2 \qquad \text{III-20}$$

Knowing the velocity distribution, one can calculate the mass flow distribution by the following equation:

$$\left(\frac{\rho V}{\rho_o a_o}\right)_{i,j} = e^{-(S_2 - S_1)_i/R} \left(\frac{V}{a_o}\right)_{i,j} \left[1 - \frac{\gamma-1}{2}\left(\frac{V}{a_o}\right)_{i,j}^2\right]^{1/\gamma-1} \qquad \text{III-21}$$

where:

$$e^{-(S_2 - S_1)_i/R} = \left(\rho_2/\rho_1\right)_i^{\gamma/\gamma-1} \Big/ \left(P_2/P_1\right)^{1/\gamma-1} \qquad \text{III-22}$$

Equations III-19 and III-21 are utilized in an iterative procedure in order to satisfy the boundary condition.

$$\frac{\psi_s}{\rho_o a_o \ell \left(\frac{\ell}{2}\right)^\epsilon} \equiv \int_o^{n_s/\ell} \frac{\rho V}{\rho_o a_o}\left(2\frac{y}{\ell}\right)^\epsilon d\left(\frac{n}{\ell}\right) = \int_o^{y_1/\ell} \frac{\rho_1 V_1}{\rho_o a_o}\left(2\frac{y}{\ell}\right)^\epsilon d\left(\frac{y}{\ell}\right) \qquad \text{III-23}$$

When the upstream flow is uniform, the right hand side of equation III-23 can be integrated into:

$$\int_o^{y_1/\ell} \frac{\rho_1 V_1}{\rho_o a_o}\left(2\frac{y}{\ell}\right)^\epsilon d\left(\frac{y}{\ell}\right) = \left(\frac{2^\epsilon}{\epsilon+1}\right)\frac{\rho_1 V_1}{\rho_o a_o}\frac{y_1}{\ell}\left(\frac{y_1}{\ell}\right)^\epsilon \qquad \text{III-24}$$

The steps in detail are:

(1) Assume a velocity at the shock wave $V_s = V_{i+1,j}$

(2) Use equation III-19 to compute $V_{i,j}$ the velocity at the point $(x, y)_{i,j}$. Knowing $V_{i,j}$, again use equation III-19 to compute the velocity $V_{i-1,j}$, at the point $(x, y)_{i-1,j}$. Continue along the j normal until all velocities are computed.

(3) Use equation III-21 to compute the mass flow at each point along the j normal

(4) Knowing the mass flow along the j normal, numerically integrate equation III-23

(5) If $$\int_0^{n_s/\ell} \frac{\rho V}{\rho_o a_o} \left(2\,\frac{y}{\ell}\right)^{\epsilon} d\left(\frac{n}{\ell}\right) - \frac{2^{\epsilon}}{\epsilon+1}\,\frac{\rho_1 V_1 y_1}{\rho_o a_o}\left(\frac{y_1}{\ell}\right)^{\epsilon} \leq \zeta$$

the boundary condition is satisfied. If not, vary V_s and repeat the above from Step 2 until the above criterion is satisfied.

The distribution of the stream function along the j normal at the given β lines (streamlines) is found by

$$\frac{\psi_i}{\ell \rho_o a_o \left(\frac{\ell}{2}\right)^{\epsilon}} = \int_0^{n_i/\ell} \frac{\rho V}{\rho_o a_o} \left(\frac{2y}{\ell}\right)^{\epsilon} d\left(\frac{n}{\ell}\right) \qquad \text{III-25}$$

and the following type relation is obtained.

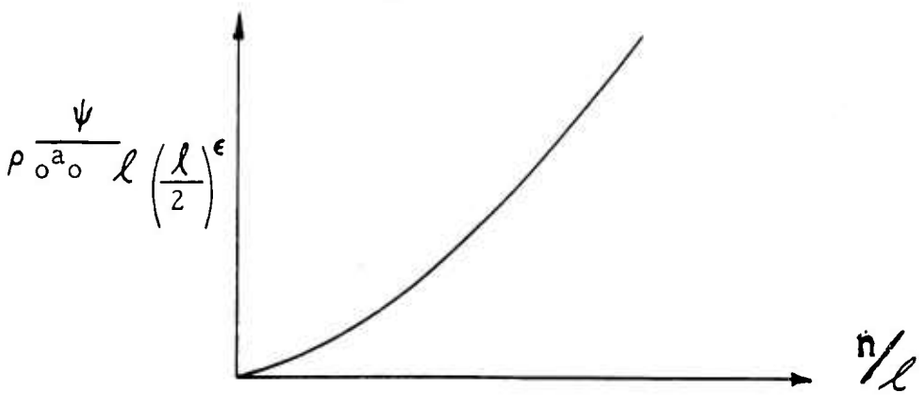

Figure III-3. Flux Distribution Along A Normal

The location of the streamlines is corrected by entering Figure III-3 with the stream function values of the streamline and finding the corrected n/ℓ location along the normal.

This procedure is followed on every normal and the new streamlines are obtained by connecting the newly obtained corresponding points on adjacent normals. New normals are drawn thus completing the present field iteration. This new flow pattern will serve as the co-ordinate axes for the next iteration.

For a given shock shape the above iterative procedure is repeated until a consistent field solution is obtained.

2. Shock Calculations

Fulfillment of the boundary condition requires that the shock stream deflection angles coincide with the streamline angle immediately behind the shock obtained from the field calculations. That is:

$$\delta_i = (\theta_s)_i$$

This condition will not be satisfied at every shock point unless a solution has been attained.

A parameter indicating the completeness of the solution is defined as:

$$K = (\theta_s)_{max} / \delta_{max} \qquad \text{III-26}$$

This parameter is used to calculate new values of δ for the next shock iteration as follows:

$$\delta = \theta_s / K \qquad \text{III-27}$$

When K = 1 is obtained, the shock condition is completely satisfied. This condition will only be attained when the correct shock stand-off distance has been found.

The description that follows is the iterative scheme for shock adjustment that is employed for a given shock stand-off distance. The values of K obtained from successive iterations will approach a limit. If this limit value is not K = 1, the shock stand-off distance is varied and the entire iterative scheme of shock and field calculation is repeated. The new stand-off distance is obtained from the previously obtained value. If K (in the limit) < 1 the stand-off distance is decreased. If K > 1 the stand-off distance is increased. This procedure is pursued until a value of K = 1 is obtained. This will be achieved only when the correct shock stand-off distance is located.

The steps for shock adjustment in detail are:

(1) Upon completion of a field iteration the values of ω_i and $(\theta_s)_i$ are tabulated.

(2) From equation III-10 obtain the values of δ_i corresponding to the ω_i of step (1).

(3) Survey the lists of δ and $(\theta_s)_i$ locating the maximum of each and form the ratio $K = \dfrac{(\theta_s)_{i\ \text{max.}}}{\delta_{i\ \text{max.}}}$.

(4) Obtain a new value of δ from equation III-27.

(5) For each value of δ of step (4) use equation III-10 to obtain the corresponding values of ω_i.

(6) Draw a new shock wave starting the axis at the chosen stand-off distance. Each segment of the shock wave is drawn at the appropriate angle ω_i starting at the intersection of the shock wave segment, drawn from i - 1 streamline, and the i th streamline.

(7) The shock wave now intersects the streamline at different locations. Therefore, measure the new values of $(\theta_s)_i$ and repeat procedure from Step 3.

This procedure is repeated until K approaches a limit.

C. Circular Cylinder Problems

To obtain insight to the different aspects of the problem, the calculation presented in Reference (7) "A Circular Cylinder in Two Dimensional Flow", was performed.

The correct shock stand-off distance was obtained from Reference (7). For this stand-off distance, as shown in Figure III-4, the third shock and field iteration compared favorably with the fourth iteration as given in Reference (7).

Because of this agreement and also because the final solution as obtained in Reference (7) did not differ appreciably from the 4th iteration, the calculation was terminated.

This calculation was done as a semigraphical procedure. That is, the field calculation was performed on a high speed digital computer up to the point where the location of the corrected streamlines had been obtained.

The drawing of the new streamline and normals was done graphically as was the adjustment of the shock wave.

D. Parachute Problem

A limited effort was expended in order to obtain the flow field for a three-dimensional parachute in non-linear flow; the non linearity resulting from the presence of the vehicle wake upstream of the parachute.

In this case only the field downstream of the shock and upstream of the parachute was considered. Hence, the shock wave obtained from Schlieren photographs was assumed fixed. (In order to adjust the shock shape, the entire field must be considered.)

Field calculations were stalled when difficulties were encountered in that the governing flow equations were not able to successfully correct portions of the initial downstream field. This difficulty was not encountered in the two-dimensional cylinder in uniform flow.

Further study would be required to determine cause of the difficulties.

E. Complete Automation

In order to improve on the accuracy of the field calculation and to reduce the time involved, a method has been evolved for automating the entire field calculation. It is presented to indicate the feasibility of complete automation.

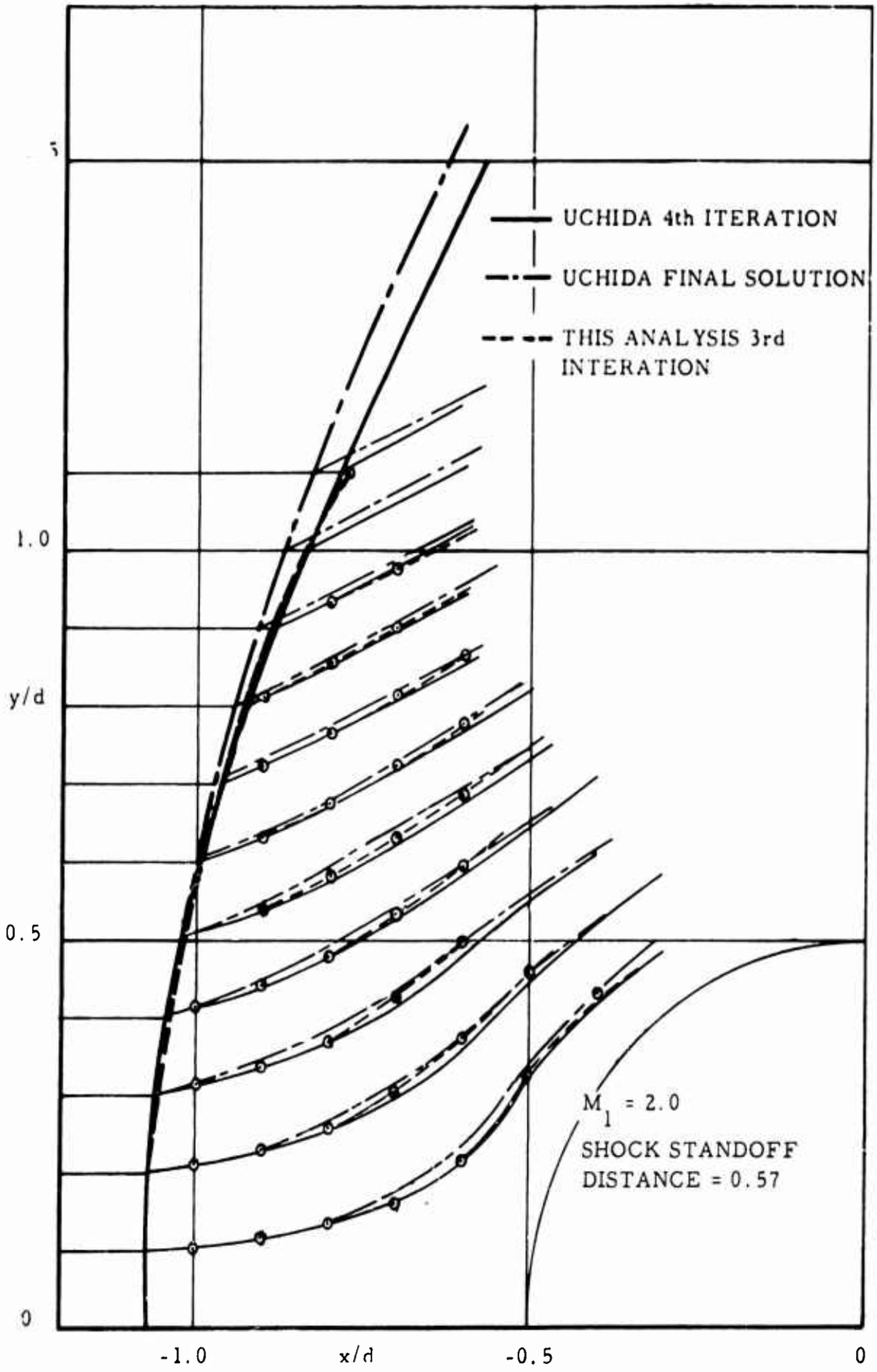

Fig. III-4. Streamlines and Bow Shock Wave for Various Iterations

1. Nomenclature

The following nomenclature will be used in the construction of streamlines and normals. (See Figure III-5)

Let f_i represent the entire i^{th} streamline and η_j represent the entire j^{th} normal.

$P_{i,j}$ shall be the corrected points used to construct the new streamline.

$P'_{i,j}$ shall be points on the new streamline.

$P''_{i,j}$ shall denote the intersection of the new streamlines with the new normals.

The points $P_{o,j}$ lie on the axis or on the body. The points $P_{i,j}$, where $i = j$, lie on the shock wave, i.e., $P_{i,i}$.

Let $f_{i,j}$ represent the second order curve passing through the points $P_{i,j}$, $P_{i,j+1}$, $P_{i,j+2}$.

Let $f^{*}_{i,j}$ represent the second order curve passing through the point $P'_{i,j}$ $(j \geq i+2)$ and satisfying a least squares fit through the points $P_{i,j+1}$, $P_{i,j+2}$, ..., $P_{i,j+r}$ were r is the number of points used in the least squares fit. It will represent the streamline in the neighborhood of the point from which it starts, $P'_{i,j}$.

2. Streamline Construction

As described previously, new streamlines are constructed by drawing a curve through corrected points. Because of the scatter that occurred in the corrected points for most portions of the field, passing a curve exactly through the points would result in an extremely rough curve. Therefore, a least squares curve technique will be used to fair in these streamlines.

The only region where streamline fitting through the exact points will be utilized is in the neighborhood of the shock wave where the correction to the streamlines are fairly uniform.

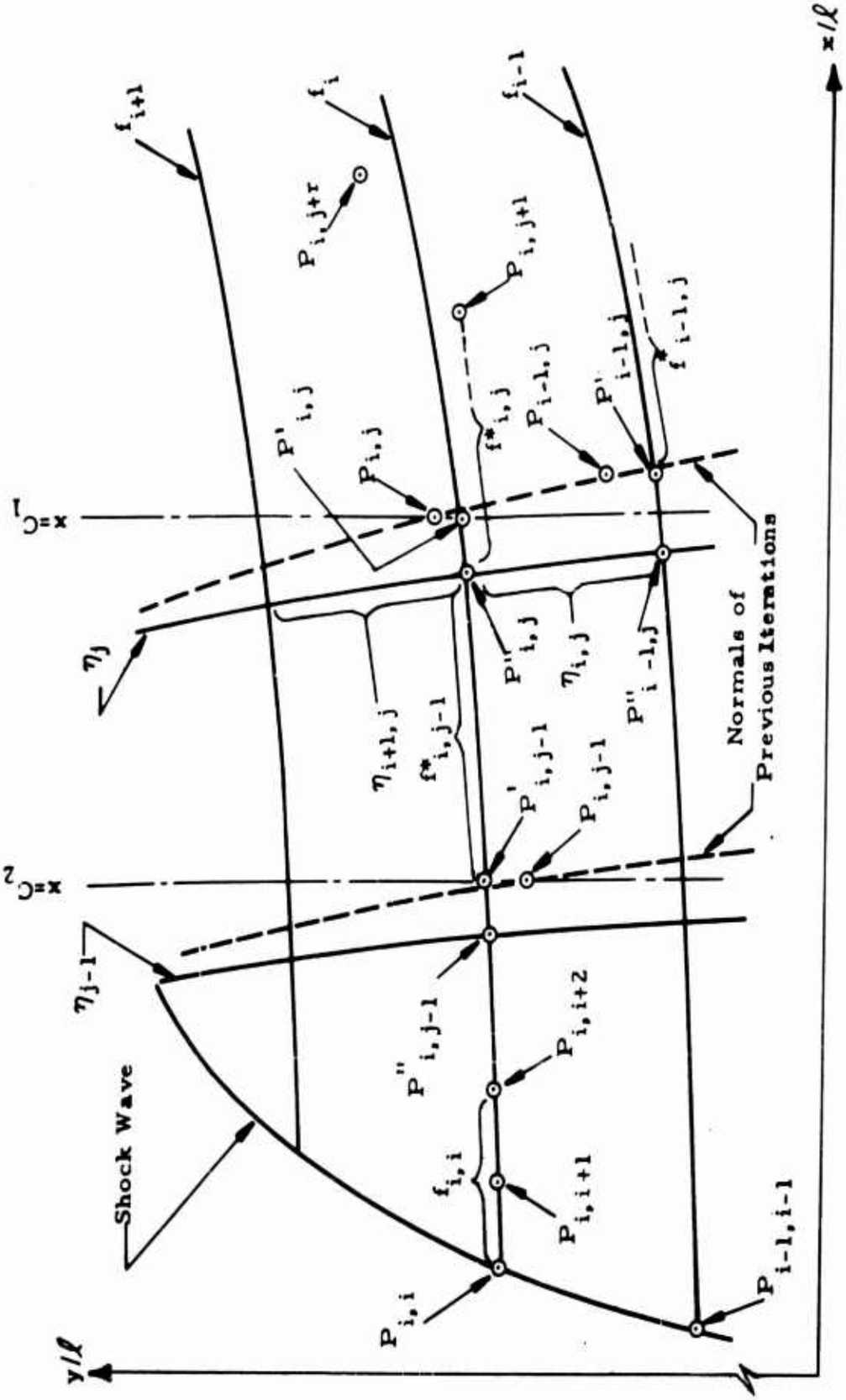

Figure III-5 Field Nomenclature

A quadratic function is used for the streamline fit since the fitting of the normals would become extremely complex if higher orders were used (with the quadratic it is necessary to solve four non-linear simultaneous equations).

Thus, to start the procedure of fitting the streamlines, a quadratic

$$f_{i,i} : y = a_{i,i} x^2 + b_{i,i} x + c_{i,i} \qquad \text{III-28}$$

is passed through three successive points,

$$P_{i,i},\ P_{i,i+1},\ P_{i,i+2}.$$

The coefficients of equation III-28 will be determined as follows:

$$\begin{aligned} y_{i,i} &= a_{i,i} x^2_{i,i} + b_{i,i} x_{i,i} + c_{i,i} \\ y_{i,i+1} &= a_{i,i} x^2_{i,i+1} + b_{i,i} x_{i,i+1} + c_{i,i} \qquad \text{III-29} \\ y_{i,i+2} &= a_{i,i} x^2_{i,i+2} + b_{i,i} x_{i,i+2} + c_{i,i} \end{aligned}$$

Thus

$$\Delta_{i,i} = \begin{vmatrix} x^2_{i,i} & x_{i,i} & 1 \\ x^2_{i,i+1} & x_{i,i+1} & 1 \\ x^2_{i,i+2} & x_{i,i+2} & 1 \end{vmatrix} \qquad \text{III-29.1}$$

$$a_{i,i} = \frac{\begin{vmatrix} y_{i,i} & x_{i,i} & 1 \\ y_{i,i+1} & x_{i,i+1} & 1 \\ y_{i,i+2} & x_{i,i+2} & 1 \end{vmatrix}}{\Delta_{i,i}} \qquad \text{III-29.2}$$

$$b_{i,i} = \frac{\begin{vmatrix} x_{i,i}^2 & y_{i,i} & 1 \\ x_{i,i+1}^2 & y_{i,i+1} & 1 \\ x_{i,i+2}^2 & y_{i,i+2} & 1 \end{vmatrix}}{\Delta_{i,i}} \qquad \text{III-29.3}$$

$$c_{i,i} = \frac{\begin{vmatrix} x_{i,i}^2 & x_{i,i} & y_{i,i} \\ x_{i,i+1}^2 & x_{i,i+1} & y_{i,i+1} \\ x_{i,i+2}^2 & x_{i,i+2} & y_{i,i+2} \end{vmatrix}}{\Delta_{i,i}} \qquad \text{III-29.4}$$

A similar curve will be obtained for $f_{i-1,\ i-1}$, the next lower streamline

$$f_{i-1,\ i-1}: \ y = a_{i-1,i-1}\, x^2 + b_{i-1,i-1}\, x + c_{i-1,\ i-1} \qquad \text{III-30}$$

From the point $P_{i,i+2}$ working downstream, the streamlines will be fitted by a least squares technique.

In order to maintain some relationship between the $P_{i,j}$ and $P'_{i,j}$ points let $x'_{i,j} = x_{i,j}$.

Two conditions are to be satisfied at each $P'_{i,j}$ point; continuity and continuous first derivative.

The problem is to determine f^*_{ij}.

$$x'_{i,j} = x_{i,j} \qquad \text{III-31}$$

$$y'_{i,j} = f^*_{i,j-1}\ (x_{i,j};\ y_{i,j}) \qquad \text{III-32}$$

$$\dot{f}^*_{i,j-1}\ (x_{i,j};\ y_{i,j}) \qquad \dot{f} \equiv dy/dx \qquad \text{III-33}$$

$F'_{i,j+1}$ will be given by $\left[x_{i,j+1};\ f^*_{i,j}\ (x_{i,j+1},\ y_{i,j+1})\right]$

It is now required to determine $f^*_{i,j}$ which is of the form

$$f^*_{i,j}(x) = a_{i,j}x^2 + b_{i,j}x + c_{i,j} \qquad \text{III-34}$$

for which

$$f^*_{i,j}(x_{i,j}) = f^*_{i,j-1}(x_{i,j}) \qquad \text{III-35}$$

$$\dot{f}^*_{i,j}(x_{i,j}) = \dot{f}^*_{i,j-1}(x_{i,j}) \qquad \text{III-36}$$

and the sum of squares of the deviations

$$E^2_{i,j} = \sum_{s=1}^{r} \left[f^*_{i,j}(x_{i,j+s}) - y_{i,j+s} \right]^2 \qquad \text{III-37}$$

is minimized

From III-34 and III-35

$$f^*_{i,j-1}(x_{i,j}) = a_{i,j} x^2_{i,j} + b_{i,j} x_{i,j} + c_{i,j} \qquad \text{III-38}$$

Taking the derivative of III-34 and using III-36 renders

$$\dot{f}^*_{i,j-1}(x_{i,j}) = 2 a_{i,j} x_{i,j} + b_{i,j} \qquad \text{III-39}$$

From III-39

$$b_{i,j} = \dot{f}^*_{i,j-1}(x_{i,j}) - 2 a_{i,j} x_{i,j} \qquad \text{III-40}$$

Substituting III-40 into III-38 renders

$$f^*_{i,j-1}(x_{i,j}) = c_{i,j} + x_{i,j} \dot{f}^*_{i,j-1}(x_{i,j}) - a_{i,j} x^2_{i,j}$$

Solving for $c_{i,j}$

$$c_{i,j} = f^*_{i,j-1}(x_{i,j}) - x_{i,j} \dot{f}^*_{i,j-1}(x_{i,j}) + a_{i,j} x^2_{i,j} \qquad \text{III-41}$$

Substituting III-40 and III-41 into III-34 gives

$$f^{*}_{i,j}(x) = a_{i,j}x^2 + \left[\dot{f}^{*}_{i,j-1}(x_{i,j}) - 2a_{i,j}x_{i,j}\right] x + f^{*}_{i,j-1}(x_{i,j}) - x_{i,j}\dot{f}^{*}_{i,j-1}(x_{i,j}) + a_{i,j}x^2_{i,j} \qquad \text{III-42}$$

From III-37 since $a_{i,j}$ is the only variable of the function to be determined

$$\frac{\partial E^2_{i,j}}{\partial a_{i,j}} = 2\sum_{s=1}^{r}\left[\left[f^{*}_{i,j}(x_{i,j+s}) - y_{i,j+s}\right]\frac{\partial f^{*}_{i,j}(x_{i,j+s})}{\partial a_{i,j}}\right] = 0 \qquad \text{III-43}$$

From III-42

$$\frac{\partial}{\partial a_{i,j}}\left[f^{*}_{i,j}(x_{i,j+s})\right] = x^2_{i,j+s} - 2x_{i,j}x_{i,j+s} + x^2_{i,j} \qquad \text{III-44}$$

Substituting III-42 and III-44 into III-43 gives

$$\sum_{s=1}^{r}\Big[\Big\{f^{*}_{i,j-1}(x_{i,j}) - x_{i,j}\dot{f}^{*}_{i,j-1}(x_{i,j}) + a_{i,j}x^2_{i,j} + x_{i,j+s}\left[\dot{f}^{*}_{i,j-1}(x_{i,j}) - 2a_{i,j}x_{i,j}\right] + a_{i,j}x^2_{i,j+s} - y_{i,j+s}\Big\}\left\{x^2_{i,j} - 2x_{i,j}x_{i,j+s} + x^2_{i,j+s}\right\}\Big] = 0$$

Solving for $a_{i,j}$

$$a_{i,j} = -\sum_{s=1}^{r} \left\{ \left[f^{*}_{i,j-1}(x_{i,j}) - y_{i,j+s} + (x_{i,j+s} - x_{i,j}) \dot{f}^{*}_{i,j-1}(x_{i,j}) \right] x \right. \qquad \text{III-45}$$

$$\left. \left[x^{2}_{i,j} - 2x_{i,j} x_{i,j+s} + x^{2}_{i,j+s} \right] \right\} \Big/$$

$$\sum_{s=1}^{r} \left[x^{2}_{i,j} - 2 x_{i,j} x_{i,j+s} + x^{2}_{i,j+s} \right]^{2}$$

After $a_{i,j}$ is found, $b_{i,j}$ and $c_{i,j}$ are found from III-40 and III-41.

3. Normal Construction

Usually, the construction of normals will begin at the shock; however, a general field point will be discussed since the boundary point differs only slightly in procedure.

The equation for the normal segments, $\eta_{i,j}$, will be expressed as $x = f(y)$ since at the axis, the normality condition would require that $dy/dx \to \infty$ while in the form suggested $dy/dx = 0$

Thus

$$\eta_{i,j} : x = k_{i,j} y^{2} + \ell_{i,j} y + m_{i,j} \qquad \text{III-46}$$

To determine the coefficients, the following three conditions will be used.

(1) $\eta_{i,j}$ intersects $f^{*}_{i,j}$ at $P''_{i,j}$

(2) $\eta_{i,j} \perp f^{*}_{i,j}$ at $P''_{i,j}$

(3) $\eta_{i,j} \perp$ at some point $P''_{i-1,j}$ to be determined.

The first condition, $\eta_{i,j}$ intersects $f^{*}_{i,j}$ is obtained by substituting $x''_{i,j}$ and $y''_{i,j}$ for x and y in III-46 yielding.

$$x''_{i,j} = k_{i,j} y''^{2}_{i,j} + \quad _{i,j} y''_{i,j} + m_{i,j} \qquad \text{III-47}$$

The second condition, $\eta_{i,j} \perp f^{*}_{i,j}$ at $P''_{i,j}$ is obtained from III-34 and III-46 by determining the slopes of the two curves at the point $P''_{i,j}$.

From III-34 $$\frac{df^{*}_{i,j}}{dx} = \frac{dy}{dx} = 2a_{i,j} x + b_{i,j}$$

From III-46 $$\frac{d\eta_{i,j}}{dy} = \frac{dx}{dy} = 2 k_{i,j} y + \ell_{i,j}$$

The normality condition is satisfied by setting

$$\frac{df^{*}_{i,j}}{dx} = - \frac{d\eta_{i,j}}{dy} \qquad \text{III-48}$$

and substituting $x''_{i,j}$ and $y''_{i,j}$ for x and y.

or

$$2a_{i,j} x''_{i,j} + b_{i,j} = - (2 k_{i,j} y''_{i,j} + \quad _{i,j}) \qquad \text{III-49}$$

The third condition $\eta_{i,j} \perp f^{*}_{i-1,j}$ would be met by a condition similar to III-49. However, the point of intersection is not known and this becomes a fourth variable. A fourth condition will be obtained by the generalized condition

4) $\eta_{i,j}$ intersects $f^{*}_{i-1,j}$

Substituting the expression for $f^{*}_{i-1,j}$ into III-46 gives

$$x = k_{i,j}(a_{i-1,j}x^{2} + b_{i-1,j}x + c_{i-1,j})^{2} \qquad \text{III-50}$$

$$+ \ell_{i,j}(a_{i-1,j}x^{2} + b_{i-1,j}x + c_{i-1,j}) + m_{i,j}$$

Differentiating the expression for $f^{*}_{i-1,j}$ and III-46 and satisfying the condition of II-48 renders

$$2a_{i-1,j}x + b_{i-1,j} = -(2k_{i,j}y + \ell_{i,j}) \qquad \text{III-51}$$

Substituting $f^{*}_{i-1,j}$ into III-51 gives

$$2a_{i-i,j}x + b_{i-1,j} = -2k_{i,j}(a_{i-1,j}x^{2} + b_{i-1,j}x + c_{i-1,j}) - \ell_{i,j} \qquad \text{III-52}$$

Equations III-47, III-49, III-50 and III-52 are four equations in the four variables, $k_{i,j}$, $l_{i,j}$, $m_{i,j}$ and x where x is actually $x''_{i-1,j}$ one co-ordinate of the intersection of $\eta_{i,j}$ and $f^{*}_{i-1,j}$; $y''_{i-1,j}$ is obtained from $f^{*}_{i-1,j}$. This determines $P''_{i-1,j}$ which is used for extending the normal to the next streamline.

Because of the non-linearity of the system of four equations, simultaneous solution would be intractable. Instead, an iterative technique will be applied.

Unfortunately, there is no method of attack that will guarantee convergence. The best approach is to select initial values that will be close to the solution. In the system to be solved it is fortunate that not all equations contain all variables and it will be possible to start the iteration by estimating two of the parameters.

The parameters that can best be estimated are the second derivative of $\eta_{i,j}$, i.e., $k_{i,j}$ and the new intersection co-ordinate x.

For these estimates we use $P_{i+1,j}$; $P_{i,j}$ and $P_{i-1,j}$, where the superscripts indicate the iteration order.

$$\frac{d^2x}{dy^2} = (k_{i,j})^o = \left\{ \frac{x_{i+1,j} - x_{i,j}}{y_{i+1,j} - y_{i,j}} - \frac{x_{i,j} - x_{i-1,j}}{y_{i,j} - y_{i-1,j}} \right\} \Bigg/ \left\{ \left[(y_{i+1,j} - y_{i,j}) + (y_{i,j} - y_{i-1,j}) \right] / 2 \right\}$$

or

$$(k_{i,j})^o = \frac{2}{(y_{i+1,j} - y_{i-1,j})} \left\{ \frac{x_{i+1,j} - x_{i,j}}{y_{i+1,j} - y_{i,j}} - \frac{x_{i,j} - x_{i-1,j}}{y_{i,j} - y_{i-1,j}} \right\} \qquad \text{III-53}$$

and

$$x''^o_{i-1,j} = x'_{i,j} + (x'_{i,j} - x_{i+1,j}) = 2x'_{i,j} - x'_{i+1,j} \qquad \text{III-54}$$

With these initial values, the iteration can be ordered as follows:

From III-49

$$(\ell_{i,j})^h = 2(k_{i,j})^{h-1} y''_{i,j} + 2a_{i,j}(x'')^{h-1} + b_{i,j} \qquad \text{III-55}$$

From III-47

$$(m_{i,j})^h = (x''_{i,j})^{h-1} - (k_{i,j})^{h-1} y''^2_{i,j} - (\ell_{i,j})^h y''_{i,j} \qquad \text{III-56}$$

From III-50

$$(x'')^{h}_{i-1,j} = (k_{i,j})^{h-1}\left[a_{i-1,j}(x''^{2})^{h-1} + b_{i-1,j}(x'')^{h-1} + c_{i-1,j}\right]^{2} \qquad \text{III-57}$$

$$+(\ell_{i,j})^{h}\left[a_{i-1,j}(x''^{2})^{h-1} + b_{i-1,j}(x'')^{h-1} + c_{i-1,j}\right] + (m_{i,j})^{h}$$

Finally, from III-52

$$(k_{i,j})^{h} = \left[-(\ell_{i,j})^{h} - 2a_{i-1,j}(x'')^{h} - b_{i-1,j}\right] \Big/ \qquad \text{III-58}$$

$$2\left[a_{i-1,j}(x''^{2})^{h} + b_{i-1,j}(x'')^{h} + c_{i-1,j}\right]$$

Thus, with the initial values given by III-53 and III-54, equations III-55 through III-58 are iterated until convergence is obtained. The criteria for this will be:

where $\left|\xi^{h} - \xi^{h-1}\right| < Q$

$\xi = k,\ \ell,\ m, x$ and Q is

the precision required.

The application of the above technique was not possible in this program, due to limitation of time and funds. It is felt, however, that the analytical procedures discussed in this section are valid, and that further effort in the application of these techniques in conjunction with phenomenological insight gained in the experimental programs would lead to the accomplishment of the initial objectives of the theoretical approach to the parachute problem.

SECTION IV

CONCLUSIONS AND RECOMMENDATIONS FOR FURTHER STUDY

The evolution of a family of high Mach number, self-inflating parachute configurations in this one year program has indicated an extension of the state of the art in speed capability of parachute decelerators by a factor of about three over that capability accepted as a practical limit for such decelerators at the time of the initiation of this program. This family provides also a drag to weight ratio advantage of a factor of the order of 6 over any other known decelerator capable of operation in this Mach number range.

Work prior to this program had led to the development of parachutes capable of proper performance at Mach number of a little more than 2. Requirements for applications at high Mach numbers could not be satisfied. Indeed, it was not even well established that it was feasible to develop a parachute for applications much above Mach number 2. The maximum Mach number at which satisfactory canopy performances were exhibited in the final (Phase II) wind tunnel test program, was limited only by the Phase II wind tunnel capability (M = 4.65). While this report was being written, a test program was conducted by the contracting agency in which configurations designed during this program were successfully tested to M = 6. This also represented the speed limitation of the wind tunnel used for these tests (the Phase I test facility, Tunnel A, VKF, AEDC).

Due to the successful performance of the high speed parachute designs evolved in this program a large amount of data was gathered, however, since the test programs (particularly Phase II) were the first to be conducted at high Mach numbers with successfully performing configurations, much of the data serve only to define directions of effort in future programs.

A. Conclusions

The following specific conclusions were drawn during the conduct of this program:

(1) Although several basic geometric shapes were found to perform satisfactorily in the high Mach number environments, those configurations which consisted of a cone frustrum shape, of high inlet diameter to maximum diameter ratio (0.9) and with a 10 degree inlet cone angle, combined with a flat roof appeared to be superior. In these designs, the use of a low total porosity (8 to 18 percent), a low porosity (2 percent) inlet cone, and a high porosity roof (14 to 34 percent) resulted in

canopy configurations (C-6, C-7, CR-2) which performed in an outstanding manner throughout the tested speed range. Hereinafter these configurations employing minor variations in the basic design characteristics described above are referred to as the Hyperflo family of high performance parachutes.

(2) The use of a relatively low total canopy porosity in the Hyperflo designs provides high over-all inflation characteristics, in addition the very low porosity of the canopy inlet cone leads to high stability characteristics for these configurations, and high inflation characteristics in the inlet region. The cone frustrum shape of the canopy minimizes the total area, and, hence the total weight and bulk as compared for example, to a canopy which is designed with a preshaped hemispherical roof. The latter design results in twice the roof area for a given frontal area. The necessary porosity to satisfy mass flow and stability requirements in the Hyperflo configuration is provided by the high porosity roof.

(3) Observation of these canopies under subsonic conditions during wind tunnel shutdown has indicated excellent inflation and stability characteristics. It is therefore, felt that successful operation of the high speed canopies will be assured with perhaps minor variations in the design parameters for subsonic speed applications.

(4) Although relatively low total porosities were used in the design of the test models, as compared to previously applied (conventional) parachute designs, wide ranges of porosity (8 to 18 percent) were used with successful results.

(5) The canopy location aft of the forebody appeared to significantly affect the performance of all configurations in the high speed ranges. The most favorable location appeared to be in the close-in, or low x/d positions, (6-8 forebody diameters). This would result in a significant reduction in the over-all parachute system weight, since the riser length will be minimized. The weight of a parachute riser frequently represents a large percentage of the total parachute system weight.

(6) The effects of diameter ratio of the canopy to that of the forebody was not clearly established, although there were indications of a slight reduction in canopy performance at a ratio of 3.33 compared to a ratio of 2.5.

(7) In the event of application of the high performance parachutes to an unsymmetrical forebody, it is expected that satisfactory

parachute performance will be attained. If a symmetrical wake is essential to satisfactory canopy performance, the location of the canopy further downstream in such applications should be satisfactory. A previous application of a conventional parachute decelerator to an unsymmetrical forebody resulted in satisfactory performance at M = 2.2.

(8) The effects of dynamic pressure on canopy performance are not definitely established, although some data gathered in this program appear to indicate high drag coefficients with low dynamic pressure. The effects of dynamic pressure, or of Reynolds number were not investigated sufficiently in this program to establish a definite correlation with canopy performance.

(9) Several roof designs were employed in the models tested in this program. No significant effect on canopy performance could be attributed to the flat roof design variation. All canopies which were constructed using the basic Hyperflo design geometry performed in a comparable manner when designed with equivalent total porosities. This provides a wide latitude of techniques to be used in the fabrication of full scale canopies.

(10) Rigorous analytical procedures by means of which canopy performance at supersonic speeds might be predicted was completed but not applied in this program. The validity of the formulation appeared to be established. The results of the program, however, indicate that relatively non-rigorous procedures may be fruitful. Careful data analysis coupled with relatively non-rigorous analytical procedures led to the indication of configurational requirements for satisfactory high Mach number parachute performance and some of the associated air flow phenomena. Although the non-rigorous procedures applied in this program resulted in successful supersonic canopy performance, a positive prediction of supersonic parachute requirements will be established only by rigorous analytical methods.

B. Recommendations

1. Experimental Programs

a. A study of the effects of dynamic pressure on canopy performance in the high Mach number range is essential, due to possible dynamic pressure effects observed in the Phase II test program.

b. The effects of diameter ratio of parachute to forebody should be investigated to determine if a practical limit to this ratio exists. Although two such ratios were investigated in the final test program (2.5 and 3.33), larger diameter ratios should be investigated.

c. Further investigation to determine the upper and lower limits of total porosity, within which successful canopy performance is assured, should be conducted.

2. Analytical Study

Inherent complexities in the formulation, and necessary mechanization of the flow field solution prevented a useful contribution of this approach to the canopy designs achieved in this program. It is felt that the feasibility and validity of the analytical procedures discussed in Section III appear to be established, however, further study and experience with the application of this procedure, by matching test data and incorporating observed phenomena, should result in an invaluable contribution to future parachute canopy designs, and the further understanding of these phenomena.

APPENDIX I

THE PHASE I TEST FACILITY DESCRIPTION

The VKF Tunnel A, AEDC Tennessee is a continuous, closed circuit, variable density wind tunnel with a Mach number range of 1.5 to 6.0. The tunnel is served by the main compressor system which provides a wide range of mass flows and pressure ratios up to a maximum pressure of 200 PSIA.

The test section is 40 by 40 inches, with its effective test chambers approximately centered at the downstream end of the flexible nozzle plates. Three-pane windows are located in the test section side walls.

A variable-geometry, five-hinge diffuser is located downstream of the test section.

An ERA-1102 digital computer is shared by all VKF tunnels, with individual tunnels equipped with a digital scanner, raw-data punch, and related output equipment.

A double-pass Schlieren system with a 35 inch diameter optical path is provided for observation of flow fields through any of the three test section windows.

APPENDIX II

THE PHASE I, AND Ia TEST FACILITY DESCRIPTION

The Cook Technological Center wind tunnel is a continuous flow open circuit atmosphere induction type with either fixed or variable flow nozzles. The test sections are of the two-dimensional type with airflow available by adjustment of two General Electric J-47 turbojet engines. The facility was designed to provide continuous variation of Mach numbers from low supersonic to a Mach number of approximately 2.7 in a test section 22 inches by 24 inches.

Flow visualization is accomplished by the utilization of a Schlieren optical system which is adjustable by sliding on rails to permit recording access to all sections of the test chambers. Two window ports in the side walls are utilized to photograph shock wave patterns at different sections of the test area.

APPENDIX III

THE PHASE II TEST FACILITY DESCRIPTION

The Langley Large Supersonic Tunnel, Langley Field, Virginia is capable of test Mach numbers from 2.3 to 4.65, with a maximum stagnation pressure of 150 PSIA. The test section of this facility is 4 feet high, 4 feet wide, and 7 feet long, and will permit variation of Mach number at any desired increment throughout its range with tunnel operating.

Both stagnation pressure and stagnation temperature may be controlled independently.

The tunnel window has a field of 59 inches by 48 inches, and is made up of nine strips of optical plate glass, each 5-1/2 inches wide, and separated from each other by 1-1/4 inches of supporting structure.

The Schlieren system has a 49 inch diameter field, and adjustable so as to allow complete coverage of the 59 inch window.

A semi-automatic force data readout system provides tabulated raw data and IBM punch card storage of raw data concurrent with tunnel operation.

LIST OF REFERENCES

1. Fredette, R. O., Parachute Reasearch Above Critical Aerodynamic Velocities, Cook Electric Company 1961

2. Love, Eugene S., Base Pressure at Supersonic Speeds on Two-Dimensional Surfaces and on Bodies of Revolution With and Without Fins Having Turbulent Boundary Layers, NACA TN 3819, January 1959

3. Schlichting, H., Boundary Layer Theory, McGraw-Hill Book Company, Inc., 1955

4. Charezenko, N., and McShera, J. T., Aerodynamic Characteristics of Towed Cones Used as Decelerators at Mach Numbers From 1.57 to 4.65, NASA TN D-994, December 1961

5. Coats, J. D., Static and Dynamic Testing of Conical Trailing Decelerators for the Pershing Re-Entry Vehicle, AEDC-TN-60-188, October 1960

6. Liepmann, H. W., and Roshko, A., Elements of Gasdynamics, John Wiley & Sons, Inc., New York, 1960

7. Uchida, S. and Yasuhara, M., The Rotational Field Behind a Curved Shock Wave Calculated by the Method of Flux Analysis, J. IAS, Vol. 23, September 1956, No. 9

Aeronautical Systems Division, Dir/Aeromechanics, Flight Accessories Lab, Wright-Patterson AFB, Ohio.
Rpt Nr ASD-TDR-62-844. ANALYTICAL AND EXPERIMENTAL INVESTIGATION OF SUPERSONIC PARACHUTE PHENOMENA(U). Final report, Feb 63, 133p. incl illus., tables, 7 refs.
Confidential Report

Two parallel efforts were conducted consisting of (1) analytical studies to describe the flow field surrounding a trailing parachute decelerator in the wake of a forebody traveling at supersonic speeds and (2) a wind tunnel test program employing both conventional and unconventional parachute canopy designs. The wind tunnel program consisted of approximately 200 tests in the Mach number range from M=1.5 to M=4.65 using 6 and 8 inch inflated diameter models. Wind tunnel test data, and high speed Schlieren photographs are included to illustrate the test results of a program in which a new family of high speed self inflating parachutes evolved. Satisfactory performance of this new parachute family was demonstrated through Mach 4.65.

Unclassified Abstract

(over)

1. Parachutes
2. Fluid Mechanics
3. Tests
4. Supersonics
5. Drag and recovery
I. AFSC Project 6065, Task 606505
II. Contract AF 33(616)-8459
III. Cook Technological Center, Chicago, Illinois
IV. L. W. Sims
V. Secondery Rpt No. C00299
VI. Not aval fr OTS
VII. In ASTIA collection

Aeronautical Systems Division, Dir/Aeromechanics, Flight Accessories Lab, Wright-Patterson AFB, Ohio.
Rpt Nr ASD-TDR-62-844. ANALYTICAL AND EXPERIMENTAL INVESTIGATION OF SUPERSONIC PARACHUTE PHENOMENA(U). Final report, Feb 63, 133p. incl illus., tables, 7 refs.
Confidential Report

Two parallel efforts were conducted consisting of (1) analytical studies to describe the flow field surrounding a trailing parachute decelerator in the wake of a forebody traveling at supersonic speeds and (2) a wind tunnel test program employing both conventional and unconventional parachute canopy designs. The wind tunnel program consisted of approximately 200 tests in the Mach number range from M=1.5 to M=4.65 using 6 and 8 inch inflated diameter models. Wind tunnel test data, and high speed Schlieren photographs are included to illustrate the test results of a program in which a new family of high speed self inflating parachutes evolved. Satisfactory performance of this new parachute family was demonstrated through Mach 4.65.

Unclassified Abstract

(over)

1. Parachutes
2. Fluid Mechanics
3. Tests
4. Supersonics
5. Drag and recovery
I. AFSC Project 6065, Task 606505
II. Contract AF 33(616)-8459
III. Cook Technological Center, Chicago, Illinois
IV. L. W. Sims
V. Secondery Rpt No. C00299
VI. Not aval fr OTS
VII. In ASTIA collection

Aeronautical Systems Division, Dir/Aeromechanics, Flight Accessories Lab, Wright-Patterson AFB, Ohio.
Rpt Nr ASD-TDR-62-844. ANALYTICAL AND EXPERIMENTAL INVESTIGATION OF SUPERSONIC PARACHUTE PHENOMENA(U). Final report, Feb 63, 133p. incl illus., tables, 7 refs.
Confidential Report

Two parallel efforts were conducted consisting of (1) analytical studies to describe the flow field surrounding a trailing parachute decelerator in the wake of a forebody traveling at supersonic speeds and (2) a wind tunnel test program employing both conventional and unconventional parachute canopy designs. The wind tunnel program consisted of approximately 200 tests in the Mach number range from M=1.5 to M=4.65 using 6 and 8 inch inflated diameter models. Wind tunnel test data, and high speed Schlieren photographs are included to illustrate the test results of a program in which a new family of high speed self inflating parachutes evolved. Satisfactory performance of this new parachute family was demonstrated through Mach 4.65.
Unclassified Abstract

(over)

1. Parachutes
2. Fluid Mechanics
3. Tests
4. Supersonics
5. Drag and recovery
I. AFSC Project 6065, Task 606505
II. Contract AF 33(616)-8459
III. Cook Technological Center, Chicago, Illinois
IV. L. W. Sims
V. Secondary Rpt No. C00299
VI. Not avail fr OTS
VII. In ASTIA collection

Aeronautical Systems Division, Dir/Aeromechanics, Flight Accessories Lab, Wright-Patterson AFB, Ohio.
Rpt Nr ASD-TDR-62-844. ANALYTICAL AND EXPERIMENTAL INVESTIGATION OF SUPERSONIC PARACHUTE PHENOMENA(U). Final report, Feb 63, 133p. incl illus., tables, 7 refs.
Confidential Report

Two parallel efforts were conducted consisting of (1) analytical studies to describe the flow field surrounding a trailing parachute decelerator in the wake of a forebody traveling at supersonic speeds and (2) a wind tunnel test program employing both conventional and unconventional parachute canopy designs. The wind tunnel program consisted of approximately 200 tests in the Mach number range from M=1.5 to M=4.65 using 6 and 8 inch inflated diameter models. Wind tunnel test data, and high speed Schlieren photographs are included to illustrate the test results of a program in which a new family of high speed self inflating parachutes evolved. Satisfactory performance of this new parachute family was demonstrated through Mach 4.65.
Unclassified Abstract

(over)

1. Parachutes
2. Fluid Mechanics
3. Tests
4. Supersonics
5. Drag and recovery
I. AFSC Project 6065, Task 606505
II. Contract AF 33(616)-8459
III. Cook Technological Center, Chicago, Illinois
IV. L. W. Sims
V. Secondary Rpt No. C00299
VI. Not avail fr OTS
VII. In ASTIA collection

Aeronautical Systems Division, Dir/Aeromechanics, Flight Accessories Lab, Wright-Patterson AFB, Ohio.
Rpt Nr ASD-TDR-62-844. ANALYTICAL AND EXPERIMENTAL INVESTIGATION OF SUPERSONIC PARACHUTE PHENOMENA(U). Final report, Feb 63. 133p. incl illus., tables, 7 refs.
Confidential Report

Two parallel efforts were conducted consisting of (1) analytical studies to describe the flow field surrounding a trailing parachute decelerator in the wake of a forebody traveling at supersonic speeds and (2) a wind tunnel test program employing both conventional and unconventional parachute canopy designs. The wind tunnel program consisted of approximately 200 tests in the Mach number range from M=1.5 to M=4.65 using 6 and 8 inch inflated diameter models. Wind tunnel test data, and high speed Schlieren photographs are included to illustrate the test results of a program in which a new family of high speed self inflating parachutes evolved. Satisfactory performance of this new parachute family was demonstrated through Mach 4.65.
Unclassified Abstract

(over)

1. Parachutes
2. Fluid Mechanics
3. Tests
4. Supersonics
5. Drag and recovery

I. AFSC Project 6065, Task 606505
II. Contract AF 33(616)-8459
III. Cook Technological Center, Chicago, Illinois
IV. L. W. Sims
V. Secondary Rpt No. C00299
VI. Not avel fr OTS
VII. In ASTIA collection

Aeronautical Systems Division, Dir/Aeromechanics, Flight Accessories Lab, Wright-Patterson AFB, Ohio.
Rpt Nr ASD-TDR-62-844. ANALYTICAL AND EXPERIMENTAL INVESTIGATION OF SUPERSONIC PARACHUTE PHENOMENA(U). Final report, Feb 63. 133p. incl illus., tables, 7 refs.
Confidential Report

Two parallel efforts were conducted consisting of (1) analytical studies to describe the flow field surrounding a trailing parachute decelerator in the wake of a forebody traveling at supersonic speeds and (2) a wind tunnel test program employing both conventional and unconventional parachute canopy designs. The wind tunnel program consisted of approximately 200 tests in the Mach number range from M=1.5 to M=4.65 using 6 and 8 inch inflated diameter models. Wind tunnel test data, and high speed Schlieren photographs are included to illustrate the test results of a program in which a new family of high speed self inflating parachutes evolved. Satisfactory performance of this new parachute family was demonstrated through Mach 4.65.
Unclassified Abstract

(over)

1. Parachutes
2. Fluid Mechanics
3. Tests
4. Supersonics
5. Drag and recovery
I. AFSC Project 6065, Task 606505
II. Contract AF 33(616)-8459
III. Cook Technological Center, Chicago, Illinois
IV. L. W. Sims
V. Secondary Rpt No. C00299
VI. Not avel fr OTS
VII. In ASTIA collection

Aeronautical Systems Division, Dir/Aeromechanics, Flight Accessories Lab, Wright-Patterson AFB, Ohio.
Rpt Nr ASD-TDR-62-844. ANALYTICAL AND EXPERIMENTAL INVESTIGATION OF SUPERSONIC PARACHUTE PHENOMENA(U). Final report, Feb 63, 133p. incl illus., tables, 7 refs.

Confidential Report

Two parallel efforts were conducted consisting of (1) analytical studies to describe the flow field surrounding a trailing parachute decelerator in the wake of a forebody traveling at supersonic speeds and (2) a wind tunnel test program employing both conventional and unconventional parachute canopy designs. The wind tunnel program consisted of approximately 200 tests in the Mach number range from M=1.5 to M=4.65 using 6 and 8 inch inflated diameter models. Wind tunnel test data, and high speed Schlieren photographs are included to illustrate the test results of a program in which a new family of high speed self inflating parachutes evolved. Satisfactory performance of this new parachute family was demonstrated through Mach 4.65.

Unclassified Abstract

1. Parachutes
2. Fluid Mechanics
3. Tests
4. Supersonics
5. Drag and recovery
I. AFSC Project 6065, Task 606505
II. Contract AF 33(616)-8459
III. Cook Technological Center, Chicago, Illinois
IV. L. W. Sipp
V. Secondary Rpt No. C00299
VI. Not avail fr OTS
VII. In ASTIA collection

Aeronautical Systems Division, Dir/Aeromechanics, Flight Accessories Lab, Wright-Patterson AFB, Ohio.
Rpt Nr ASD-TDR-62-844. ANALYTICAL AND EXPERIMENTAL INVESTIGATION OF SUPERSONIC PARACHUTE PHENOMENA(U). Final report, Feb 63, 133p. incl illus., tables, 7 refs.

Confidential Report

Two parallel efforts were conducted consisting of (1) analytical studies to describe the flow field surrounding a trailing parachute decelerator in the wake of a forebody traveling at supersonic speeds and (2) a wind tunnel test program employing both conventional and unconventional parachute canopy designs. The wind tunnel program consisted of approximately 200 tests in the Mach number range from M=1.5 to M=4.65 using 6 and 8 inch inflated diameter models. Wind tunnel test data, and high speed Schlieren photographs are included to illustrate the test results of a program in which a new family of high speed self inflating parachutes evolved. Satisfactory performance of this new parachute family was demonstrated through Mach 4.65.

Unclassified Abstract

1. Parachutes
2. Fluid Mechanics
3. Tests
4. Supersonics
5. Drag and recovery
I. AFSC Project 6065, Task 606505
II. Contract AF 33(616)-8459
III. Cook Technological Center, Chicago, Illinois
IV. L. W. Sipp
V. Secondary Rpt No. C00299
VI. Not avail fr OTS
VII. In ASTIA collection